Anonymous Referee #1

This contribution presents number size distribution and concentration of non-volatile particle fractions and the volatile composition of ambient aerosols based on VTDMA data. In particular, even though volatility analysis of ambient aerosols in general have been intensively studied in different fields, it is the first time to provide the chemical composition based on volatility of aerosols in PRD region with a different synoptic condition.

Major comments: (we have indexed the comments for easy reference)

1. *The volatility information of studied site, which this work strives to provide, could be written out more explicitly both in the introduction and results.*

1.1 According to this, the main goals of the study, given in the end of the introduction, should be revised. At least, more discussion about how the results obtained in this study would contribute to, e.g., estimating the chemical composition of size segregated aerosols and the mixing state of the non-volatile residuals, should be added, because this is given as a motivation for this work in the introduction.

1.2 In addition, the discussion of the mixing state of the non-volatile residuals is far too simplified. Please consider adding more materials from either total number size distribution measurements or chemical composition data from other instruments, or air masses origins information. Also, the literature could be rechecked for the last 2-3 years.

2. *It is highlighted in the manuscript that in urban areas "non-volatile" aerosol fraction consists mainly of soot. This statement guides the reader to think that there are no other important non-volatile aerosol compounds. However, as it is concluded the non-volatile fraction may actually consist of some extremely low-volatility organic material that does not evaporate even at 300 ℃. More discussion on the effectively non-volatile organics should be added to the manuscript; what are these organics?*

3. *The author wrote the VTDMA measurements were performed at 25, 100 and 300 ℃, while in the discussion section; only the results at 300 ℃ were present. The definition of VSF, LV, MV, HV and all relevant quantities actually were based on number size distribution after heating at 300 ℃. The author did not write clearly in the methodology part, please revise it.*

4. *Conventionally, ammonium sulfate can be considered to be of low-volatility and it tends to evaporate at around 200 ℃. It seems that in this manuscript low volatile refers to material that is elsewhere referred to as extremely low volatile of effectively non-volatile (see recent literature, e.g. Donahue et al., 2013 in Faraday Discussions; Murphy et al., 2014 in ACP).*

5. *The author should avoid using too many abbreviations or use them in cautions especially they are not conventionally used elsewhere.*

6. *The discussion of the fraction of low volatile, medium volatile and high volatile materials on the non-volatile cores as well as the complete volatile materials was mainly related to meteorological conditions and traffic emissions. I thus strongly recommend that the general meteorological parameters, e.g. temperature, relative humilities as well as traffic densities are given, since all results only represent concurrent conditions. For example, plot time series or diurnal variations of air mass origins and traffic densities around by can also help for the discussion.*

7. *Concerning the number fractions, isn't it possible that the finest particles (initial diameter of 40 nm) get below the detection limit of the instrument upon heating? If so, it cannot be assumed that these particles would be completely evaporated. These particles may include an extremely low volatility "non-volatile" fraction, which cannot be detected because of the small size of the remaining particles after the heating. This issue should be discussed in the manuscript.*

8. *Please provide the residence time in your heating unit; is it long enough for all the volatile material to evaporate? Please add this information to the manuscript.*

9. *If available, the particle number size distribution from DMPS or SMPS during the whole campaign should be given. Was new particle formation seen in this site? How does the number size distribution vary during day and night?*

Response:

We thank the reviewer for the useful comments. Below please find our response to each of the points above. Major changes to the manuscript are shown in blue.

1. In the introduction, we have revised the background of VTDMA studies, volatility of organics and goals of this work, which were:

i) To characterize the volatility of ambient aerosols at a suburban site in Guangzhou, a mega city in China; and

ii) To better characterize the composition of non-volatile materials in VTDMA measurements at 300 ℃.

In the results and discussion section, we have added the following new materials and discussions to achieve the goals above:

i) Meteorological conditions including wind speed, wind direction, temperature, and relative humidity;

ii) Particle number size distribution from the SMPS;

iii) Time series and diurnal variations in OC and EC concentrations; and

iv) Back trajectory analysis

With the addition of the new materials, the subsections in the results and discussion section of the revised manuscript are re-organized:

- 3.1 Overview
- 3.2 Diurnal variations
- 3.3 Back trajectory analyses
- 3.4 New particle formation
- 3.5 Closure analysis for LV and MV residuals at 300 ℃, OC and EC

The response below will focus on the new materials added. We do not have time series data of traffic density at the sampling site, but we cited Zhang et al. (2015)

for the diurnal traffic pattern measured in a tunnel experiment in Guangzhou to aid the discussion.

1.1 Revised Introduction

1.1.1 Background of VTDMA studies and volatility of organics

Philippin et al. (2004) later developed a VTDMA capable of evaporating volatile materials in aerosols at temperatures up to 300 ℃. Non-volatile materials at 300 ℃, such as EC, non-volatile organics and sea salt can externally or internally mix (or be coated) with volatile materials. Note that the terms "volatile" and "non-volatile" are defined at the heating temperature of 300 ℃ in the VTDMA. They are different from the volatilities defined under ambient conditions (Donahue et al., 2009; Murphy et al., 2014) or in other measurement techniques (Twomey, 1968; Pinnick et al., 1987; Huffman et al., 2009). The composition of these non-volatile residuals can vary spatially and temporally in VTDMA measurements. Previous studies have demonstrated good agreement between the mass of black carbon and the mass of particles with small volatile fractions, which experienced size reductions of 5 to 10% upon heating at 300 ℃ in the VTDMA. Various studies have also used a VTDMA to estimate the mixing states of soot particles. Particles with small volatile fractions are often assumed to be soot particles externally mixed with particles with volatile materials at 300 ℃. Particles with larger volatile fractions, which experienced size reductions of more than 10% upon heating at 300 ℃ in the VTDMA, were assumed to represent soot particles internally mixed (coated) with the volatile materials (Philippin et al., 2004; Cheng et al., 2006; Frey et al., 2008; Wehner et al., 2009; Rose et al., 2011; Levy et al., 2014; Zhang et al., 2016).

Organics also contribute to light absorption by atmospheric particles (Bond 2001; Kirchstetter et al. 2004; Chen and Bond 2010). Laboratory studies have shown that organic aerosols may form low volatility oligomers after aging for a long time (e.g. Kalberer et al., 2004). Huffman et al. (2009) showed that highly oxygenated, aged organic aerosols exhibited similar or lower volatility than the primary organic aerosols or the less oxygenated ones. Recently, Häkkinen et al. (2012) found that the mass fraction remaining of non-BC residuals, i.e. the difference between the residual mass derived from a volatility differential mobility particle sizer at 280 ℃ and the black

carbon mass derived from an aethalometer, is positively correlated with the mass fraction of organics measured with an aerosol mass spectrometer.

1.1.2 Goals of this study

In this study, simultaneous measurements of aerosol volatility and carbonaceous matter were made at a suburban site in Guangzhou, China during wintertime in February and March 2014 using a VTDMA and a semi-continuous OC/EC analyzer, respectively. Volatility measurements were made for ambient aerosols ranging from 40 nm to 300 nm in diameter. Residuals remaining after heating at 300 ℃ in the VTDMA are referred to as non-volatile in this study. We report the average values, time series and diurnal variations in the number and volume fractions of the volatile and non-volatile materials, as well as the OC and EC concentrations. We examine the relationships of the non-volatile materials upon heating at 300 ℃ to EC and to the non-volatile OC, based on analyses of the diurnal patterns and mass closures of the OC/EC and VTDMA data. Finally, we discuss the influence of air mass origins on the volatility of the sampled aerosols and concentrations of OC and EC based on back trajectory analysis.

1.2 Revised Results and Discussions (with new materials added)

1.2.1 Meteorological conditions, SMPS and OC/EC data

The time series of meteorological conditions, particle number size distribution, $PM_{2.5}$, OC and EC concentrations during the campaign are presented in Fig. R1. Overall, the campaign came under the influence of the prevailing northerly wind with an average wind speed and temperature (± one standard deviation) of 1.73 ± 0.95 m s^{-1} and 14.8 ± 5.1 ℃, respectively. The average $PM_{2.5}$ concentration was 48 ± 26 μg m^{-3}. A few cold front periods were observed, during which the wind speed increased and the temperature decreased. In general, the low wind speed favored the accumulation of $PM_{2.5}$. OC concentrations ranged from 0.5 to 47.0 μg m^{-3} with an average of 9.0 ± 6.0 μg m^{-3}, while EC concentrations ranged from 0.2 to 23.0 μg m^{-3} with an average of 3.4 ± 3.0 μg m^{-3}. OC_1, the most volatile group among OC_1 to OC_4 in OC/EC analysis, accounted for one-third of the total carbon mass (Fig. R2).

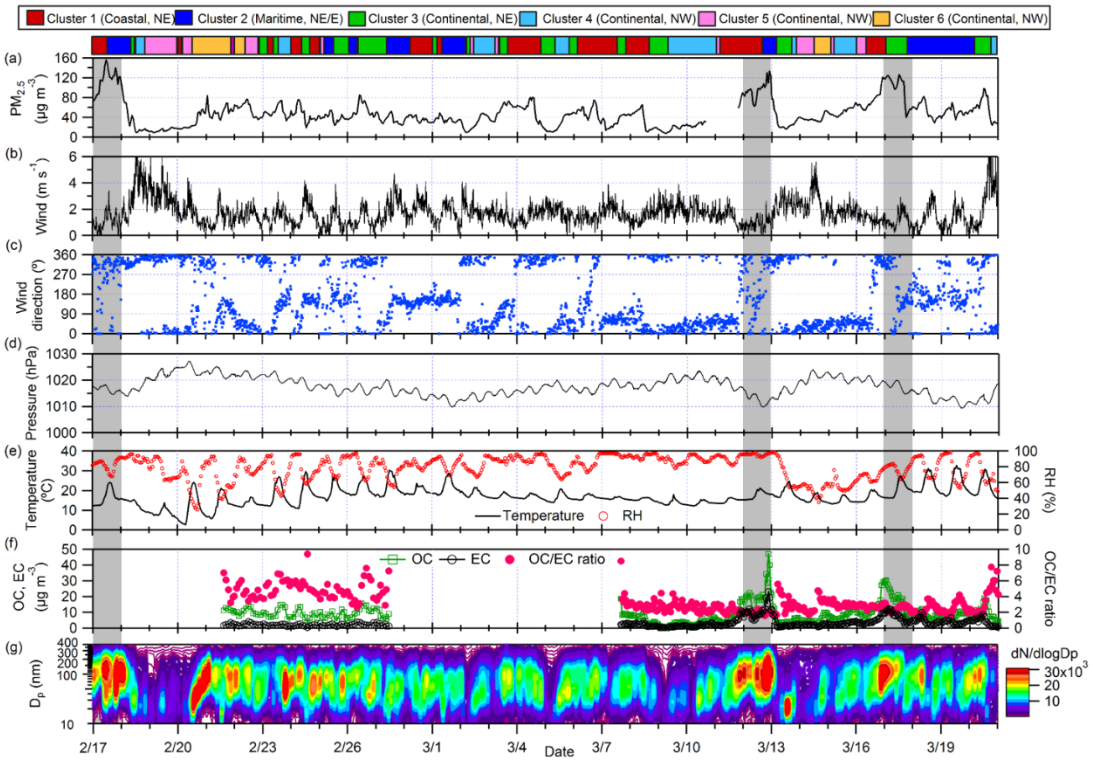

Fig. R1. Overview of major meteorological parameters, $PM_{2.5}$, OC and EC concentrations, OC/EC ratio and particle number size distributions in the campaign. Air mass clusters are depicted at the top and the shaded areas indicate days with daily-averaged $PM_{2.5}$ concentrations exceeding 95 μg m^{-3}.

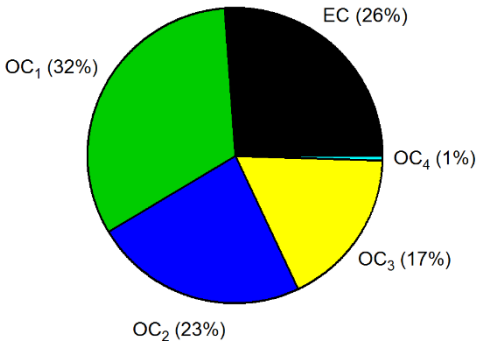

Fig. R2. Average mass fractions of EC, OC_1, OC_2, OC_3 and OC_4 in $PM_{2.5}$.

On Feb 17, and Mar 12 and 17, the daily-averaged $PM_{2.5}$ concentrations exceeded 95 μg m^{-3}; they were nearly twice the daily-averaged values on other days (Fig. R1, shaded area in grey). Results of 72 h back trajectories (Stein et al., 2015; Rolph, 2016) showed that air masses arriving at the site on or before these three days mostly originated from the continental or oceanic area close to Eastern China (Fig. R3). The SMPS data also showed a mode near 100 nm with a high particle number concentration (Fig. R1).

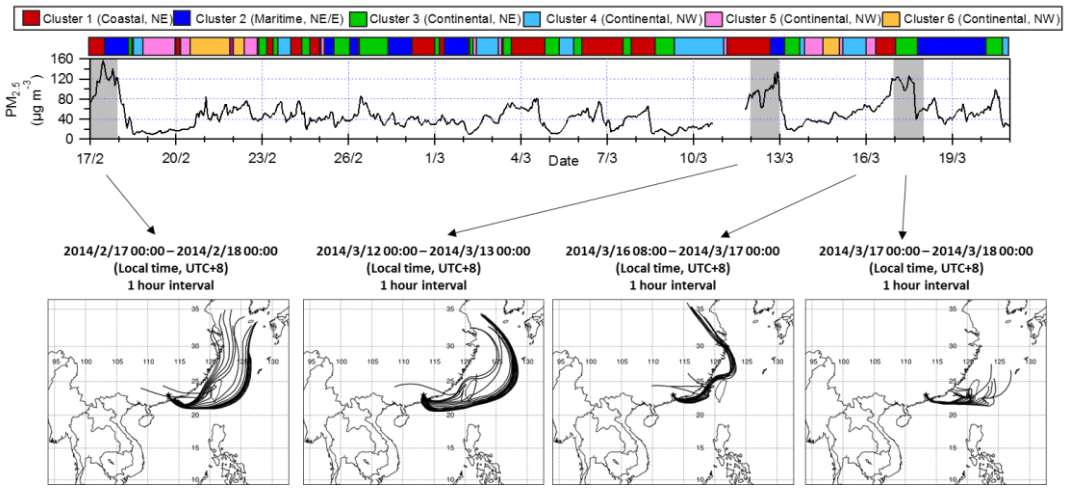

Fig. R3. Time series of $PM_{2.5}$ concentrations and 72 h back trajectories at hourly intervals on Feb 17, and Mar 12, 16 and 17.

Two new particle formation (NPF) events were observed in the campaign on Feb 20 and Mar 13 (Fig. R1). Since VTDMA data were not available during the NPF event on Mar 13, we only focus on the NPF event on Feb 20 which happened after a cold front under a low $PM_{2.5}$ concentration. On Feb 20, a sub-20 nm particle mode was first observed at 12:00. This particle mode grew continuously until it reached 120 nm at 02:00 on Feb 21. In VTDMA measurements, a sharp increase in the number concentration of HV particles having an initial diameter of 40 nm was observed at 17:00 on Feb 20 (Fig. R4). This event is likely related to the growth of the newly formed particles when they mixed with the volatile materials via condensation or adsorption. As these particles aged further, they grew larger as reflected in the increase in number concentrations of larger MV particles and the increase in $PM_{2.5}$ mass (Fig. R4). The growth of the newly formed particles can also be observed from the number size distributions of HV, MV and LV particles at different times on Feb 20 and 21 (Fig. R5). The mode of HV particles increased from 40 nm at 17:00 to 80 nm at 21:00 on Feb 20 Feb. The mode stayed at 80 nm while the corresponding number concentration decreased at 02:00 on Feb 21 Feb. In contrast, the number concentrations of MV particles grew continuously. The HV and MV particle concentrations and diameter modes underwent much smaller changes on the non-event day of Feb 28 (Fig. R5).

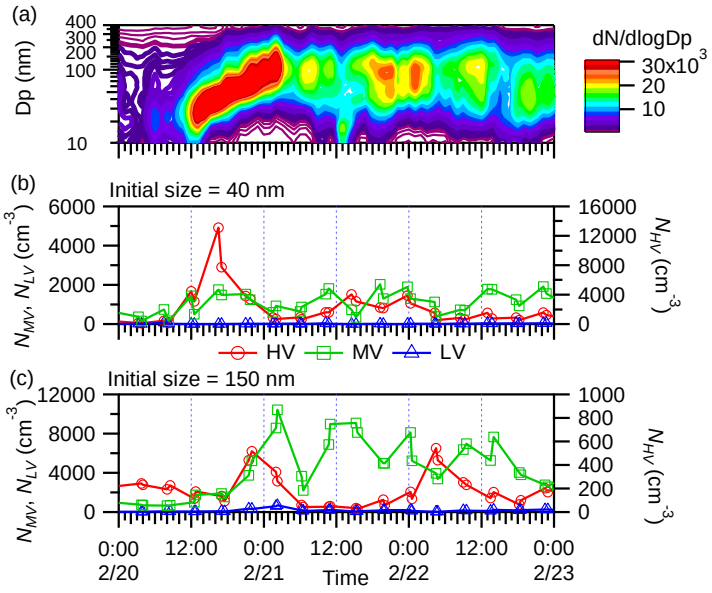

Fig. R4. Time series of (a) particle number size distribution, (b) number concentrations of HV, MV and LV in 40 nm particles and (c) number concentrations of HV, MV and LV in 150 nm particles.

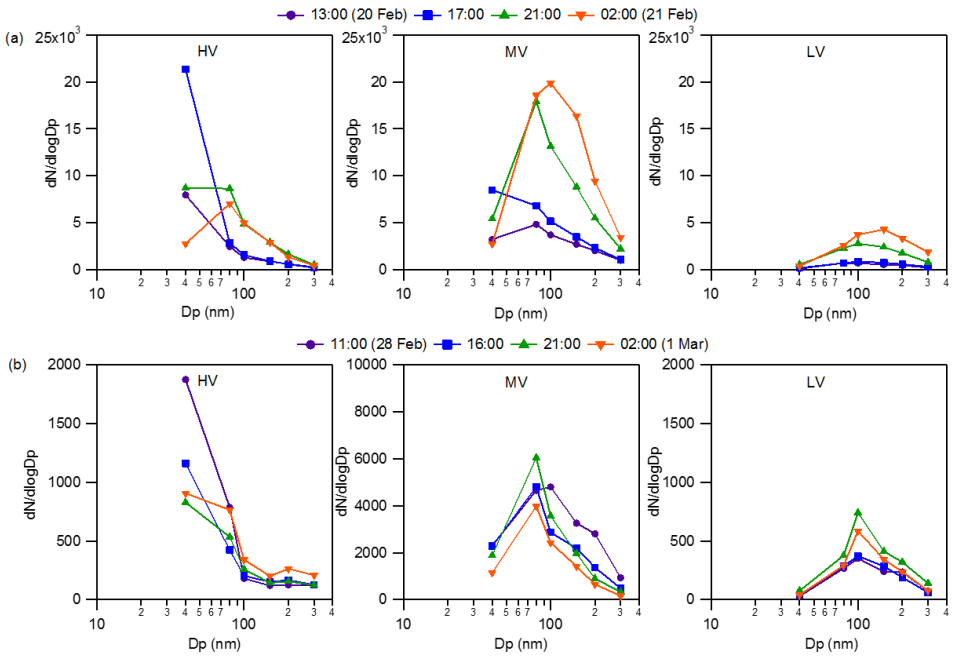

Fig. R5. Particle number size distribution of (columns from left to right) HV, MV and LV particles (a) at 13:00, 17:00, 21:00 on 20 Feb and 02:00 on 21 Feb and (b) at 11:00, 16:00, 21:00 on 28 Feb and 02:00 on 1 Mar.

1.2.2 Comparison of the diurnal variations in OC/EC and VTDMA data

The diurnal variations in the mass fractions of OC and EC in $PM_{2.5}$ are compared with the volume fractions of CV, HV residual, MV residual, LV residual and VM in particles of dry initial diameters of 40, 150 and 300 nm. The OC and EC data on Mar 12 and 17 were excluded since they were more than two standard deviations higher than those on other days. Subtle morning peaks between 06:00 and 10:00 were observed for the volume fraction of LV residuals (Fig. R6). A similar peak was observed for the mass fraction of EC in $PM_{2.5}$ in the morning (Fig. R7). This suggests that LV particles may be related to the EC from vehicle emissions in the morning. This EC was relatively less aged and externally mixed with other volatile materials. In the late afternoon, LV residuals showed another peak between 17:00 and 19:00 whereas the mass fraction of EC in $PM_{2.5}$ exhibited a minimum at 15:00, after which it increased continuously. The continuous increase in EC at night is likely related to the increase of heavy-duty diesel vehicles (Zhang et al., 2015), which was restricted during daytime (Bradsher, 2007).

Although OC_1 contributed to about half of the total OC mass, the diurnal variation in the mass fraction of OC in $PM_{2.5}$ was driven by the total mass of OC_2, OC_3 and OC_4 ($OC_{2\text{-}4}$), which reached a minimum between 05:00 and 09:00 and increased until 19:00. OC can be attributed to both primary and secondary sources. The increased mass fraction of OC in $PM_{2.5}$ and OC-to-EC ratio in the afternoon suggest that the sources of OC were less related to traffic but more to the aging and formation of secondary organic aerosols (Turpin et al., 1990; Chow et al., 1996). These OC_2, OC_3 and OC_4 may be highly oxygenated species or oligomers that are less volatile than primary or less oxygenated organics (Kalberber et al., 2004; Huffman et al., 2009).

It is interesting to note that the volume fraction of LV residuals and the *VFR* of MV particles at different sizes showed a dip in the afternoon (Fig. R6, third column from the left). The *VFR* of 40 nm MV particles showed a dip at 14:00 while those in 150 nm and 300 nm particles showed a dip at 15:00. The volume fraction of LV residuals in 150 nm and 300 nm particles reached a minimum at 13:00 and 15:00, respectively. Because EC decreased between 12:00 and 15:00, the increase in the volume fraction of LV residuals in 150 nm particles since 13:00 and the *VFR* of 40 nm MV particles

since 14:00 may be related to the increased presence of aged organics as well as the EC particles which aged via coagulation and condensation.

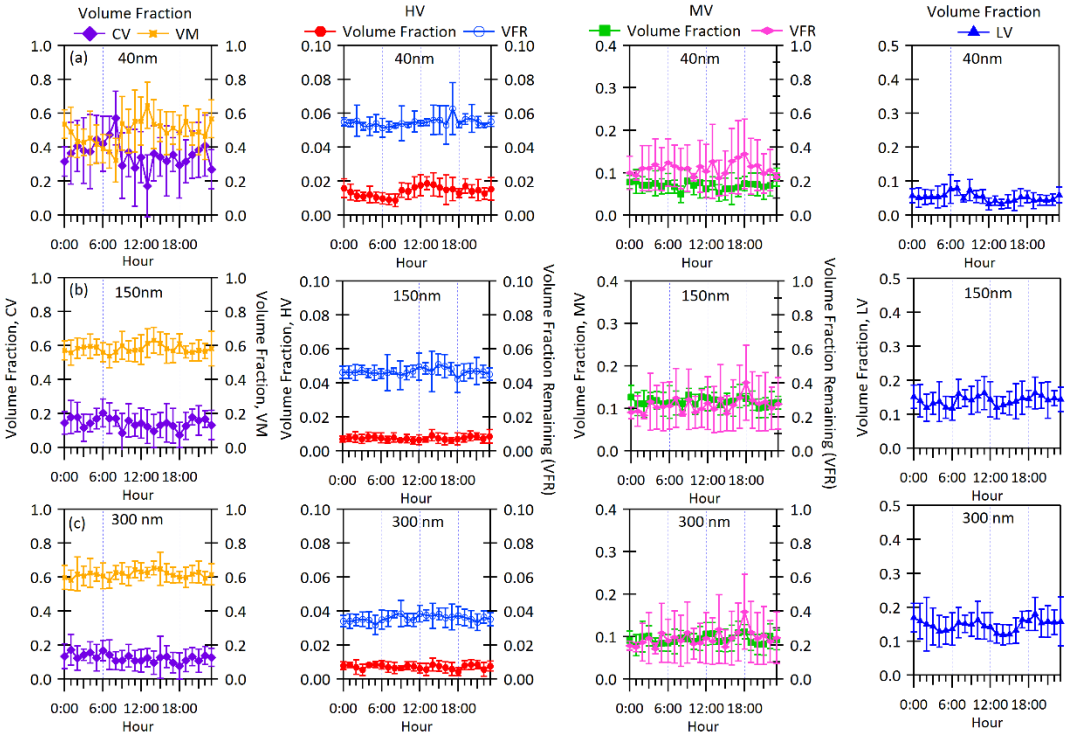

Fig. R6. Diurnal variations in volume fractions of (columns from left to right) CV, VM, HV residual, MV residual and LV residual in (a) 40 nm, (b) 150 nm and (c) 300 nm particles. Diurnal variations in the volume fraction remaining (*VFR*) of HV and MV particles are plotted on the right axis. Error bars represent one standard deviation.

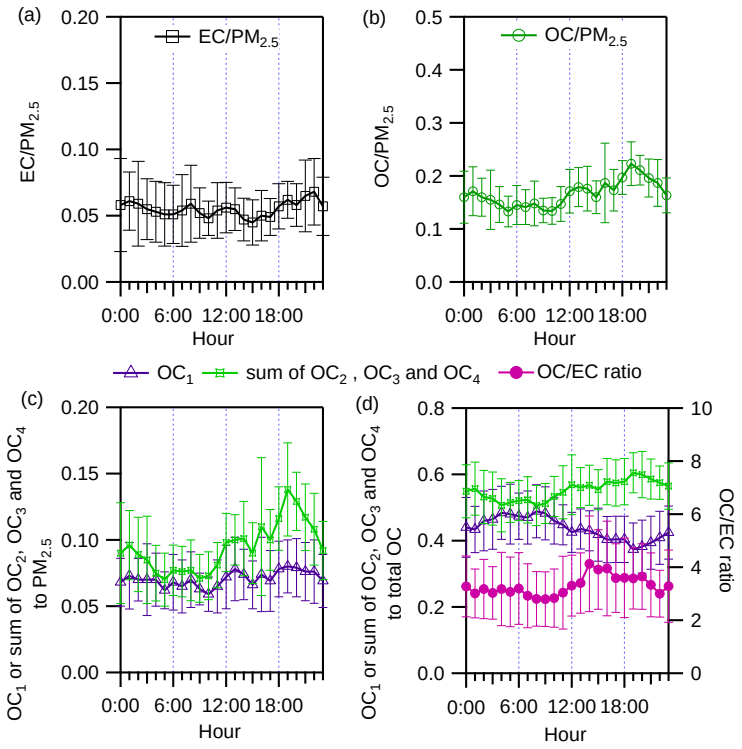

Fig. R7. Diurnal variations in the mass fractions of EC, OC, OC_1 and the sum of OC_2, OC_3 and OC_4 in $PM_{2.5}$, the ratio of OC to EC, mass fractions of OC_1 and the sum of OC_2, OC_3 and OC_4 to total OC in February and March. Error bars represent one standard deviation.

1.2.3 Back trajectory analyses

We calculated the 72 h back trajectories of the air masses arriving at the sampling site (23°00 N, 113°25" E) at 4 h intervals (at 00:00, 04:00, 08:00, 12:00, 16:00 and 20:00 local time, UTC +8) using the PC version of the HYSPLIT4 (Hybrid Single Particle Lagrangian Integrated Trajectory, version 4) model (Stein et al., 2015; Rolph, 2016). Archived meteorological data from the Global Data Assimilation System (GDAS) 1-deg was employed and the receptor height was set at 500 m above ground level (a.g.l.). The 191 back trajectories calculated were grouped into six clusters based on their spatial distribution (Fig. R8).

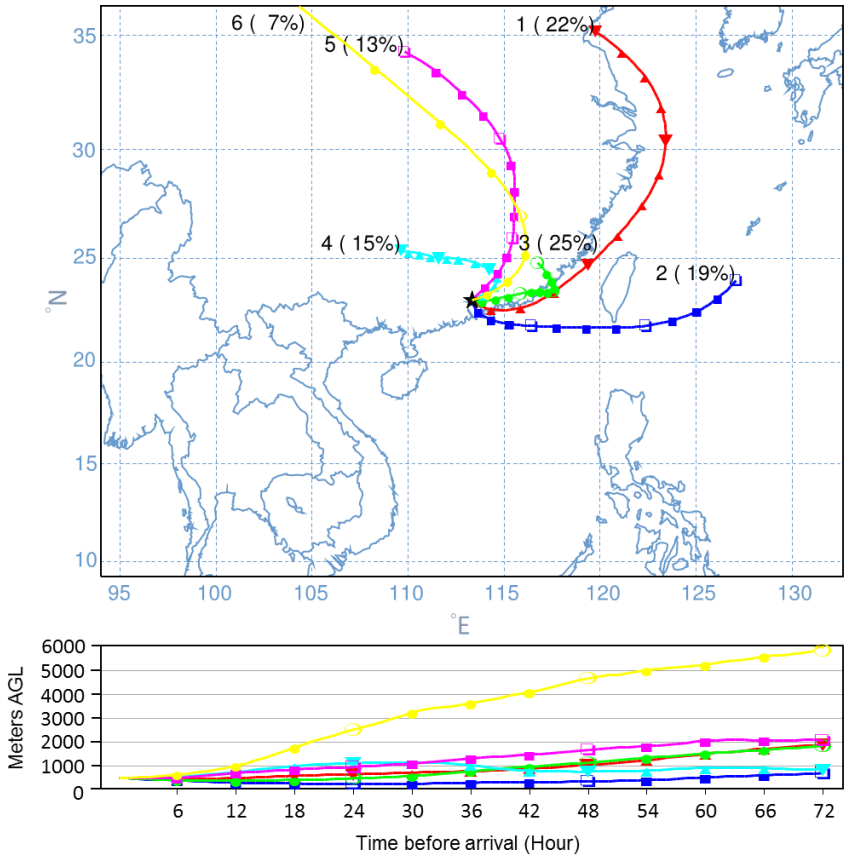

Fig. R8. Mean back trajectories of the six types of air masses arriving at the sampling site.

Overall, the sampling site was mostly affected by northwesterly and northeasterly air masses. Cluster 1 and 3 are coastal and continental air masses, respectively, although both originated from the northeast. Clusters 4, 5 and 6 represent continental air masses originating from the northwest. Cluster 2 is a group of maritime air masses originating from the East China Sea northeast or east of Guangzhou. While air masses in cluster 6 were transported at relatively high speeds and altitudes (over 3000 m a.g.l.), air masses in all the other clusters were transported at an altitude below 1500 m a.g.l. for over 40 h before arriving at the site. Nevertheless, air masses in cluster 6 only persisted for less than three days. Since the corresponding VTDMA and OC/EC data were sometimes unavailable, cluster 6 will be excluded from the following discussion.

The average $PM_{2.5}$, OC and EC concentrations associated with air masses from the northeast of Guangzhou (clusters 1, 2 and 3) were higher than those from the northwest (clusters 4 and 5, Table R1). Days associated with coastal and maritime air masses were more polluted than days associated with continental air masses for several reasons. First, south China as a region is often affected by the high pressure system moving eastward or southward from the continent out to sea in winter. When the maritime or coastal air streams entered from the southeast of the sampling site at Panyu, the atmosphere at the sampling site became more stable with low local wind speeds (e.g. the polluted days on Feb 17 and Mar 12, 16 and 17, Fig. R1 and R3). Local pollutants accumulated and the city was also affected by pollutants from the southeastern areas of the site (e.g. Shenzhen, Nansha and Dongguan). Second, land-sea breeze cycles were observed when the sampling site was under the influence of maritime air masses from Mar 18 to 20. During the day, southeasterly wind prevailed and the wind speed was higher. In the evening, the southeasterly wind was gradually replaced by a southwesterly or northwesterly wind and the wind speed decreased (Fig. R1). The cycle started again in the morning when the westerly wind was gradually replaced by southeasterly wind. Such land-sea breeze effects can result in an effective redistribution and accumulation of air pollutants within the PRD region (Lo et al., 2006).

Table R1. Summary of concentrations of $PM_{2.5}$, OC, EC and the ratio of OC to EC (OC/EC) in the five clusters.

	Cluster				
	Coastal	Maritime	Continental		
	1	2	3	4	5
Origin (to the site)	NE	NE/E	NE	NW	NW
$PM_{2.5}$ (μg m^{-3})	58.5 ±24.4	58.9 ±30.9	47.5 ±28.4	33.9 ±15.9	33.8 ±19.3
OC (μg m^{-3})	10.8 ±6.01	10.84 ±7.22	10.13 ±6.89	5.51 ±3.3	7.32 ±2.75
EC (μg m^{-3})	4.38 ±2.97	4.98 ±4.21	3.43 ±3.12	1.8 ±0.98	2.46 ±0.59
OC/EC	2.83 ±1.05	2.62 ±1.03	3.65 ±1.6	3.18 ±1.26	2.94 ±0.73

Furthermore, $PM_{2.5}$ in the northeastern parts of China can exceed 200 μg m^{-3} due to both enhanced emissions from coal combustion for heating and poor dispersion during wintertime (Gu et al., 2014). Under the influence of the prevailing northerly or northeasterly wind in China, these pollutants were often transported to southern China and the East China Sea (Chen et al., 2012). Pollutants might also have accumulated when the maritime air masses spent about two days across Taiwan and the coast of south China. In contrast, continental air masses in cluster 5 moved slightly faster, and were often associated with the cold front period during which the local wind speed and pressure increased but the temperature decreased (Fig. R1). As the cold air masses passed through the city, dispersion and clearance of pollutants were promoted, resulting in lower $PM_{2.5}$ concentrations (Tan et al., 2013a). Therefore, unlike in other coastal cities like Hong Kong (Lee et al., 2013), in Panyu maritime air masses could lead to more severe pollution than the continental ones in winter.

The five clusters were further analyzed to study the influence of air mass history on aerosol volatility. The number fractions of CV, HV, MV and LV of the six selected diameters in VTDMA measurements are regrouped based on the clusters as shown in Fig. R9. The total number fractions of the non-volatile residuals (sum of HV, MV and LV) were similar in all clusters. Maritime air masses (cluster 2) had a slightly higher fraction of LV particles while continental air masses originating from the northwest of the site (clusters 4 and 5) had a higher fraction of HV particles. Although the air masses in clusters 1 and 5 originated from farther away and traveled at relatively higher speeds

than those in clusters 2, 3 and 4, all clusters involved transport at low altitudes (below 1500 m) for over 40 h, likely due to the generally lower mixing heights in winter. Therefore, aerosols in these air masses were all well-aged upon arrival (Wehner et al., 2009). This could be another reason for the lack of size dependence of the number, volume fractions and diurnal variation for particles larger than 80 nm. When the transported air masses mixed with local pollutants, the size dependence of the number fractions of different volatility groups as well as the aging of local emissions was further reduced.

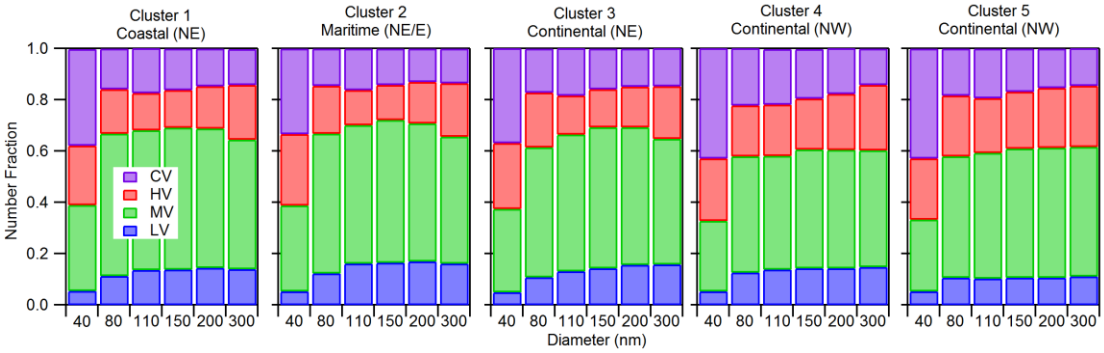

Fig. R9. Average number fractions of CV, HV, MV and LV particles in clusters 1 to 5 at different selected diameters.

We also examine at the volatility shrinkage factor (*VSF*) distributions of 40 nm, 110 nm and 300 nm particles upon heating at 300 ℃ (Fig. R10). Log-normal fittings with a three-peak solution were applied to the distributions. The average *VSF* modes of the peaks were located at 0.38 ± 0.021 (peak 1), 0.60 ± 0.066 (peak 2) and 0.95 ± 0.007 (peak 3), respectively. The standard deviation of the corresponding normal distribution (σ) of peak 3 was the smallest among the three peaks ($\sigma < 0.1$). For the same particle size, the *VSF* distributions in the *VSF* range between 0.3 and 0.8 in cluster 5 was relatively more uni-modal than those of other clusters (Fig. R10b and R10c). This suggests that the composition in cluster 5 was more homogeneous. Cluster 1 also consisted of long-range transported air masses but they likely passed through areas that are more polluted and mixed with different types of pollutants. Note that the fractions of HV, MV and LV have been traditionally defined based on the values of *VSF*, i.e. HV < 0.4; 0.4 < MV < 0.9; LV > 0.9 (Wehner et al., 2009). The *VSF* distributions above suggest that these definitions using *VSF* = 0.4 and 0.9 may need to be re-visited in the future.

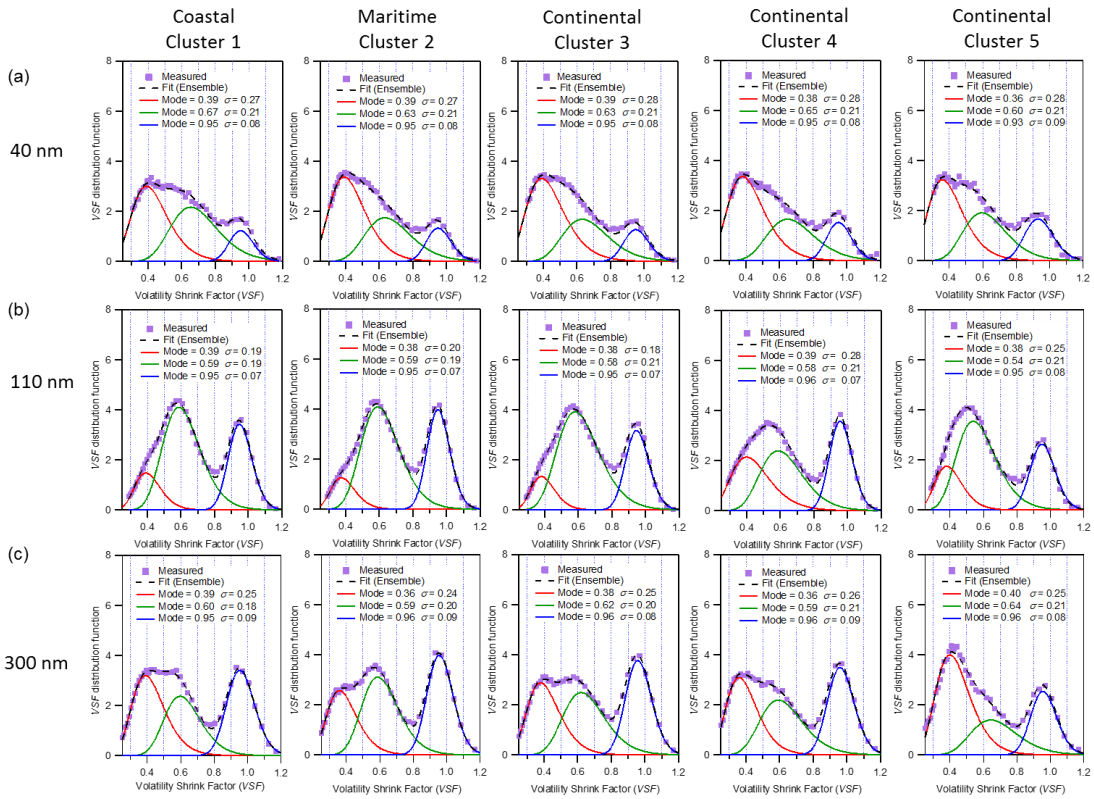

Fig. R10. Volatility shrinkage factor (*VSF*) distribution function in different clusters. Solid and dotted lines are the peaks fitted with log-normal function and the ensemble distributions, respectively.

2. We have revised the introduction to include a discussion of the non-volatile organics (see item 1.1.1).

3. The data analysis in this work focused on the measurements made after the aerosols were heated at 300 ℃. The methodology section is revised stating clearly that the definitions of *VSF*, LV, MV, HV and all relevant quantities defined in this work refer to results at 300 ℃.

3.1 Revised Methodology (Section 2.1.2, P25275 of the original manuscript, line 8 onwards):

…The *VSF* is also used to divide the particles into three groups, namely the low volatility (LV), medium volatility (MV) and high volatility (HV) particles. In this study, we focus on the measurements made at 300 ℃. The *VSF* ranges for LV, MV and HV particles upon heating at 300 ℃ are above 0.9, between 0.4 and 0.9 and below 0.4, respectively (Fig. 2) (Wehner et al., 2004; Wehner et al., 2009).

4. We agree that the term low volatility in this manuscript refers to material that is elsewhere referred to as extremely low volatile (e.g. Donahue et al., 2013, Murphy et al., 2014). In this study, the terms "volatile" and "non-volatile" are defined based on the heating temperature (i.e. 300 ℃ in this work) set in the VTDMA to characterize carbonaceous compounds. They are therefore different from the volatilities defined under ambient conditions (Donahue et al., 2009; Murphy et al., 2014) or in other measurement techniques, which aim to characterize other chemical components (Twomey, 1968; Pinnick et al., 1987; Huffman et al., 2009). We have clarified this definition in the revised introduction (see item 1.1).

5. Unnecessary abbreviations for number and volume fractions in both the methodology and results sections are avoided in the revised manuscript by using the original terms such as "number fractions" or "volume fractions".

6. Please refer to item 1.2 for the information and discussions added.

7. We agree that the residuals of the finest particles (with an initial diameter of 40 nm) might go below the detection limit of the downstream DMA and CPC in the VTDMA system, i.e. 10 nm, upon heating at 300 ℃. The number concentrations (and fractions) of HV and CV of the finest particles may therefore be underestimated and overestimated, respectively. A note is added in the results section of the revised manuscript.

7.1 Revised Section 3.1 (Discussion on average number and volume fractions):

…Nevertheless, the detection limit of the downstream DMA and CPC in the VTDMA system is 10 nm. It was assumed that the residuals having a diameter below 10 nm were small enough to be considered as completely vaporized. However, such assumption would lead to an overestimation of CV and an underestimation of the non-volatile residuals for the finest particles selected (with an initial diameter of 40 nm).

8. The heating tube was a 1/2", 80 cm long stainless steel tube with an inner diameter of 8 mm. With a sample flow rate of 1 L min^{-1}, the resulting residence time in the heated section of the VTDMA was 2.4 s. The estimated aerosol velocity on the center line was 0.33 m s^{-1}. After leaving the heating unit, particles entered a heat exchanger measuring 30 cm in length to ensure sufficient cooling before entering DMA_2. The relevant information is added to the methodology section.

8.1 Revised Methodology (Section 2.1.2 VTDMA measurements, P25375 of the original manuscript, line 5 onwards):

Afterwards, the monodisperse aerosols were directed via path (b) to a heated tube for volatility measurement (V-Mode) sequentially at 25, 100 and 300 ℃. The heating tube was a 1/2", 80 cm long stainless steel tube with an inner diameter of 8 mm. With a sample flow rate of 1 L min^{-1}, the resulting residence time in the heated section of the VTDMA was 2.4 s. The estimated aerosol velocity on the center line was 0.33 m s^{-1}. Compared to the residence time of 0.3 s to 1 s in other VTDMA systems (e.g. Brooks et al., 2002; Philippin et al., 2004; Villani et al., 2007), the residence time in our VTDMA is assumed to be long enough for the volatile materials to be effectively vaporized. After leaving the heating tube, the flow entered a heat exchanger measuring 30 cm in length to ensure sufficient cooling before entering DMA_2.

9. Please refer to item 1.2 for the information and discussions added.

Minor comments:

1. ***P25271, abstract:*** *Please explain how the medium and low-volatility aerosol fractions are determined. Also it should be clear from the abstract that by low-volatility fraction essentially "non-volatile" fraction is meant, i.e. LV aerosol fraction consists of compounds that do not evaporate significantly even at 300 ℃. Also, it is somewhat confusing to say "nonvolatile materials … contain… less volatile OC".*

Response:

The abstract is rewritten using clearer definitions.

Revised:

... Low-volatility (LV) particles, with a volatility shrinkage factor *(VSF*) at 300 ℃ exceeding 0.9, contribute to 5% of number concentrations of 40 nm particles and 11–15% of 80–300 nm particles. They were non-volatile materials externally mixed with the volatile ones and therefore did not evaporate significantly at 300 ℃. Non-volatile materials mixed internally with the volatile ones are referred to as the medium volatility (MV, 0.4 < *VSF* < 0.9) and high volatility (HV, *VSF* < 0.4) particles…

…The closure analysis of the total mass of LV and MV residuals and the mass of EC or the sum of EC and non-volatile OC also suggests that non-volatile OC, in addition to EC, was one of the components of the non-volatile residuals measured by the VTDMA in this study.

***2. P25271, abstract**: OC contents are named from OC_1 to OC_4. It is not clear in the abstract what is meant by OC_2-OC_4 compounds. Does it refer to the amount of carbon in the compound? Please clarify.*

Response:

In the revised abstract, the term non-volatile OC, which evaporated at 475 ℃ or above, is used instead of OC_2-OC_4.

Revised:

… Non-volatile OC evaporating at 475 ℃ or above, together with EC, contributed to 67% of the total carbon mass.

***3. P25271, l 24-26**: check the references during recent years.*

Response:

Two references in recent years are added.

Original:

P25271, l 24-26

Carbonaceous aerosols comprising organic carbon (OC) and elemental carbon (EC) or black carbon (BC) are one of the major light absorption constituents and are abundant in particulate matter (PM) (Rosen et al. 1978; Hansen et al. 1984; Japar et al. 1986; Chow et al. 1993; Horvath 1993; Liousse et al. 1993; Fuller et al. 1999; Putaud et al. 2010).

Revised:

Carbonaceous aerosols comprising organic carbon (OC) and elemental carbon (EC) or black carbon (BC) are major light absorption constituents and occur abundantly in particulate matter (PM) (Rosen et al. 1978; Hansen et al. 1984; Japar et al. 1986; Chow et al. 1993; Horvath 1993; Liousse et al. 1993; Fuller et al. 1999; Putaud et al. 2010; Tao et al., 2014; Zhang et al., 2015).

4. ***P25272, l 4-6****: were the data reported in 2007, or the measurements were performed in 2007, please clarify it.*

Response:

The measurements were performed in 2007 but reported by Yu et al. (2010). However, the mass of OC was incorrectly reported. It should be 13.4 to 22.5 μg m^{-3}. The sentence is revised.

Original:

P25272, l 4-6

In 2007, the mass concentrations of EC and OC at an urban Guangzhou (GZ) site were reported to be 6.8 to 9.4 and 6.6 to 22.5 μg m^{-3} respectively (Yu et al., 2010).

Revised:

In 2007, the mass concentrations of EC and OC measured at an urban Guangzhou (GZ) site ranged from 6.8 to 9.4 and from 13.4 to 22.5 μg m^{-3} respectively (Yu et al., 2010).

5. ***P25273, l 1-4****: Firstly, I think the definition is not clear. It should be particles with LV, MV and HV fractions, but not LV, MV and HV particles according to Wehner et al. (2009). Secondly, they performed the measurements at 300 ℃. Please add the temperature reference in the text. Thirdly, what do these completely vaporized aerosols refer to ambient aerosols, from what you wrote in the discussion part, it could be sulfate, ammonium nitrate?*

Response:

Sorry for the confusing definitions. The definitions are revised to show that they follow the definitions by Wehner et al. (2004) and Rose et al. (2006): LV particles are particles containing a less volatile fraction and do not evaporate significantly upon heating at 300 ℃; MV and HV particles are particles with more volatile fractions.

The completely vaporized aerosols at 300 ℃ can be sulfate, nitrate and volatile organics. Please refer to item 1.1 of the major comments for the revised content.

6. ***P25273, line 13****: Please write what AMS stands for.*

Original:

P25273, line 13

…with the mass fraction of organics measured by an AMS.

Revised:

… with the mass fraction of organics measured using an aerosol mass spectrometer.

7. ***P25273, line 15-21****: "However, because of its higher volatility compared to EC, they were often considered completely evaporated upon heating at temperatures above 300 C in VTDMA studies" contradicts with "It is therefore possible, that a significant amount of non-volatile OC can exist together with EC in ambient aerosol, even after heating in a VTDMA." Clarify what is meant by the former sentence. Also, using "its" and "they" causes some confusion.*

Response:

We apologize for the contradicting sentence. The paragraphs in the introduction are revised. Please refer to item 1.1 in the major comments for the revised content.

8. P25274, section 2.1.2*: The approach to determine the LV/MV/HV aerosol fractions is explained in the end of the section. I suggest that it is explained whenever LV/MV/HV are mentioned for the first time in this section.*

Response:

LV, MV and HV are now defined when the terms first appear. It is also assumed that LV particles represent EC particles externally mixed with volatile materials while MV and HV particles represent EC particles internally mixed with volatile materials.

Original:

Section 2.1.2, P25275 line 8 onwards

Upon heating at 100 ℃ and above, volatile components of particles such as sulfate, nitrate and volatile organics would vaporize at different temperatures depending on their volatilities.

Revised:

Upon heating at 100 ℃ and above, volatile components of particles such as sulfate, nitrate and volatile organics would vaporize at different temperatures depending on their volatilities. A volatility shrinkage factor, *VSF*, is defined as the ratio of particle diameter after heating at temperature *T*, $D_{p,T}$, to that before heating, D_0, to indicate the size reduction of the ambient particles (Eq. (1)). The value of *VSF* is always smaller than or equal to one, depending on the amount of volatile materials vaporized at the heating temperature *T*.

$$VSF(T) = \frac{D_{p,T}}{D_0} \quad (1)$$

The *VSF* is also used to divide the particles into three groups, namely the low volatility (LV), medium volatility (MV) and high volatility (HV) particles. In this study, we focus on the measurements made at 300 ℃. The *VSF* ranges for LV, MV and HV particles upon heating at 300 ℃ are above 0.9, between 0.4 and 0.9 and below 0.4, respectively (Fig. 2) (Wehner et al., 2004; Wehner et al., 2009). The LV particles are assumed to represent EC particles externally mixed with the volatile materials, while MV and HV particles are assumed to represent EC particles internally mixed with volatile materials. While the volatile materials in the MV and HV particles are referred to as VM, those exist as external mixtures with the LV, MV and HV particles are referred to as completely vaporized (CV) particles. The CV particles evaporate completely without leaving behind any residuals at 300 ℃.

9. ***P25275, l 5-7:*** *Please provide the residence time in your heating unit as well as the time after the heating unit but before being sampling by the CPC as mentioned above.*

Response:

Please refer to item 8 in the major comments.

10. ***P25275, l 13-15****: The complete run took around two hours, during which the chemical composition of ambient aerosols might vary a lot, especially related to traffic emissions. Can this be added into your discussion part?*

Response:

The chemical composition of ambient aerosols might vary a lot in two hours. However, the campaign lasted for about two months, and clear diurnal patterns were observed. The variations in aerosol compositions within a two-hour span are likely not affect any of our conclusions.

Furthermore, although a complete run took around two hours, the sampling time at each set temperature (25 ℃, 100 ℃ and 300 ℃) only took about half an hour. SMPS scans were made between each temperature. A sentence is added for clarification.

Original:

P25275, l 13-15

Overall it took around one and a half to two hours to complete a cycle of measurements which consisted of SMPS scans and V-Mode measurements at 25, 100 and 300 ℃.

Revised:

Overall it took around one and a half to two hours to complete a cycle of measurements which consisted of SMPS scans and V-Mode measurements at 25, 100 and 300 ℃. At each temperature, the sampling time for the six selected diameters from DMA_1 (40 nm, 80 nm, 110 nm, 150 nm, 200 nm and 300 nm) took about half an hour and SMPS scans were made in-between.

11. P25275, l 24-25*: This is based on the assumptions that diffusion losses are neglected.*

Response:

Yes. The sentence is modified with a mention of this assumption.

Original:

P25275, l 24-25

Evaporation of VM and CV does not change the number concentrations of LV, MV and HV particles.

Revised:

Excluding particle diffusional and thermophoretic losses, the evaporation of VM and CV does not change the number concentrations of LV, MV and HV particles.

12. P25276, l 1-4*: VSF is depending on chemical composition of your particles, but also depending on which temperature you are using in your measurement. The definition regarding to LV, MV and HV is not valid without giving the temperature you are using for the number size distribution (Fig. 2) after heating. Also for Fig. 2, please explain VSF in the figure caption. Figure 2 is referred in the text prior to introducing VSF.*

Response:

The description is revised to emphasize the fact that the analysis was performed on data collected at 300 ℃. The definition of *VSF* is moved to the earlier part of Section 2.1.2. It is now introduced before the reference to Figure 2 is made. Please refer to item 3.1 in the major comments and item 8 in minor comments for the revised methodology.

Original:

P25292, Fig. 2, Caption

Examples of particle size distributions of (left) ambient aerosols before entering DMA_1 and (right) residuals of the size-selected particles (D_0) after heating. The left and right distributions correspond to (1) and (2) in Fig. 1 respectively. Residuals are divided into several groups—LV (blue), MV (green) and HV (red)—based on their volatilities.

Revised:

Examples of particle size distributions of (a) ambient aerosols before entering DMA_1 and (b) residuals of the size-selected particles (D_0) after heating at 300 ℃. The distributions in Fig. 2a and 2b correspond to (1) and (2) in Fig. 1 respectively. The residuals are divided into three groups—LV (blue), MV (green) and HV (red)—based on their *VSF*.

13. P25276, l 8-14*: Should this part be moved to either introduction part or discussion section? It is more relevant to general picture about volatility.*

Response:

In the revised introduction, the possible volatile and non-volatile materials at 300 ℃ are discussed. This part is thus removed from the methodology section. Please refer to item 1.1 in the major comments for the revised content.

14. P25276, l 12*: Provide references here please.*

Response:

The sentence is removed while it is revised in the introduction.

15. P25276, l 21-22*: Please add references here.*

Response:

The sentence is revised with more information added for a better description of OC_1 to OC_4.

Original:

P 25276, line 19 – 22

"The OC/EC Analyzer adopts the ACE-Asia protocol (a NIOSH-derived protocol), where OC evaporates at four set temperatures of 310, 475, 615 and 870 ℃, and EC is combusted at temperature above 550 ℃ (Schauer et al., 2003). Based on volatility and refractoriness, the OC contents are named OC_1 to OC_4 with OC_1 being most volatile"

Revised:

The OC/EC analyzer adopts the ACE-Asia protocol (a NIOSH-derived protocol), where OC evaporates at four set temperatures of 310, 475, 615 and 870 ℃ with pure helium (He) as the carrier gas, and EC is combusted at temperatures between 550 ℃ and 870 ℃ under He and 2% oxygen (O_2, Schauer et al., 2003, Wu et al., 2012). The OC contents are named OC_1 to OC_4 based on the temperature protocol of the OC/EC analyzer (Table R2). The mass of EC determined at different temperatures will be grouped together for discussions.

Table R2. Temperature (T) and residence time (RT) protocol of the semi-continuous Sunset OC/EC analyzer (Wu et al., 2012)

Carbon Fraction	Carrier Gas	T (℃)	RT (s)
OC_1	He	310	80
OC_2		475	60
OC_3		615	60
OC_4		870	90
EC_1	He + 2% O_2	550	45
EC_2		625	45
EC_3		700	45
EC_4		775	45
EC_5		850	45
EC_6		870	45

16. P25277, l 4*: Which section, please clarify.*

Response:

It should be Section 3.1 Overview. The average volume fraction of HV residuals only contributed to less than 1% of the total volume (P25282 of the original manuscript, lines 9-10). The sentence on P25277 is revised.

Original:

P25277, l 4

We have ignored the HV residuals as their contributions are insignificant when compared to LV and MV residuals (see later).

Revised:

We have ignored the HV residuals as their contributions to the total volume of the particles are insignificant when compared to the contributions of the LV and MV residuals (Section 3.1).

***17. P25277, l 8**: I don't agree it is the number fraction of LV, MV and HV residuals, but rather the number fraction of particles containing LV, MV and HV materials.*

Response:

The number fractions of LV, MV and HV residuals (after accounting for corrections with CV particles and diffusional and thermophoretic losses) should be the same as the number fractions of LV, MV and HV particles before heating. However, we understand that in many studies number fraction is used for LV, MV and HV particles. In the revised manuscript, we will only use "number fractions of LV, MV and HV residuals ($\Phi'_{N,LV}$, $\Phi'_{N,MV}$ and $\Phi'_{N,HV}$, with their sum being equal to unity)" to represent the measured values before any correction with CV particles and diffusional and thermophoretic losses.

Original:

P25277, l 8 onwards:

The number fractions of LV, MV and HV residuals ($\Phi'_{N,LV}$, $\Phi'_{N,MV}$ and $\Phi'_{N,HV}$, with their sum equals unity) in Stream 2 on Fig. 1 were obtained from $dN'/dlogD_p$ measured by the CPC. However, these fractions are not the actual number fractions of LV, MV and HV residuals ($\Phi_{N,LV}$, $\Phi_{N,MV}$ and $\Phi_{N,HV}$) of the selected particles before heating because they have not taken into account the CV particles and particle diffusional and thermophoretic losses.

Revised:

The number fractions of LV, MV and HV residuals ($\Phi'_{N,LV}$, $\Phi'_{N,MV}$ and $\Phi'_{N,HV}$, with their sum being equal to unity) in Stream 2 in Fig. 1 were obtained from $dN'/dlogD_p$ measured with the CPC. However, these fractions do not represent the actual number fractions of LV, MV and HV particles ($\Phi_{N,LV}$, $\Phi_{N,MV}$ and $\Phi_{N,HV}$) before heating because they have not taken into account the CV particles and particle diffusional and thermophoretic losses.

18. P25277, l 20-23*: it will be good to provide a calibration curve or transmission curve from NaCl.*

Response:

A figure of the transport efficiency of NaCl in the VTDMA is added to the supplementary information as Figure S2 (Fig. R11). A note is added in the methodology section.

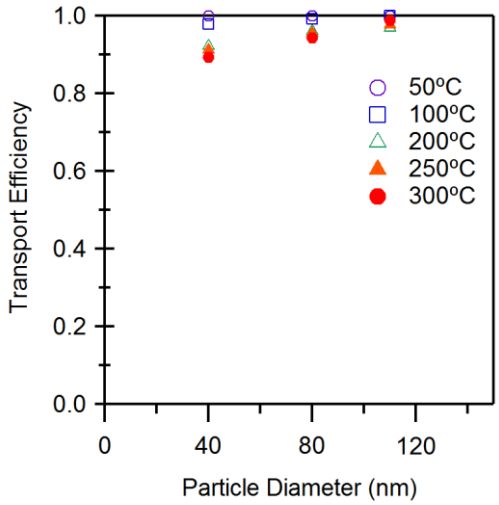

Fig. R11. Transport efficiency of NaCl in the VTDMA as a function of particle diameter and heating temperature.

Revised:

P25277 l20-23

…was determined by laboratory calibrations with sodium chloride (NaCl) particles, which do not evaporate (i.e. $\Phi_{N,CV} = 0$) at the temperatures used in our experiments. The transmission efficiency of NaCl of several selected diameters heated at temperatures between 50 ℃ and 300 ℃ is provided in the supplemental information (Fig. S2).

19. P25279, l 5*: We use VFR (volume fraction remaining) conventionally here to define the ratio between the volume of the residuals and the host particles; please consider changing it.*

Response:

We have changed the term to *VFR*. Changes are made in both the methodology and results sections.

Original:

P25279 l3-5:

Furthermore, we define the volume ratio if the residuals to their host particles for MV and HV ($\Theta_{V,\mathrm{MV}}$ and $\Theta_{V,\mathrm{HV}}$) for our discussions later:

$$\Theta_{V,\mathrm{i}} = \frac{N_i \times \frac{\pi}{6} D_{p,i}^3}{N_i \times \frac{\pi}{6} D_0^3} = \frac{D_{p,i}^3}{D_0^3} \quad (6)$$

Revised:

Furthermore, we also calculated the volume fraction remaining (*VFR*), defined as the volume ratio of the residual to its host particle, to aid our discussions later:

$$VFR_i = \frac{N_i \times \frac{\pi}{6} D_{p,i}^3}{N_i \times \frac{\pi}{6} D_0^3} = \frac{D_{p,i}^3}{D_0^3} \quad (6)$$

20. P25280, l 14-15*: Could the reason be due to the detection limit of the CPC as mentioned above?*

Response:

Yes it is a possibility. Please refer to item 7 in the major comments.

21. P25280, l 20*: What kind of atmospheric processes could be? Please clarify.*

Response:

The discussion on the lack of size dependence of number and volume fractions is moved to section 3.2 diurnal variations of the revised manuscript. The diurnal variations for particles larger than 80 nm were found much less obvious than those for 40 nm particles in this study and in others (Fig. R6) (Rose et al., 2011; Cheng et al., 2012; Zhang et al., 2016). In winter, the atmosphere is more stable, resulting in a poorer dilution of aged particles with the less polluted aerosols from higher up (Rose et al., 2006). When the aged pollutants were trapped near the ground surface, the effect of aging of fresh emissions weakened. The information is included in section 3.2 of the revised manuscript.

On the other hand, most of the air masses arriving at the site traveled at low altitudes (below 1500 m) for over 40 h (Fig. R8). The aerosols in these air masses contained mainly MV and HV particles and were likely to be well-aged. When they mixed with local pollutants, the size dependence of the number fractions of the volatility groups was further reduced. Details are given in the trajectory analysis in item 1.2 of the major comments.

Original:

P25280, l 20:

The lack of size dependence of number fractions for particles larger than 80 nm suggests that they may be the result of similar atmospheric processes.

Revised:

Section 3.2 Diurnal variation of the revised manuscript:

The diurnal variations for particles larger than 80 nm were much less obvious than those for 40 nm particles in this study and in others (Rose et al., 2011, Cheng et al., 2012, Zhang et al., 2016). In winter, the atmosphere is more stable, resulting in a poorer dilution of aged particles with the less polluted aerosols from higher up (Rose et al., 2006). When the aged pollutants were trapped near the ground surface, the effect of aging of fresh emissions weakened. Therefore, although a daily maximum and a daily minimum were still observed for particles larger than 80 nm, the variation was mostly within 15%.

22. P25280, l 23*: I don't agree with this, please rephrase the sentence.*

Response:

The whole sentence is rewritten for a proper explanation.

Original:

P25280, l 20:

The large fraction of CV in 40 nm particles is likely due to nucleation of fresh emissions from more volatile primary sources or volatile secondary pollutants.

Revised:

As in Rose et al. (2006), fresh emissions like soot adsorbed or absorbed volatile materials during atmospheric processing. Smaller particles grew to a greater extent than the larger ones because of their higher ratios of surface area to volume. When they were heated in the VTDMA at 300 ℃, these smaller particles reduced more substantially in size, as reflected in the higher CV and HV fractions and lower MV and LV fractions.

23. P25280, l 24-25*: Please add appropriate references.*

Response:

The sentence here is combined with the sentence in the next comment and revised for a more coherent discussion with references added.

Original:

P25280, l 24-25

Freshly emitted non-volatile primary sources such as EC and OC are in a larger size range.

P25281, l 1-3

Yu et al. (2010) reported that the mass median aerodynamic diameter of urban EC in the condensation mode in Guangzhou is about 380 nm.

Revised:

Yu et al. (2010) reported that the condensation and droplet modes of EC and OC in urban sites of Guangzhou were approximately 400 nm and 900 nm, respectively. The mode of fresh EC emitted from vehicles is also approximately 400 nm (Huang et al., 2006).

24. P25281, l 1-3*: The sentence is not clearly written; please rephrase it.*

Response:

Please refer to the comment above (item 23).

25. P25281, l 10-12*: How do you define polluted days? Please clarify. Also, please add references here.*

Response:

The whole description was rewritten for a proper explanation.

Original:

N_{MV} tracks reasonably well with $PM_{2.5}$ mass because of its dominance in the number concentrations. Internally mixed soot particles, manifested as MV particles, play an important role in Guangzhou, especially during polluted days.

Revised:

The temporal variation of the number concentration of MV particles having an initial diameter of 80 nm or above tracked reasonably well with the accumulation of $PM_{2.5}$ as particles aged and became more internally mixed. Furthermore, a size dependence was observed for 80 nm to 300 nm MV particles. There were days, e.g., from Feb 24 to Mar 10, when the number concentration of 300 nm MV particles did not track well with $PM_{2.5.}$ The mode of total particle number size distribution was below 100 nm and the number concentrations of 300 nm particles were low (Fig. R12). $PM_{2.5}$ tracked better with the number concentrations of 80 nm to 150 nm MV particles (Fig. R12a to R12c) than those of 200 nm to 300 nm MV particles (Fig. R12d and R12e).

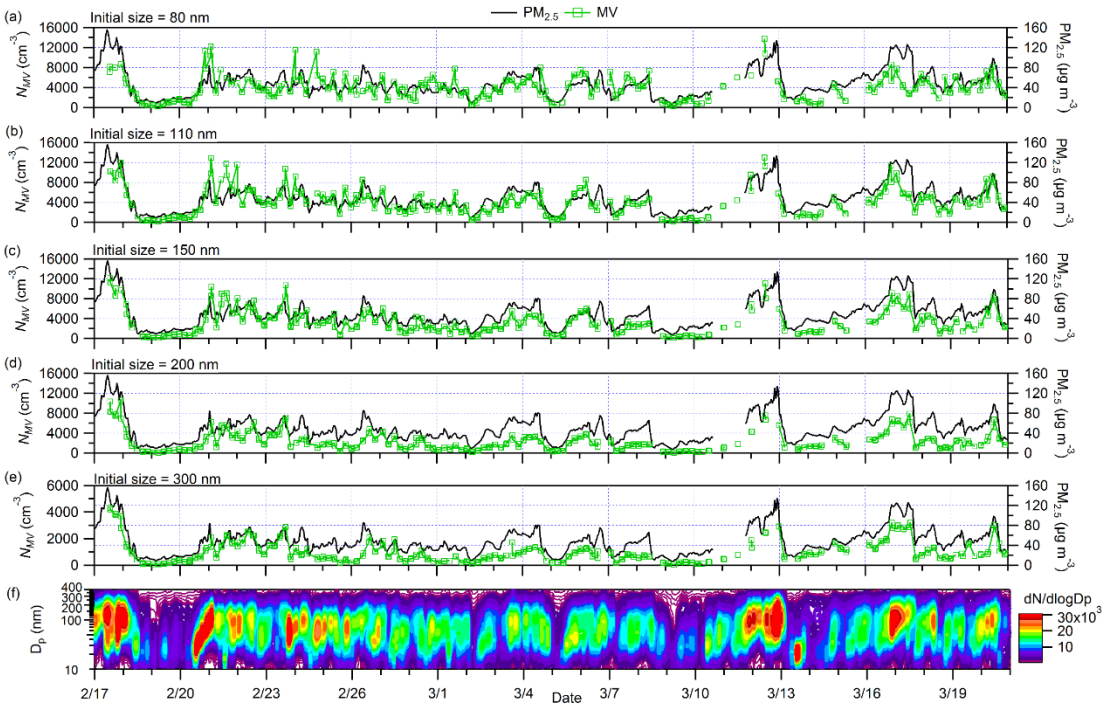

Fig. R12. (a–e) Time series of number concentrations of MV particles having initial diameters of 80 nm to 300 nm and (f) particle number size distributions during the campaign. Time series of $PM_{2.5}$ concentrations are plotted on the right axis in (a) to (e).

26. P25282, l 1-3*: The logics behind are not clear here; please rephrase the sentence.*

Response:

Please refer to item 21 for the revised content.

27. P25282, l 10-13*: Please consider rewriting it.*

Response:

The sentence is removed when the overall discussion of number and volume fractions is rewritten for simplicity and clarity.

28. P25282*: Please add error bars in Fig. 5 and Fig. 7.*

Response:

The number and volume fractions of different groups are plotted separately after adding the error bars (Fig. R13 and R14). Since their diurnal patterns were similar, we only add the diurnal patterns of volume fractions of 40 nm, 150 nm and 300 nm particles in the revised manuscript (Fig. R6).

Original:

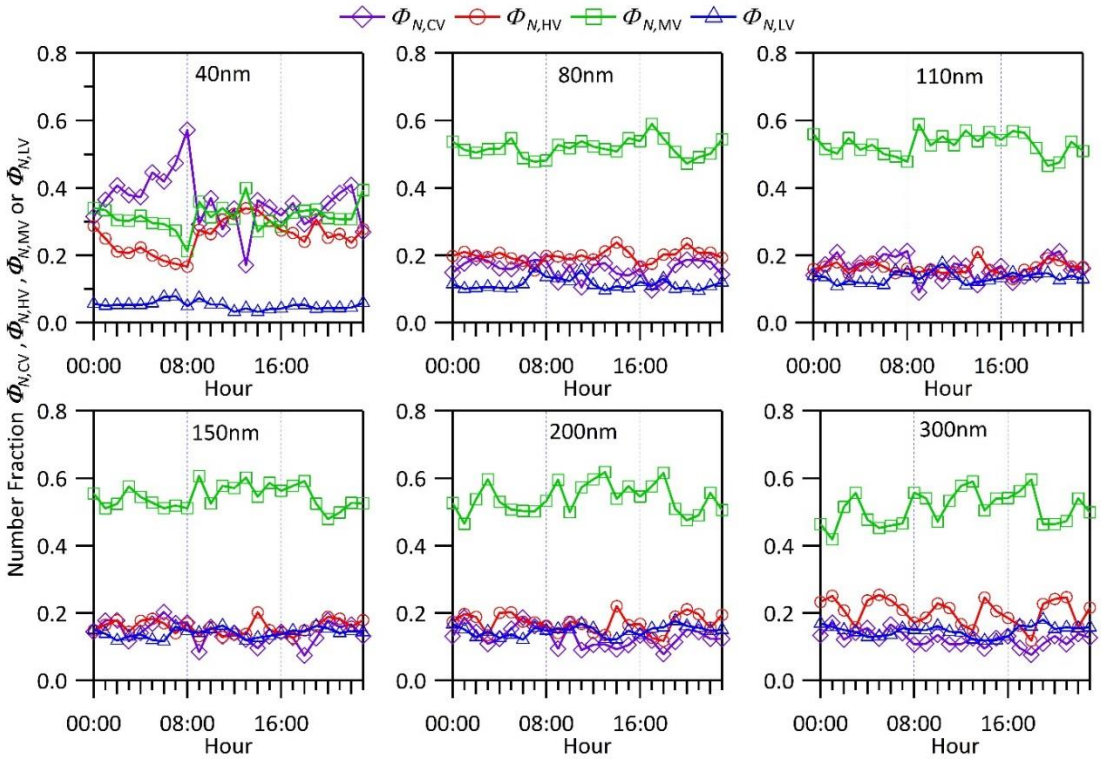

Fig. 5 (original manuscript). Diurnal variations in the number fractions of CV (diamond (purple)), HV (circle (red)), MV (square (green)) and LV (triangle (blue)) particles that are 40 nm, 80 nm, 110 nm, 150 nm, 200 nm and 300 nm in dry size.

Revised:

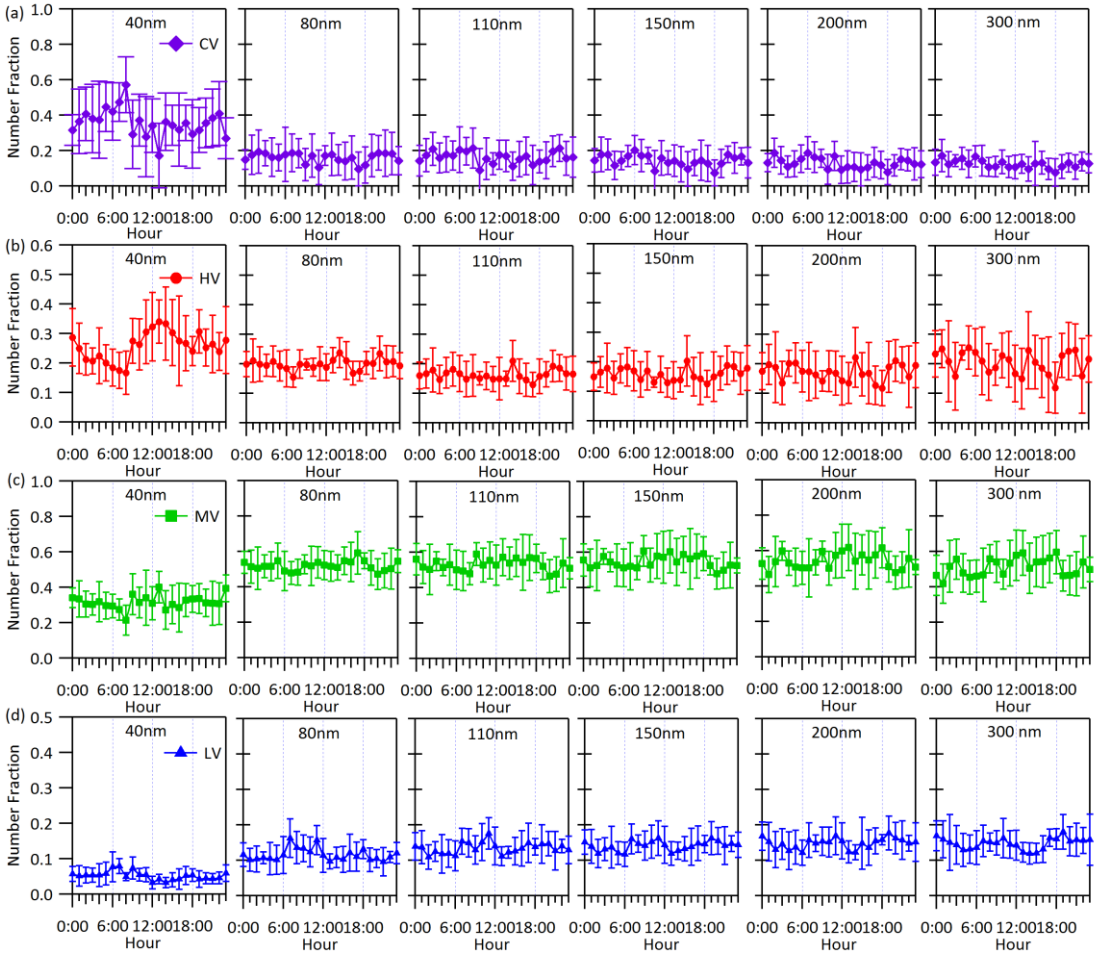

Fig. R13. (a–d) Diurnal variations in the number fractions of CV, HV, MV and LV particles having (from left to right) the six selected diameters ranging from 40 nm to 300 nm. Error bars represent one standard deviation.

Original:

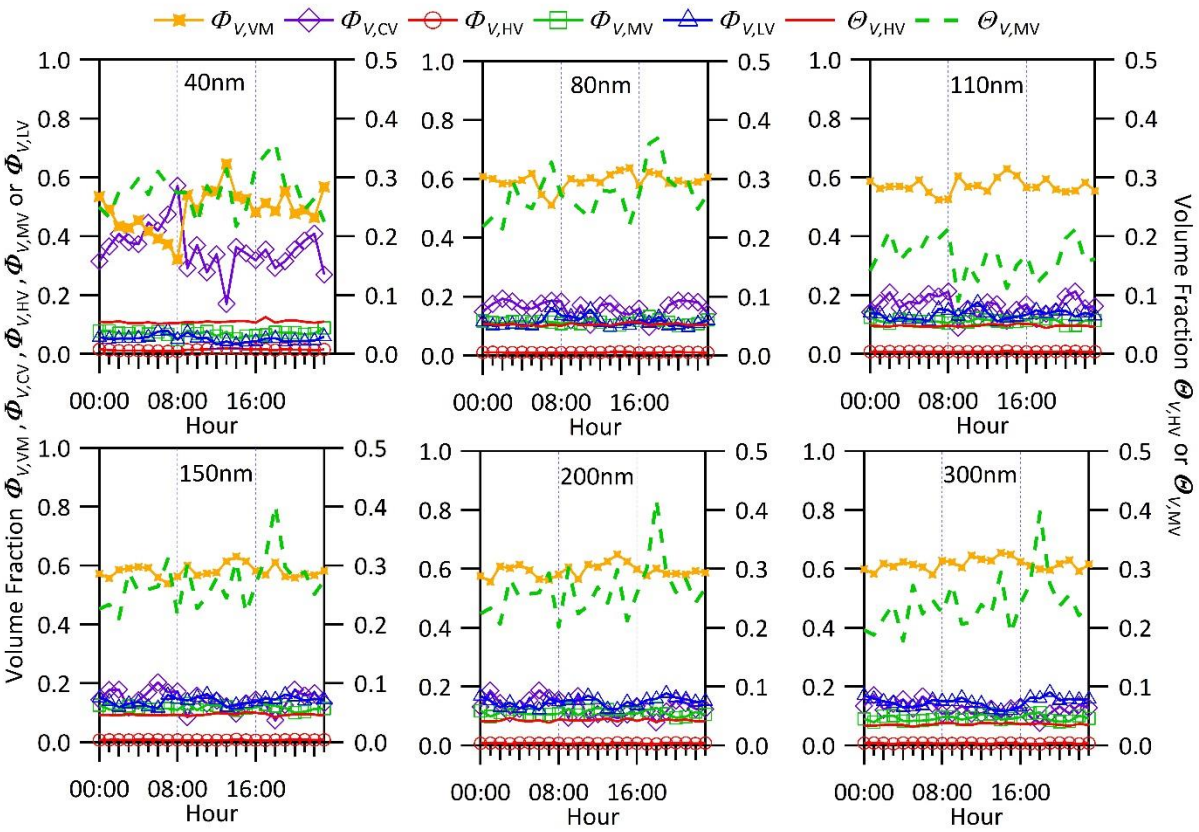

Fig. 7 (original manuscript). Diurnal variation in (left axis) $\Phi_{V,VM}$ (cross (orange)), $\Phi_{V,CV}$ (diamond (purple)), $\Phi_{V,HV}$ (circle (red)), $\Phi_{V,MV}$ (square (green)), $\Phi_{V,LV}$ (triangle (blue)), (right axis) $\Theta_{V,HV}$ (solid line (red)) and $\Theta_{V,MV}$ (dashed line (green)) particles that are 40 nm, 80 nm, 110 nm, 150 nm, 200 nm and 300 nm in dry size.

Revised:

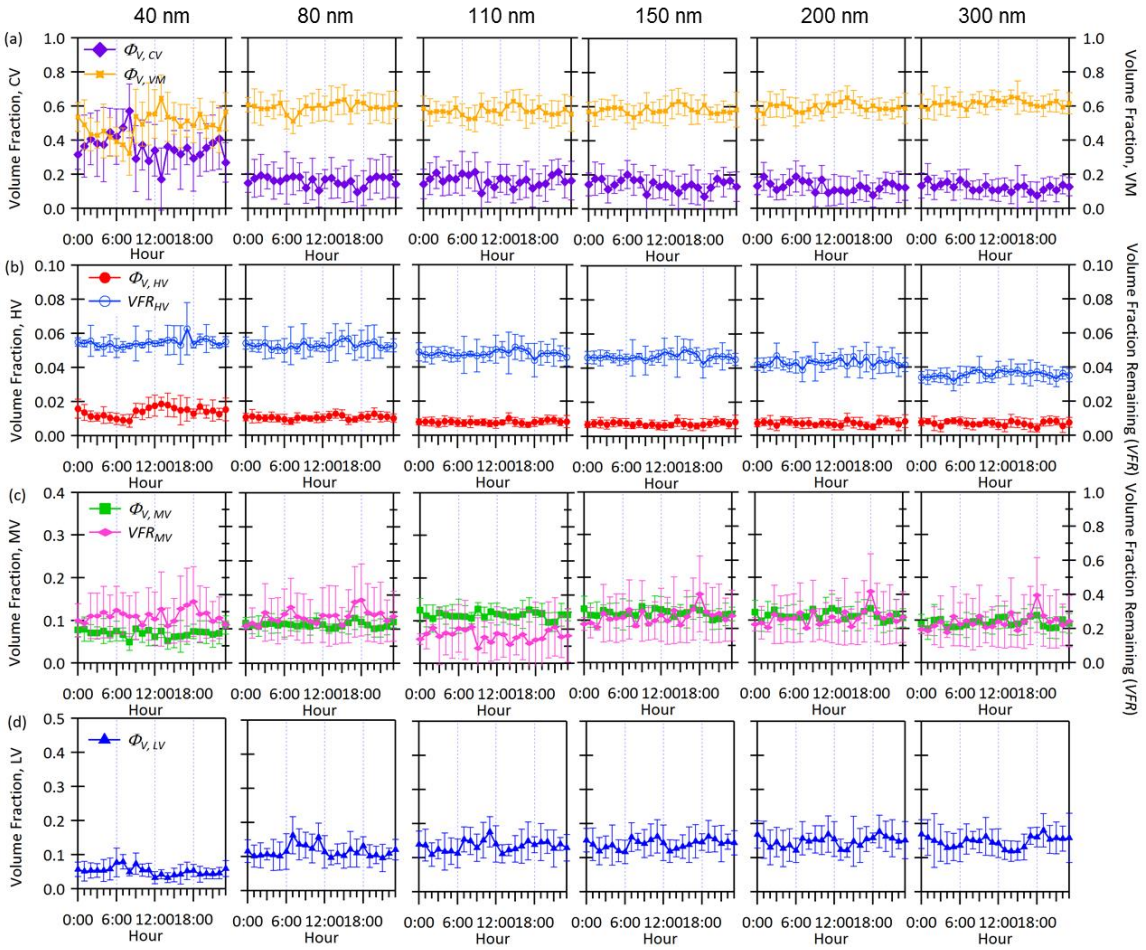

Fig. R14. (a–d) Diurnal variations in the volume fractions of CV particles, VM, HV residuals, MV residuals and LV residuals having the diameters of (from left to right) the six selected diameters ranging from 40 nm to 300 nm. Diurnal variations in the volume fraction remaining (*VFR*) of HV and MV are plotted on the right axis. Error bars represent one standard deviation.

29. P25282, l 19-21*: What does the number concentration of MV+HV mean? Do you mean number concentration of particles containing MV+HV materials or what you wrote 'MV+HV residuals' at other part? Please rephrase the sentence. This kind of confusing statement is elsewhere along the text; please check the language before writing them into the text.*

Response:

We mean the number concentration of MV and HV particles, i.e., particles containing a larger fraction of volatile materials. Similar notations in Section 3.3 such as "EC + OC_{2-4}" and "LV + MV" are all replaced by "the sum of EC, OC_2, OC_3 and OC_4" and "the total of LV and MV residuals". We apologize for the mistake and the confusing statements.

30. P25282, l 24-28*: The sentence is too long; please try to make the statement clear in short sentences.*

Response:

The sentence and the analysis are rewritten. We have also taken the reviewer's suggestion to use the more commonly used term "volume fraction remaining (*VFR*)" for the volume ratio of the residual to its host particle instead of $\Theta_{V,MV}$ and $\Theta_{V,HV}$.

Original:

P25282, l 24-28

There was no obvious diurnal variation of $\Theta_{V,MV}$ and $\Theta_{V,HV}$ for all sizes (except for a minor peak at about 06:00 p.m. for $\Theta_{V,MV}$, which may be related to traffic), even for 40 nm particles where there is an obvious diurnal trend of $\Phi_{V,VM}$, which is the volume ratio of volatile materials internally mixed with non-volatile components to total volume before heating.

Revised:

We also used the diurnal variations in the volume fraction remaining (*VFR*), again defined as the volume ratio of the residual to its *host* particle (not to the total volume of all particles), to examine the size changes of the non-volatile residuals of HV and MV particles (Fig. R6). The *VFR* of HV did not exhibit any obvious diurnal variations but the *VFR* of MV peaked near 18:00. The *VFR* of 40nm MV particles increased after 14:00 while those of 150 nm and 300 nm MV particles increased after 15:00.

***31. P25283**, section 3.3: When you use extrapolation fitting the number size distribution of 300 nm particles to 5 um particles, you have to either assume the number size distribution is constant along the time or their mixing state is constant along different sizes. This did not reduce the uncertainties when comparing VTDMA results with OC/EC results. Please add appropriate discussions on the possible chemical composition within the size gap or refer to other studies.*

Response:

When we conducted the extrapolation fitting, it was for the six diameters (from 40 nm to 300 nm) selected in each measurement cycle. We therefore only assumed that the mixing state or the size distributions of each of LV, MV or HV followed log-normal distributions.

Nevertheless, we agree with the reviewer that while the VTDMA measured the size distribution of particles between 10 and 400 nm in diameter, the OC/EC analyzer took into account particles up to 2.5 μm in diameter. Yu et al. (2010) reported three EC and OC modes between 0.4 μm and 10 μm in ambient aerosols in Guangzhou: 0.4, 0.9 and 5 μm. The 0.4 μm mode accounted for 44% to 49% of the measured EC but only 17% to 20% of the measured OC. A discussion is added to the manuscript.

Original:

P25283 l 20 onwards:

The extrapolated lognormal fitting of the size distribution of non-volatile particles can cause errors if the mode diameter of the fitting is beyond the range of measurements of the VTDMA.

Revised:

The extrapolated lognormal fitting of the size distribution of non-volatile particles can also cause errors if the mode diameter of the fitting is beyond the VTDMA's range of measurements. While the VTDMA measured the size distribution of particles between 10 and 400 nm in diameter, the OC/EC analyzer took into account particles up to 2.5 μm in diameter. Yu et al. (2010) reported three EC and OC modes between 0.4 μm and 10 μm in ambient aerosols in Guangzhou: 0.4, 0.9 and 5 μm. The 0.4 μm mode accounted for 44% to 49% of the measured EC but only 17% to 20% of the measured OC.

***32. P25283, l 19**: What kind of errors could be related to the measurements; please clarify.*

Response:

The discussion of the presence of oxygen in the VTDMA on P25283, l 25-27 has been moved up to l 19 as a possible source of error in the measurement.

Original:

P25283, l 19

…The presence of other refractory materials, as well as errors during the measurements, could also be a reason for the difference.

Original:

P25283, l 25-27

In the VTDMA, aerosols were heated in the presence of oxygen, while in the OC/EC Analyzer, samples were heated in the presence of helium for OC. In the presence of oxygen, it is possible that $OC_{2\text{-}4}$ in the aerosols may have evaporated in the VTDMA even at 300 ℃.

Revised:

…The presence of other refractory materials and the assumption made about the density of LV and MV are two other possible explanations.

Other possible errors for the closure could be related to the different heating environments in the VTDMA and the OC/EC analyzer. In the OC/EC analyzer, OC was measured when the samples were heated in the presence of a non-oxidative carrier gas (He). In the VTDMA, aerosols were heated in air which contained O_2. Therefore, some "$OC_{2\text{-}4}$" that evaporated at 475 ℃ or above in the OC/EC analyzer may have been oxidized at 300 ℃ in the VTDMA. Charring of organic matter could also occur (Philippin et al., 2004).

33. P25283, l 25-27*: Do you mean oxidation might take place in the presence of oxygen? Please rephrase the sentence and add references there.*

Response:

Yes. The content is revised with the comment above (item 32).

34. P25283, l 13-15*: What does 'that LV and MV may contain non-volatile OC' mean? Do you mean LV+MV residuals contain non-volatile OC?*

Response:

We mean both LV and MV residuals contain non-volatile OC. In the VTDMA, all the residuals (HV, MV and LV residuals) were non-volatile upon heating at 300 ℃. We cannot assume that non-volatile OC would only be present in MV residuals while EC is only present in LV residuals. All the terms using "LV+MV" are replaced by "the total mass of LV and MV" to avoid confusion. The sentence is also revised.

Original:

P25283, L13-15

Including non-volatile OC give better mass closure for LV+MV and this observation supports our initial postulation that LV and MV may contain non-volatile OC.

Revised:

Including non-volatile OC (sum of OC_2 to OC_4) gives better mass closure with the total mass of LV and MV. This further supports our initial postulation that the non-volatile residuals which remained intact upon heating at 300 ℃ in the VTDMA may contain a significant amount of non-volatile OC.

***35. P25284**, Section 4: I did not get a clear picture that what the authors want to conclude for the manuscript. Please consider revising it.*

Response:

The section is rewritten.

Revised:

This study presents the first VTDMA measurements in a suburban area of Guangzhou in the Pearl River Delta, China during wintertime. The LV fraction was assumed to be EC particles. These particles were externally mixed with volatile materials at 300 ℃ and contributed to less than 20% of the total particle number concentration at the sampling site. The diurnal variations in the number and volume fractions of LV, MV and HV were much less obvious in this study than in other studies, likely because of the more stable atmosphere and poorer dilution of aged aerosols in winter. Back trajectory analysis showed that the measured $PM_{2.5}$, EC and OC concentrations were higher when the sampling site came under the influence of maritime and coastal air masses originating from the east or northeast of the site. These observations are attributed to the high pressure system on the continent, the prevailing northerly wind and the enhanced pollution from north China in winter. Long-range transport continental trajectories were often associated with the cold front periods during which the dispersion of pollutants was promoted. The number fractions of LV, MV and HV particles did not show much variations among the clusters, likely because the air masses in all clusters were transported at low altitudes (below 1500 m) for over 40 h. They were therefore well-aged upon arrival at the site.

While previous studies have demonstrated soot as a major component of the non-volatile residuals at 300 ℃ measured by the VTDMA, this work identified non-volatile organics as another possible component. The diurnal variations in the LV fractions and the size of the MV residuals may be related to the variation in the abundance of both EC and non-volatile OC, which evaporated at 475 ℃ and above in the OC/EC analyzer. Analyses of the diurnal variations in the LV fractions and the *VFR* of MV particles, the latter of which reflects the change in size of the non-volatile materials in the MV particles, suggest that the increase in non-volatile fractions and size in the early

afternoon may be related to the increase in non-volatile OC in addition to the effects of EC coagulation and condensation. The mass closure analysis of EC and non-volatile OC and the total mass of LV and MV residuals also suggest that non-volatile OC may have contributed to non-volatile residuals in our VTDMA measurements.

References

Bradsher, K.: http://www.nytimes.com/2007/12/08/world/asia/08trucks.html, 2007.

Brooks, B. J., Smith, M. H., Hill, M. K., and O'Dowd, C. D.: Size-differentiated volatility analysis of internally mixed laboratory-generated aerosol, Journal of Aerosol Science, 33, 555-579, 2002.

Chen, B., Du, K., Wang, Y., Chen, J., Zhao, J., Wang, K., Zhang, F., and Xu, L.: Emission and transport of carbonaceous aerosols in urbanized coastal areas in China, 2012. 2012.

Cheng, Y. F., Eichler, H., Wiedensohler, A., Heintzenberg, J., Zhang, Y. H., Hu, M., Herrmann, H., Zeng, L. M., Liu, S., Gnauk, T., Brüggemann, E., and He, L. Y.: Mixing state of elemental carbon and non-light-absorbing aerosol components derived from in situ particle optical properties at Xinken in Pearl River Delta of China, Journal of Geophysical Research: Atmospheres, 111, D20204, 2006.

Cheng, Y. F., Su, H., Rose, D., Gunthe, S. S., Berghof, M., Wehner, B., Achtert, P., Nowak, A., Takegawa, N., Kondo, Y., Shiraiwa, M., Gong, Y. G., Shao, M., Hu, M., Zhu, T., Zhang, Y. H., Carmichael, G. R., Wiedensohler, A., Andreae, M. O., and Pöschl, U.: Size-resolved measurement of the mixing state of soot in the megacity Beijing, China: diurnal cycle, aging and parameterization, Atmos. Chem. Phys., 12, 4477-4491, 2012.

Chow, J. C., Watson, J. G., Lu, Z., Lowenthal, D. H., Frazier, C. A., Solomon, P. A., Thuillier, R. H., and Magliano, K.: Descriptive analysis of PM2.5 and PM10 at regionally representative locations during SJVAQS/AUSPEX, Atmos. Environ., 30, 2079-2112, 1996.

Donahue, N. M., Robinson, A. L., and Pandis, S. N.: Atmospheric organic particulate matter: From smoke to secondary organic aerosol, Atmospheric Environment, 43, 94-106, 2009.

Frey, A., Rose, D., Wehner, B., Müller, T., Cheng, Y., Wiedensohler, A., and Virkkula, A.: Application of the Volatility-TDMA Technique to Determine the Number Size Distribution and Mass Concentration of Less Volatile Particles, Aerosol Science and Technology, 42, 817-828, 2008.

Gu, J., Du, S., Han, D., Hou, L., Yi, J., Xu, J., Liu, G., Han, B., Yang, G., and Bai, Z.-P.: Major chemical compositions, possible sources, and mass closure analysis of PM2.5 in Jinan, China, Air Quality, Atmosphere & Health, 7, 251-262, 2014.

Huang, X.-F., Yu, J. Z., He, L.-Y., and Hu, M.: Size Distribution Characteristics of Elemental Carbon Emitted from Chinese Vehicles: Results of a Tunnel Study and Atmospheric Implications, Environmental Science & Technology, 40, 5355-5360, 2006.

Huffman, J. A., Docherty, K. S., Aiken, A. C., Cubison, M. J., Ulbrich, I. M., DeCarlo, P. F., Sueper, D., Jayne, J. T., Worsnop, D. R., Ziemann, P. J., and Jimenez, J. L.: Chemically-resolved aerosol volatility measurements from two megacity field studies, Atmos. Chem. Phys., 9, 7161-7182, 2009.

Kalberer, M., Paulsen, D., Sax, M., Steinbacher, M., Dommen, J., Prevot, A. S. H., Fisseha, R., Weingartner, E., Frankevich, V., Zenobi, R., and Baltensperger, U.: Science, 303, 1659, 2004.

Lee, B. P., Li, Y. J., Yu, J. Z., Louie, P. K. K., and Chan, C. K.: Physical and chemical characterization of ambient aerosol by HR-ToF-AMS at a suburban site in Hong Kong during springtime 2011, Journal of Geophysical Research: Atmospheres, 118, 8625-8639, 2013.

Levy, M. E., Zhang, R., Zheng, J., Tan, H., Wang, Y., Molina, L. T., Takahama, S., Russell, L. M., and Li, G.: Measurements of submicron aerosols at the California–Mexico border during the Cal–Mex 2010 field campaign, Atmos. Environ., 88, 308-319, 2014.

Lo, J. C. F., Lau, A. K. H., Fung, J. C. H., and Chen, F.: Investigation of enhanced cross-city transport and trapping of air pollutants by coastal and urban land-sea breeze circulations, Journal of Geophysical Research: Atmospheres, 111, n/a-n/a, 2006.

Murphy, B. N., Donahue, N. M., Robinson, A. L., and Pandis, S. N.: A naming convention for atmospheric organic aerosol, Atmos. Chem. Phys., 14, 5825-5839, 2014.

Philippin, S., Wiedensohler, A., and Stratmann, F.: Measurements of non-volatile fractions of pollution aerosols with an eight-tube volatility tandem differential mobility analyzer (VTDMA-8), Journal of Aerosol Science, 35, 185-203, 2004.

Pinnick, R., Jennings, S., and Fernandez, G.: Volatility of aerosols in the arid southwestern United States, Journal of the atmospheric sciences, 44, 562-576, 1987.

Rolph, G. D.: Real-time Environmental Applications and Display sYstem (READY) Website (http://www.ready.noaa.gov). NOAA Air Resources Laboratory, College Park, MD., 2016.

Rose, D., Wehner, B., Ketzel, M., Engler, C., Voigtländer, J., Tuch, T., and Wiedensohler, A.: Atmospheric number size distributions of soot particles and estimation of emission factors, Atmos. Chem. Phys., 6, 1021-1031, 2006.

Rose, D., Gunthe, S. S., Su, H., Garland, R. M., Yang, H., Berghof, M., Cheng, Y. F., Wehner, B., Achtert, P., Nowak, A., Wiedensohler, A., Takegawa, N., Kondo, Y., Hu, M., Zhang, Y., Andreae, M. O., and Pöschl, U.: Cloud condensation nuclei in polluted air and biomass burning smoke near the mega-city Guangzhou, China

– Part 2: Size-resolved aerosol chemical composition, diurnal cycles, and externally mixed weakly CCN-active soot particles, Atmos. Chem. Phys., 11, 2817-2836, 2011.

Stein, A. F., Draxler, R. R., Rolph, G. D., Stunder, B. J. B., Cohen, M. D., and Ngan, F.: NOAA's HYSPLIT Atmospheric Transport and Dispersion Modeling System, Bulletin of the American Meteorological Society, 96, 2059-2077, 2015.

Tan, H. B., Yin, Y., Gu, X. S., Li, F., Chan, P. W., Xu, H. B., Deng, X. J., and Wan, Q. L.: An observational study of the hygroscopic properties of aerosols over the Pearl River Delta region, Atmos. Environ., 77, 817-826, 2013.

Tao, J., Zhang, L., Ho, K., Zhang, R., Lin, Z., Zhang, Z., Lin, M., Cao, J., Liu, S., and Wang, G.: Impact of PM2.5 chemical compositions on aerosol light scattering in Guangzhou — the largest megacity in South China, Atmospheric Research, 135–136, 48-58, 2014.

Turpin, B. J., Cary, R. A., and Huntzicker, J. J.: An In Situ, Time-Resolved Analyzer for Aerosol Organic and Elemental Carbon, Aerosol Science and Technology, 12, 161-171, 1990.

Twomey, S.: On the composition of cloud nuclei in the northeastern United States, J. Rech. Atmos, 3, 281-285, 1968.

Villani, P., Picard, D., Marchand*, N., and Laj, P.: Design and Validation of a 6-Volatility Tandem Differential Mobility Analyzer (VTDMA), Aerosol Science and Technology, 41, 898-906, 2007.

Wehner, B., Philippin, S., Wiedensohler, A., Scheer, V., and Vogt, R.: Variability of non-volatile fractions of atmospheric aerosol particles with traffic influence, Atmos. Environ., 38, 6081-6090, 2004.

Wehner, B., Berghof, M., Cheng, Y. F., Achtert, P., Birmili, W., Nowak, A., Wiedensohler, A., Garland, R. M., Pöschl, U., Hu, M., and Zhu, T.: Mixing state of nonvolatile aerosol particle fractions and comparison with light absorption in the polluted Beijing region, Journal of Geophysical Research: Atmospheres, 114, D00G17, 2009.

Wu, C., Ng, W. M., Huang, J. X., Wu, D., and Yu, J. Z.: Determination of Elemental and Organic Carbon in PM2.5 in the Pearl River Delta Region: Inter-Instrument (Sunset vs. DRI Model 2001 Thermal/Optical Carbon Analyzer) and Inter-Protocol Comparisons (IMPROVE vs. ACE-Asia Protocol), Aerosol Science and Technology, 46, 610-621, 2012.

Zhang, S. L., Ma, N., Kecorius, S., Wang, P. C., Hu, M., Wang, Z. B., Größ, J., Wu, Z. J., and Wiedensohler, A.: Mixing state of atmospheric particles over the North China Plain, Atmos. Environ., 125, Part A, 152-164, 2016.

Zhang, Y., Wang, X., Li, G., Yang, W., Huang, Z., Zhang, Z., Huang, X., Deng, W., Liu, T., Huang, Z., and Zhang, Z.: Emission factors of fine particles, carbonaceous aerosols and traces gases from road vehicles: Recent tests in an urban tunnel in the Pearl River Delta, China, Atmos. Environ., 122, 876-884, 2015.

Anonymous Referee #2

Summary

Cheung et al. conducted a set of ambient measurements from which they calculated size dependent volatility shrinkage factors (VSF) of aerosols in Guangzhou after heating to 300°C in a tandem differential mobility analyzer. Size-selected particles ranging from D_m = 40 to 300 nm were examined. Mass concentrations of OC and EC were also measured. Particles were classified as "completely volatile" (CV; VSF ~ 0), "high volatility" (HV; VSF< 0.4), "medium volatility" (MV; 0.4<VSF< 0.9) and "low volatility" (LV; VSF > 0.9). Three primary results are reported: (1) the number and volume fraction of CV particles decreases with increasing particle size, while the LV particle number and volume fractions increase with increasing diameter (2) size-resolved measurements combined with average diurnal patterns suggest that 40 nm CV and LV particles represent local, fresh emissions, whereas >80 nm HV and MV particles represent aged emissions. (3) A closure analysis of VHTDMA and OC/EC analyzer measurements suggests that organics comprise a significant fraction of the measured MV and LV. Overall, the results are interesting, but I suggest additional analysis of the data before I would support publication in ACP. In particular, I think it would be useful to present more of the OC/EC results to assist with, and expand on, the interpretation of the VHTDMA measurements.

Main Comments

1. *In my opinion, the closure analysis -- which currently focuses on a comparison of EC + OC2 + OC3 + OC4 versus LV + MV – is incomplete. The volatility resolved VHTMDA and OC/EC analyzer measurements should in principle allow for a more comprehensive closure/inter comparison study. Because the volatility fractions in both instruments are affected by the specific operation conditions, I think expanding on this subject in Section 3.3 would be interesting and possibly help with the interpretation of the VHTDMA measurements. I suggest that this subject be a major focus of a revised manuscript. For example:*
    a) *CV versus OC1*
    b) *HV versus OC1 and/or OC2*
    c) *MV and OC2 and/or OC3*

2. *I think the authors should plot and discuss campaign-average mass fractions of OC1, OC2, OC3, OC4 and EC to accompany the volume fractions of VM, CV, HV, MV and LV that are presented in Figure 6 and related discussion.*

3. *Similarly, the authors could plot time series and diurnal patterns of OC1, OC2, OC3, OC4 and EC mass fractions as is done in Figure 7 and related discussion of the volume fractions of VM, CV, HV, MV and LV.*

Response:

We thank the reviewer for the useful comments. Below please find our response to each of the points above. Major changes to the manuscript are shown in blue.

We have added the following new results in conjunction with the discussions of the VTDMA results:

v) Time series and diurnal variations in OC and EC concentrations;

vi) Meteorological conditions including wind speed, wind direction, temperature, and relative humidity;

vii) Particle number size distribution from the SMPS; and

viii) Back trajectory analysis

With the addition of the new materials, the subsections in the results and discussion section of the revised manuscript are re-organized:

- 3.1 Overview
- 3.2 Diurnal variations
- 3.3 Back trajectory analyses
- 3.4 New particle formation
- 3.5 Closure analysis for LV and MV residuals at 300 ℃, OC and EC

The response below will focus on the new discussions related to the OC and EC data in addition to the main comments raised by the reviewer. Detailed discussions about the meteorological conditions can be found in item 1.2 of the major comments for Reviewer 1 or the revised manuscript.

1. For suggested closure b) and c), we would like to point out that LV, MV, and HV particles differ in the relative abundance of the volatile fraction over the non-volatile fraction at 300^{o}C but not the volatility of the evaporated materials. On the other hand, OC_1, OC_2, OC_3 and OC_4 represent OC of different volatilities, as measured at different evaporation temperatures. Since the differentiation of LV, MV and HV relies on a different set of principles than the differentiation of OC_1, OC_2, OC_3 and OC_4, we do not think it useful to conduct any closure analysis related to b) and c).

We agree that it would be useful to carry out the suggested closure a) of CV versus OC_1 as proposed by the reviewer. However, a closure analysis between VM or CV and OC_1 was not conducted because there is a large uncertainty in the calculation of the vaporized mass (VM and CV). The estimation of the mass of vaporized materials (VM and CV) requires subtracting the volumes of LV and MV particles from the total particle volume, which was estimated by SMPS. However, unlike LV, MV, and HV particles, which had volume distributions peaking at diameters below 400 nm, the SMPS data suggest that the total volume almost always peaked at sizes above 400 nm. The calculation of VM and CV would involve large uncertainties due to the need to extrapolate the volume contributions of particles larger than 400 nm in size. Hence, we are not confident that one can draw meaningful conclusions from such analysis.

2. New materials added

2.1 Overview of OC/EC data

The time series of EC and OC concentrations and the OC/EC ratio during the campaign are shown in Fig. R1. OC concentrations ranged from 0.5 to 47.0 μg m^{-3} with an average of 9.0 ± 6.0 μg m^{-3}, while EC concentrations ranged from 0.2 to 23.0 μg m^{-3} with an average of 3.4 ± 3.0 μg m^{-3}. OC_1, the most volatile group among OC_1 to OC_4 in OC/EC analysis, accounted for one-third of the total carbon mass (Fig. R2). Similar to the number concentrations of MV particles (with an initial diameter of 80 nm and above) measured by the VTDMA at 300 ℃, OC and EC mass correlated well with $PM_{2.5}$. The r^2 values of the correlations between OC and $PM_{2.5}$ and between EC and $PM_{2.5}$ are 0.8 and 0.7, respectively (Fig. R3).

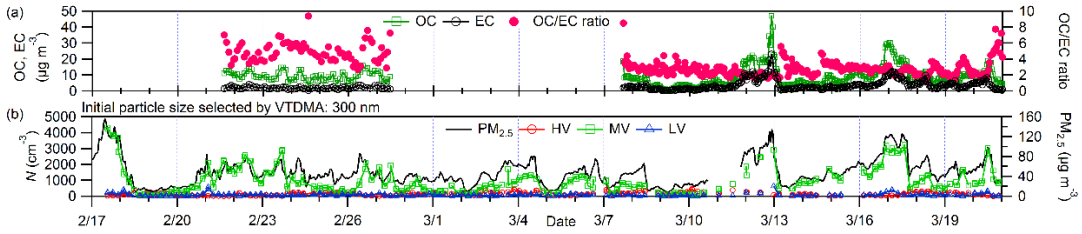

Fig. R1. Time series of (a) OC and EC concentrations and the OC/EC ratio, (b) number concentrations of HV, MV and LV particles having an initial diameter of 300 nm upon heating at 300 ℃ (left axis) and concentration of $PM_{2.5}$ (right axis).

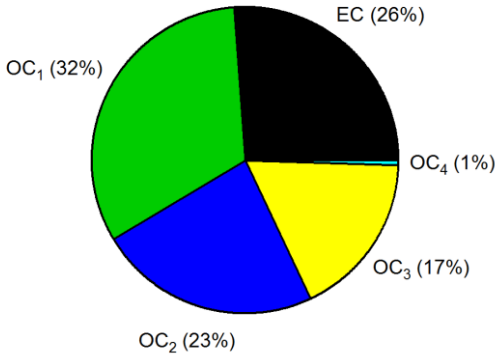

Fig. R2. Average mass fractions of EC, OC_1, OC_2, OC_3 and OC_4 in $PM_{2.5}$.

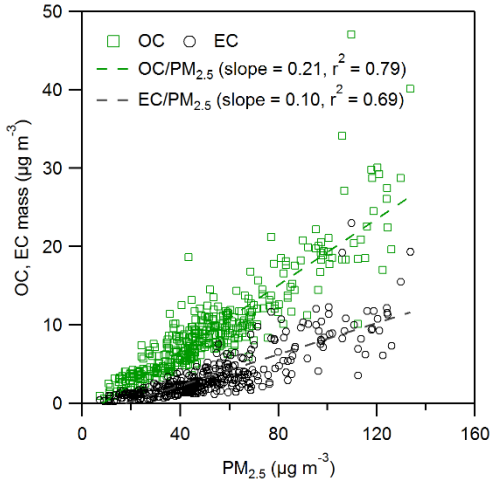

1397

1398 Fig. R3. Concentrations of OC and EC versus $PM_{2.5}$.

2.2 Comparison of the diurnal variations of OC/EC and VTDMA data

The diurnal variations in the mass fractions of OC and EC in $PM_{2.5}$ are compared with the volume fractions of CV, HV residual, MV residual, LV residual and VM in particles of dry initial diameters of 40, 150 and 300 nm. The OC and EC data on Mar 12 and 17 were excluded since they were more than two standard deviations higher than those on other days. Subtle morning peaks between 06:00 and 10:00 were observed for the volume fraction of LV residuals (Fig. R4). A similar peak was observed for the mass fraction of EC in $PM_{2.5}$ in the morning (Fig. R5). This suggests that LV particles may be related to the EC from vehicle emissions in the morning. This EC was relatively less aged and externally mixed with other volatile materials. In the late afternoon, LV residuals showed another peak between 17:00 and 19:00 whereas the mass fraction of EC in $PM_{2.5}$ exhibited a minimum at 15:00, after which it increased continuously. The continuous increase in EC at night is likely related to the increase of heavy-duty diesel vehicles (Zhang et al., 2015), which was restricted during daytime (Bradsher, 2007).

Although OC_1 contributed to about half of the total OC mass, the diurnal variation in the mass fraction of OC in $PM_{2.5}$ was driven by the total mass of OC_2, OC_3 and OC_4 ($OC_{2\text{-}4}$), which reached a minimum between 05:00 and 09:00 and increased until 19:00. OC can be attributed to both primary and secondary sources. The increased mass fraction of OC in $PM_{2.5}$ and OC-to-EC ratio in the afternoon suggest that the sources of OC were less related to traffic but more to the aging and formation of secondary organic aerosols (Turpin et al., 1990; Chow et al., 1996). These OC_2, OC_3 and OC_4 may be highly oxygenated species or oligomers that are less volatile than primary or less oxygenated organics (Kalberber et al., 2004; Huffman et al., 2009).

It is interesting to note that the volume fraction of LV residuals and the *VFR* of MV particles at different sizes showed a dip in the afternoon (Fig. R4, third column from the left). The *VFR* of 40 nm MV particles showed a dip at 14:00 while those in 150 nm and 300 nm particles showed a dip at 15:00. The volume fraction of LV residuals in 150 nm and 300 nm particles reached a minimum at 13:00 and 15:00, respectively. Because EC decreased between 12:00 and 15:00, the increase in the volume fraction of LV residuals in 150 nm particles since 13:00 and the *VFR* of 40 nm MV particles

since 14:00 may be related to the increased presence of aged organics as well as the EC particles which aged via coagulation and condensation.

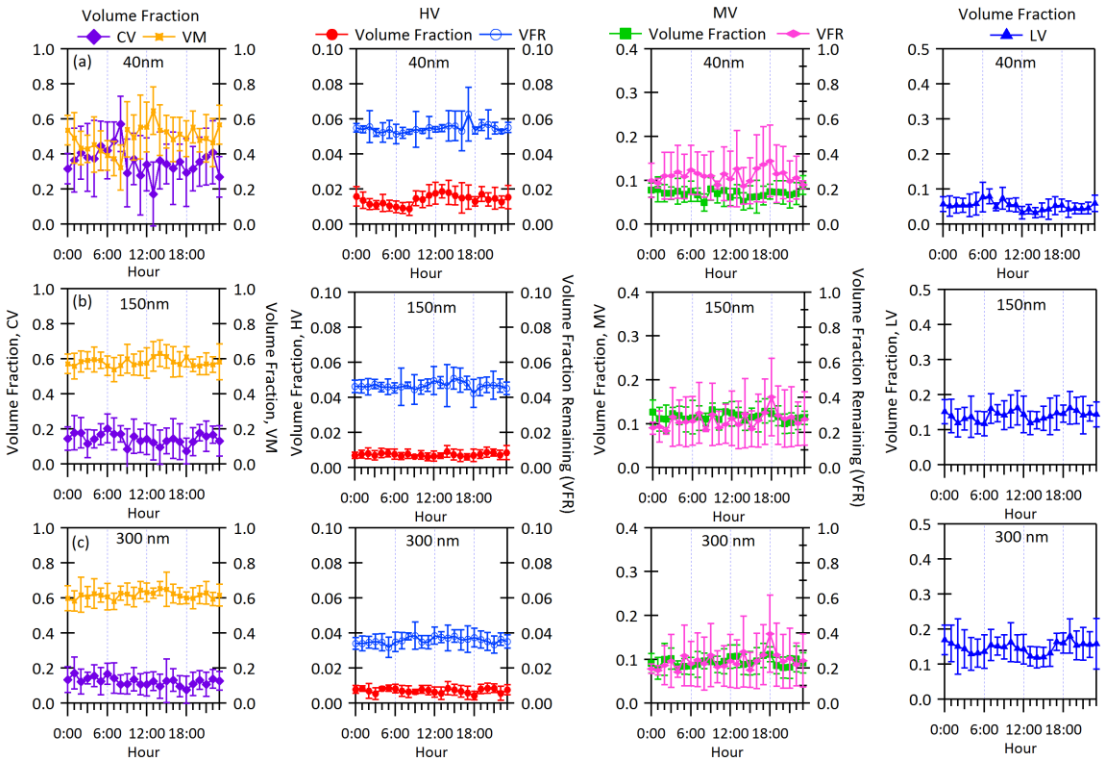

Fig. R4. Diurnal variations in volume fractions of (columns from left to right) CV, VM, HV residual, MV residual and LV residual in (a) 40 nm, (b) 150 nm and (c) 300 nm particles. Diurnal variations in the volume fraction remaining (*VFR*) of HV and MV particles are plotted on the right axis. Error bars represent one standard deviation.

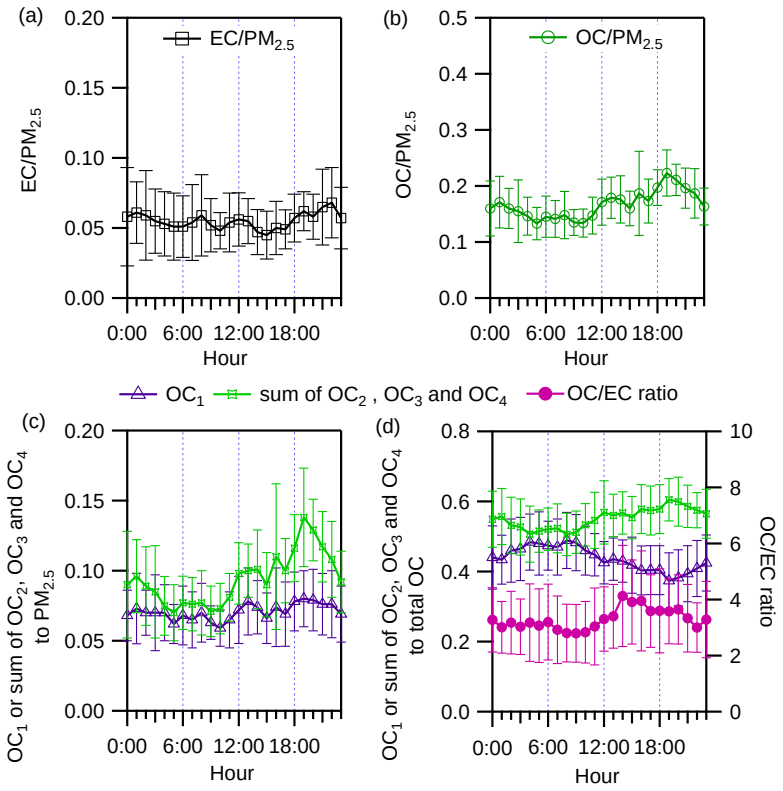

Fig. R5. Diurnal variations in the mass fractions of EC, OC, OC_1 and the sum of OC_2, OC_3 and OC_4 in $PM_{2.5}$, the ratio of OC to EC, mass fractions of OC_1 and the sum of OC_2, OC_3 and OC_4 to total OC in February and March. Error bars represent one standard deviation.

2.3 Back Trajectory Analysis

We calculated the 72 h back trajectories of the air masses arriving at the sampling site (23°00 N, 113°25'' E) at 4 h intervals (at 00:00, 04:00, 08:00, 12:00, 16:00 and 20:00 local time, UTC +8) using the PC version of the HYSPLIT4 (Hybrid Single Particle Lagrangian Integrated Trajectory, version 4) model (Stein et al., 2015; Rolph, 2016). Archived meteorological data from the Global Data Assimilation System (GDAS) 1-deg was employed and the receptor height was set at 500 m above ground level (a.g.l.). The 191 back trajectories calculated were grouped into six clusters based on their spatial distribution (Fig. R6).

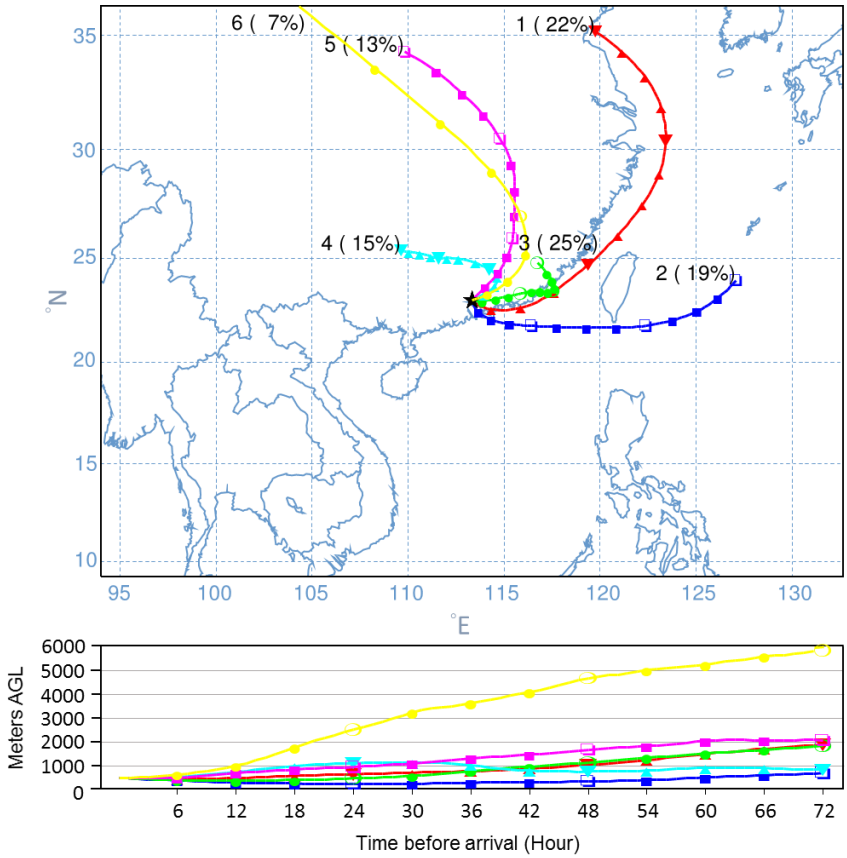

Fig. R6. Mean back trajectories of the six types of air masses arriving at the sampling site.

Overall, the sampling site was mostly affected by northwesterly and northeasterly air masses. Cluster 1 and 3 are coastal and continental air masses, respectively, although both originated from the northeast. Clusters 4, 5 and 6 represent continental air masses originating from the northwest. Cluster 2 is a group of maritime air masses originating from the East China Sea northeast or east of Guangzhou. While air masses in cluster 6 were transported at relatively high speeds and altitudes (over 3000 m a.g.l.), air masses in all the other clusters were transported at an altitude below 1500 m a.g.l. for over 40 h before arriving at the site. Nevertheless, air masses in cluster 6 only persisted for less than three days. Since the corresponding VTDMA and OC/EC data were sometimes unavailable, cluster 6 will be excluded from the following discussion.

The average $PM_{2.5}$, OC and EC concentrations associated with air masses from the northeast of Guangzhou (clusters 1, 2 and 3) were higher than those from the northwest (clusters 4 and 5, Table R1). Days associated with coastal and maritime air masses were more polluted than days associated with continental air masses for several reasons. First, south China as a region is often affected by the high pressure system moving eastward or southward from the continent out to sea in winter. When the maritime or coastal air streams entered from the southeast of the sampling site at Panyu, the atmosphere at the sampling site became more stable with low local wind speeds (e.g. the polluted days on Feb 17 and Mar 12, 16 and 17, Fig. R7 and R8). Local pollutants accumulated and the city was also affected by pollutants from the southeastern areas of the site (e.g. Shenzhen, Nansha and Dongguan). Second, land-sea breeze cycles were observed when the sampling site was under the influence of maritime air masses from Mar 18 to 20. During the day, southeasterly wind prevailed and the wind speed was higher. In the evening, the southeasterly wind was gradually replaced by a southwesterly or northwesterly wind and the wind speed decreased (Fig. R7). The cycle started again in the morning when the westerly wind was gradually replaced by southeasterly wind. Such land-sea breeze effects can result in an effective redistribution and accumulation of air pollutants within the PRD region (Lo et al., 2006).

Table R1. Summary of concentrations of $PM_{2.5}$, OC, EC and the ratio of OC to EC (OC/EC) in the five clusters.

	Cluster				
	Coastal	Maritime	Continental		
	1	2	3	4	5
Origin (to the site)	NE	NE/E	NE	NW	NW
$PM_{2.5}$ (μg m^{-3})	58.5 ±24.4	58.9 ±30.9	47.5 ±28.4	33.9 ±15.9	33.8 ±19.3
OC (μg m^{-3})	10.8 ±6.01	10.84 ±7.22	10.13 ±6.89	5.51 ±3.3	7.32 ±2.75
EC (μg m^{-3})	4.38 ±2.97	4.98 ±4.21	3.43 ±3.12	1.8 ±0.98	2.46 ±0.59
OC/EC	2.83 ±1.05	2.62 ±1.03	3.65 ±1.6	3.18 ±1.26	2.94 ±0.73

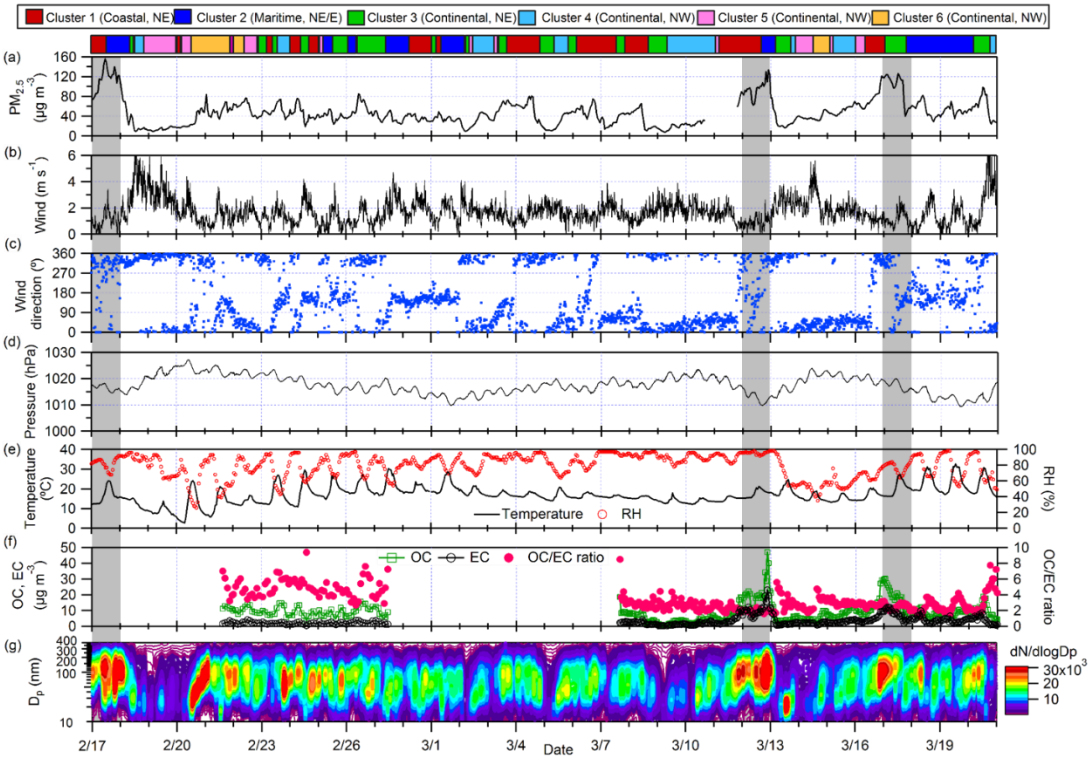

Fig. R7. Overview of major meteorological parameters, $PM_{2.5}$, OC and EC concentrations, OC/EC ratio and particle number size distributions in the campaign. Air mass clusters are depicted at the top and the shaded areas indicate days with daily-averaged $PM_{2.5}$ concentrations exceeding 95 μg m^{-3}.

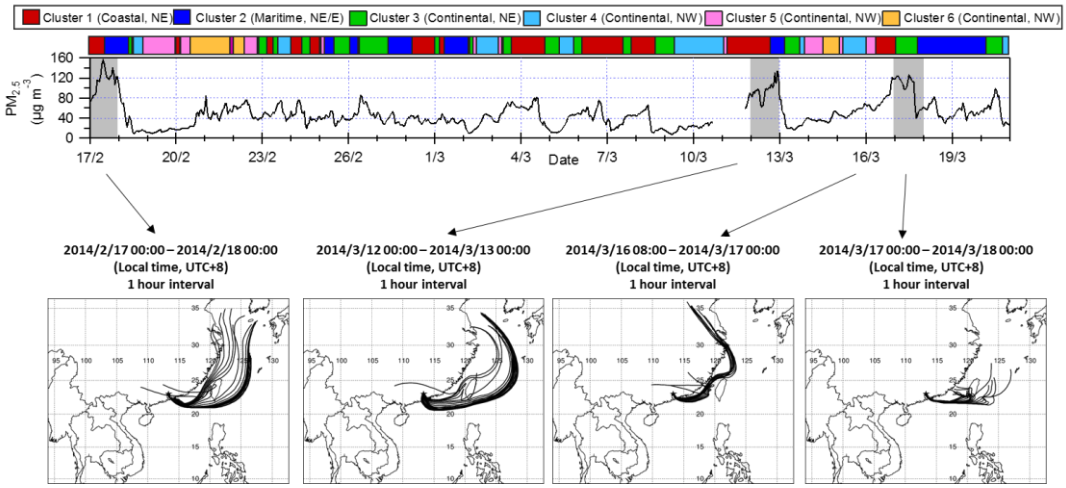

Fig. R8. Time series of $PM_{2.5}$ concentrations and 72 h back trajectories at hourly intervals on Feb 17, and Mar 12, 16 and 17.

Furthermore, $PM_{2.5}$ in the northeastern parts of China can exceed 200 μg m^{-3} due to both enhanced emissions from coal combustion for heating and poor dispersion during wintertime (Gu et al., 2014). Under the influence of the prevailing northerly or northeasterly wind in China, these pollutants were often transported to southern China and the East China Sea (Chen et al., 2012). Pollutants might also have accumulated when the maritime air masses spent about two days across Taiwan and the coast of south China. In contrast, continental air masses in cluster 5 moved slightly faster, and were often associated with the cold front period during which the local wind speed and pressure increased but the temperature decreased (Fig. R7). As the cold air masses passed through the city, dispersion and clearance of pollutants were promoted, resulting in lower $PM_{2.5}$ concentrations (Tan et al., 2013a). Therefore, unlike in other coastal cities like Hong Kong (Lee et al., 2013), in Panyu maritime air masses could lead to more severe pollution than the continental ones in winter.

The five clusters were further analyzed to study the influence of air mass history on aerosol volatility. The number fractions of CV, HV, MV and LV of the six selected diameters in VTDMA measurements are regrouped based on the clusters as shown in Fig. R9. The total number fractions of the non-volatile residuals (sum of HV, MV and LV) were similar in all clusters. Maritime air masses (cluster 2) had a slightly higher fraction of LV particles while continental air masses originating from the northwest of the site (clusters 4 and 5) had a higher fraction of HV particles. Although the air masses

in clusters 1 and 5 originated from farther away and traveled at relatively higher speeds than those in clusters 2, 3 and 4, all clusters involved transport at low altitudes (below 1500 m) for over 40 h, likely due to the generally lower mixing heights in winter. Therefore, aerosols in these air masses were all well-aged upon arrival (Wehner et al., 2009). This could be another reason for the lack of size dependence of the number, volume fractions and diurnal variation for particles larger than 80 nm. When the transported air masses mixed with local pollutants, the size dependence of the number fractions of different volatility groups as well as the aging of local emissions was further reduced.

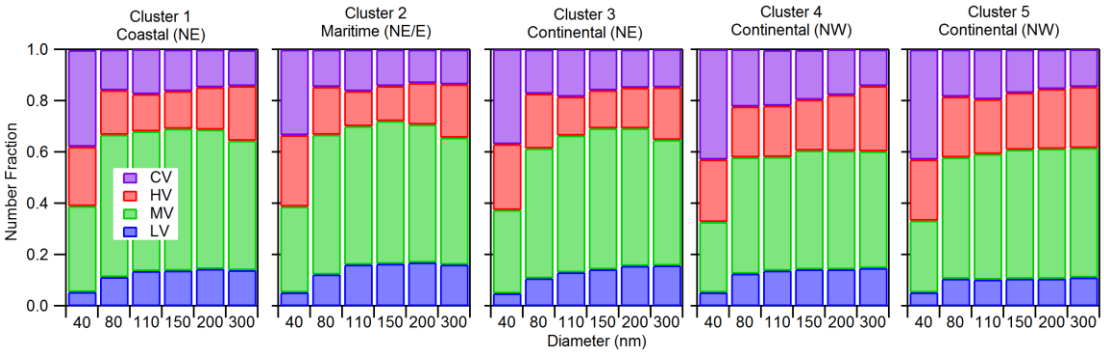

Fig. R9. Average number fractions of CV, HV, MV and LV particles in clusters 1 to 5 at different selected diameters.

We also examine at the volatility shrinkage factor (*VSF*) distributions of 40 nm, 110 nm and 300 nm particles upon heating at 300 ℃ (Fig. R10). Log-normal fittings with a three-peak solution were applied to the distributions. The average *VSF* modes of the peaks were located at 0.38 ± 0.021 (peak 1), 0.60 ± 0.066 (peak 2) and 0.95 ± 0.007 (peak 3), respectively. The standard deviation of the corresponding normal distribution (σ) of peak 3 was the smallest among the three peaks ($\sigma < 0.1$). For the same particle size, the *VSF* distributions in the *VSF* range between 0.3 and 0.8 in cluster 5 was relatively more uni-modal than those of other clusters (Fig. R10b and R10c). This suggests that the composition in cluster 5 was more homogeneous. Cluster 1 also consisted of long-range transported air masses but they likely passed through areas that are more polluted and mixed with different types of pollutants. Note that the fractions of HV, MV and LV have been traditionally defined based on the values of *VSF*, i.e. HV < 0.4; 0.4 < MV < 0.9; LV > 0.9 (Wehner et al., 2009). The *VSF* distributions above suggest that these definitions using *VSF* = 0.4 and 0.9 may need to be re-visited in the future.

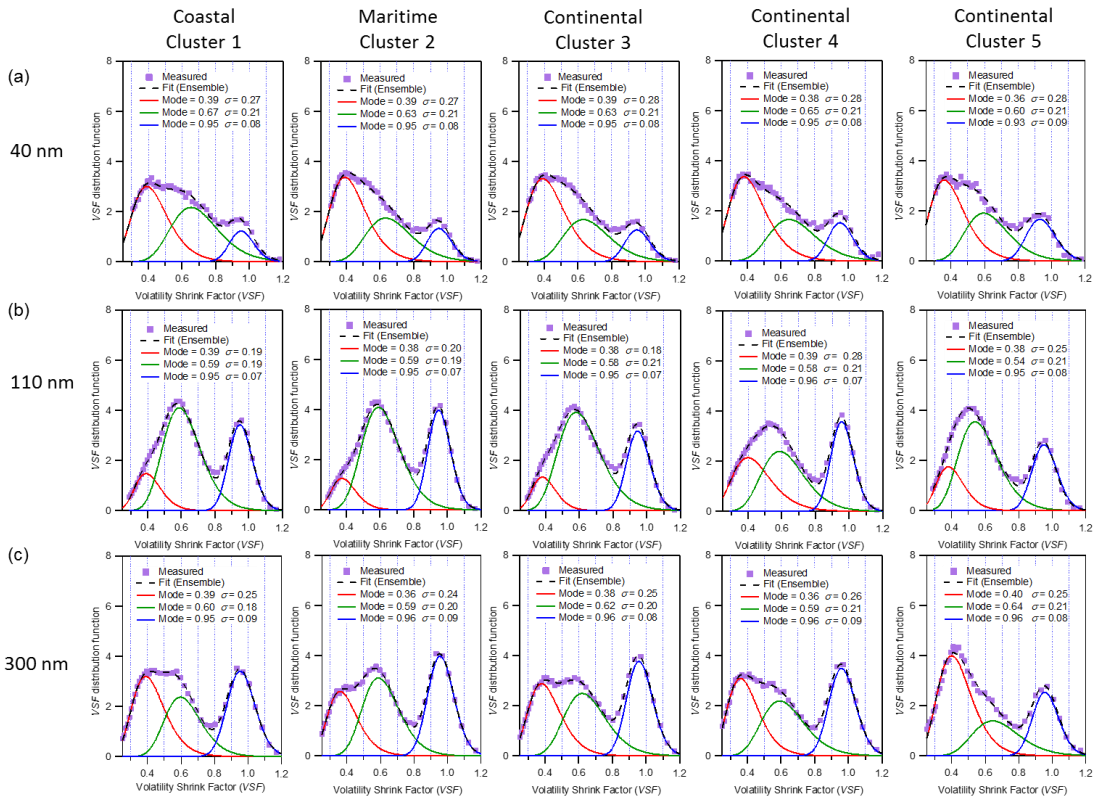

Fig. R10. Volatility shrinkage factor (*VSF*) distribution function in different clusters. Solid and dotted lines are the peaks fitted with log-normal function and the ensemble distributions, respectively.

3. Please refer to item 2.

Minor/Technical Comments

4. *It is not clear to me how understand the difference between "Volatile Materials" (VM) are defined. I assumed that "VM" becomes "CV" after heating to 300°C, but this does not seem to be the case because separate volume fractions of "VM" and "CV" are presented in Figures 6 and 7. Please clarify the definition of VM.*

Response:

VM and CV differ by how the evaporated materials mix with the non-volatile materials. VM refers to the volatile materials that are internally mixed with (or coated on) the non-volatile materials while CV refers to the volatile materials that are externally mixed with particles containing the non-volatile materials. Upon heating, VM evaporated, leaving behind HV, MV, or LV residuals. Evaporation of VM alone does not change the total number concentrations of particles. In contrast, CV particles evaporated completely without leaving any residuals behind. It reduced the total particle number concentrations.

On page 25275 of the original manuscript, Section 2.1.2, line 19 onwards, we mentioned:

Figure 2 illustrates how thermal treatment in the VTDMA affects the size distributions of the ambient aerosols. At each selected diameter D_0 (and at each temperature) in DMA_1 in the VTDMA, the particles include CV particles (purple) and **LV, MV and HV particles that have VM (orange) internally mixed with the LV (blue), MV (green) and HV (red) residuals.** After heating, the remaining particles would form LV, MV and HV residuals without any CV or VM.

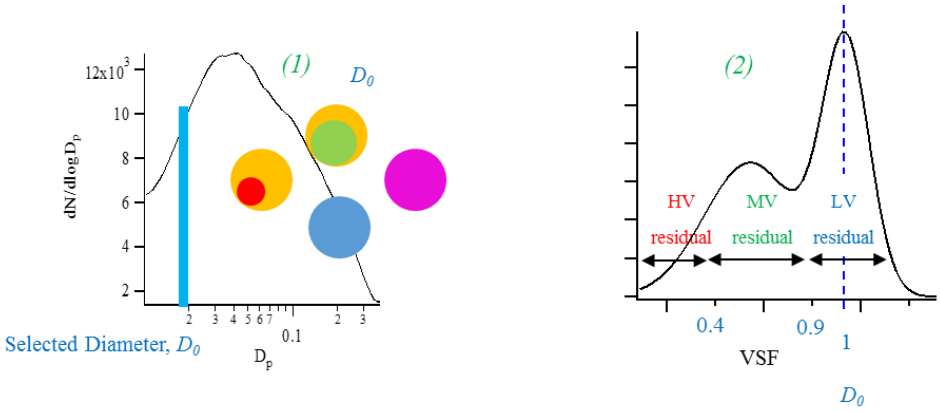

Fig. 2. Examples of particle size distributions of (a) ambient aerosols before entering DMA_1 and (b) residuals of the size-selected particles (D_0) after heating. The left and right distributions correspond to (1) and (2) in Fig. 1 respectively. Residuals are divided into three groups—LV (blue), MV (green) and HV (red)—based on their *VSF*. CV (purple) and VM (orange) are completely vaporized and hence not measured as residuals. VM appears as coating for illustration purposes only. It does not necessarily reflect the morphology of the particles.

In the revised manuscript, CV and VM are clearly defined in the methodology section instead of the introduction section. VM refers to volatile materials internally mixed with non-volatile ones while CV refers to volatile materials externally mixed with non-volatile materials.

Revised Methodology (Section 2.1.2):

…The *VSF* is also used to divide the particles into three groups, namely the low volatility (LV), medium volatility (MV) and high volatility (HV) particles. In this study, we focus on the measurements made at 300 ℃. The *VSF* ranges for LV, MV and HV particles upon heating at 300 ℃ are above 0.9, between 0.4 and 0.9 and below 0.4, respectively (Fig. 2) (Wehner et al., 2004; Wehner et al., 2009). The LV particles are assumed to represent EC particles externally mixed with the volatile materials, while the MV and HV particles are assumed to represent EC particles internally mixed with volatile materials. While the volatile materials in the MV and HV particles are referred to as VM, those exist as external mixtures with the LV, MV and HV particles are referred to as completely vaporized (CV) particles. The CV particles evaporate completely without leaving behind any residuals at 300 ℃.

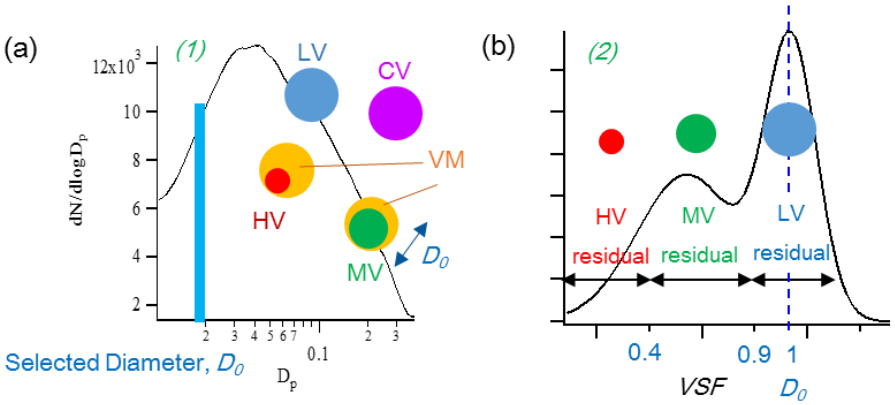

Fig. 2. Examples of particle size distributions of (a) ambient aerosols before entering DMA_1 and (b) residuals of the size-selected particles (D_0) after heating. The left and right distributions correspond to (1) and (2) in Fig. 1 respectively. Residuals are divided into three groups—LV (blue), MV (green) and HV (red)—based on their *VSF*. CV (purple) and VM (orange) are vaporized and hence not measured as residuals. VM appears as coating for illustration purposes only. It does not necessarily reflect the morphology of the particles.

5. *OC_2, OC_3 and OC_4 are never defined in the manuscript.*

Response:

On page 25276 of the original manuscript, line 19 – 22, we mentioned:

"The OC/EC Analyzer adopts the ACE-Asia protocol (a NIOSH-derived protocol), where OC evaporates at four set temperatures of 310, 475, 615 and 870 ℃, and EC is combusted at temperature above 550 ℃ (Schauer et al., 2003). Based on volatility and refractoriness, the OC contents are named OC_1 to OC_4 with OC_1 being most volatile"

We agree that the definitions did not explicitly link the terms and the heating temperatures. The revised description is shown below.

Revised:

The OC/EC analyzer adopts the ACE-Asia protocol (a NIOSH-derived protocol), where OC evaporates at four set temperatures of 310 ℃, 475 ℃, 615 ℃ and 870 ℃ with pure helium (He) as the carrier gas, and EC is combusted at temperatures between 550 ℃ and 870 ℃ under He and 2% oxygen (O_2, Schauer et al., 2003; Wu et al., 2012). The OC contents are named OC_1 to OC_4 based on the temperature protocol of the OC/EC analyzer (Table R2). The mass of EC determined at different temperatures will be grouped together for discussions.

Table R2. Temperature (T) and residence time (RT) protocol of the semi-continuous Sunset OC/EC analyzer (Wu et al., 2012)

Carbon Fraction	Carrier Gas	T (℃)	RT (s)
OC_1	He	310	80
OC_2		475	60
OC_3		615	60
OC_4		870	90
EC_1	He + 2% O_2	550	45
EC_2		625	45
EC_3		700	45
EC_4		775	45
EC_5		850	45
EC_6		870	45

6. *What is the residence time in the heated section of the VTMDA, and how sensitive are the HV/MV/LV classifications to the residence time?*

Response:

The heating tube was a 1/2'', 80 cm long stainless steel tube with an inner diameter of 8 mm. With a sample flow rate of 1 L min^{-1}, the resulting residence time in the heated section of the VTDMA was 2.4 s. The estimated aerosol velocity on the center line was 0.33 m s^{-1}. Compared to the residence time of 0.3 s to 1 s in other VTDMA systems (e.g. Brooks et al., 2002; Philippin et al., 2004; Villani et al., 2007), the residence time in our VTDMA is assumed to be long enough for the volatile materials to be effectively vaporized. After leaving the heating tube, the flow entered a heat exchanger measuring 30 cm in length to ensure sufficient cooling before entering DMA_2. The relevant information is added to the methodology section.

Revised, Page 25275 of the original manuscript, line 5 onwards:

Afterwards, the monodisperse aerosols were directed via path (b) to a heated tube for volatility measurement (V-Mode) sequentially at 25, 100 and 300 ℃. The heating tube was a 1/2'', 80 cm long stainless steel tube with an inner diameter of 8 mm. With a sample flow rate of 1 L min^{-1}, the resulting residence time in the heated section of the VTDMA was 2.4 s. The estimated aerosol velocity on the center line was 0.33 m s^{-1}. Compared to the residence time of 0.3 s to 1 s in other VTDMA systems (e.g. Brooks et al., 2002; Philippin et al., 2004; Villani et al., 2007), the residence time in our VTDMA is assumed to be long enough for the volatile materials to be effectively vaporized. After leaving the heating tube, the flow entered a heat exchanger measuring 30 cm in length to ensure sufficient cooling before entering DMA_2.

7. ***P25275, L8-10:*** *The authors state: "Upon heating at 100 ℃ and beyond, volatile components of the particle such as sulfate, nitrate and volatile organics vaporize". Please plot VSF (at 300^{o}C) of ammonium sulfate, perhaps as a supplemental figure, over a few sizes ranging from 40 nm to 300 nm. I would not have thought that ammonium sulfate completely vaporizes at only 300^{o}C.*

Response:

In a number of earlier studies, ammonium sulfate test aerosols were found to volatilize at temperatures between 160 ℃ and 280 ℃ (Table R3). The volatilization temperature of the tested aerosols varies with the initial diameter of the aerosols and their residence time in the heated section. In this work, the residence time in the heated section was 2.4 s, hence we believe that ammonium sulfate would be completely vaporized upon heating at 300 ℃ in the VTDMA. We did not mean to claim that ammonium sulfate would be completely vaporized at 100 ℃ in the original sentence ("Upon heating at 100 ℃ and beyond…"). The sentence is revised to avoid confusion.

Table R3. Volatilization temperature of ammonium sulfate test aerosols in the VTDMA (Villani et al., 2007)

	O'Dowd et al. (1992)	Philippin et al. (2004)	Burtscher et al. (2001)	Brooks et al. (2002)	Villani et al. (2007)
Volatilization temperature	280 ℃	180 ℃	180 ℃	235 ℃	160 to 180 ℃

Revised, Page 25275 of the original manuscript, line 8 – 10:

Upon heating at 100 ℃ and above, volatile components of the particle such as sulfate, nitrate and volatile organics would vaporize at different temperatures depending on their volatilities.

References

Bradsher, K.: Trucks power China's economy, at a suffocating cost., The New York Times, NY, USA, http://www.nytimes.com/2007/12/08/world/asia/08trucks.html, 2007.

Brooks, B. J., Smith, M. H., Hill, M. K., and O'Dowd, C. D.: Size-differentiated volatility analysis of internally mixed laboratory-generated aerosol, Journal of Aerosol Science, 33, 555-579, http://dx.doi.org/10.1016/S0021-8502(01)00192-6, 2002.

Burtscher, H., Baltensperger, U., Bukowiecki, N., Cohn, P., Hüglin, C., Mohr, M., Matter, U., Nyeki, S., Schmatloch, V., Streit, N., and Weingartner, E.: Separation of volatile and non-volatile aerosol fractions by thermodesorption: instrumental development and applications, Journal of Aerosol Science, 32, 427-442, http://dx.doi.org/10.1016/S0021-8502(00)00089-6, 2001.

Chen, B., Du, K., Wang, Y., Chen, J., Zhao, J., Wang, K., Zhang, F., and Xu, L.: Emission and transport of carbonaceous aerosols in urbanized coastal areas in China, 2012.

Cheng, Y. F., Eichler, H., Wiedensohler, A., Heintzenberg, J., Zhang, Y. H., Hu, M., Herrmann, H., Zeng, L. M., Liu, S., Gnauk, T., Brüggemann, E., and He, L. Y.: Mixing state of elemental carbon and non-light-absorbing aerosol components derived from in situ particle optical properties at Xinken in Pearl River Delta of China, Journal of Geophysical Research: Atmospheres, 111, D20204, 10.1029/2005JD006929, 2006.

Cheng, Y. F., Su, H., Rose, D., Gunthe, S. S., Berghof, M., Wehner, B., Achtert, P., Nowak, A., Takegawa, N., Kondo, Y., Shiraiwa, M., Gong, Y. G., Shao, M., Hu, M., Zhu, T., Zhang, Y. H., Carmichael, G. R., Wiedensohler, A., Andreae, M. O., and Pöschl, U.: Size-resolved measurement of the mixing state of soot in the megacity Beijing, China: diurnal cycle, aging and parameterization, Atmos. Chem. Phys., 12, 4477-4491, 10.5194/acp-12-4477-2012, 2012.

Chow, J. C., Watson, J. G., Lu, Z., Lowenthal, D. H., Frazier, C. A., Solomon, P. A., Thuillier, R. H., and Magliano, K.: Descriptive analysis of PM2.5 and PM10 at regionally representative locations during SJVAQS/AUSPEX, Atmos. Environ., 30, 2079-2112, http://dx.doi.org/10.1016/1352-2310(95)00402-5, 1996.

Donahue, N. M., Robinson, A. L., and Pandis, S. N.: Atmospheric organic particulate matter: From smoke to secondary organic aerosol, Atmospheric Environment, 43, 94-106, http://dx.doi.org/10.1016/j.atmosenv.2008.09.055, 2009.

Frey, A., Rose, D., Wehner, B., Müller, T., Cheng, Y., Wiedensohler, A., and Virkkula, A.: Application of the Volatility-TDMA Technique to Determine the Number

1742 Size Distribution and Mass Concentration of Less Volatile Particles, Aerosol
1743 Science and Technology, 42, 817-828, 10.1080/02786820802339595, 2008.
1744 Gu, J., Du, S., Han, D., Hou, L., Yi, J., Xu, J., Liu, G., Han, B., Yang, G., and Bai, Z.-
1745 P.: Major chemical compositions, possible sources, and mass closure analysis of
1746 PM2.5 in Jinan, China, Air Quality, Atmosphere & Health, 7, 251-262,
1747 10.1007/s11869-013-0232-9, 2014.
1748 Huang, X.-F., Yu, J. Z., He, L.-Y., and Hu, M.: Size Distribution Characteristics of
1749 Elemental Carbon Emitted from Chinese Vehicles: Results of a Tunnel Study
1750 and Atmospheric Implications, Environmental Science & Technology, 40, 5355-
1751 5360, 10.1021/es0607281, 2006.
1752 Huffman, J. A., Docherty, K. S., Aiken, A. C., Cubison, M. J., Ulbrich, I. M., DeCarlo,
1753 P. F., Sueper, D., Jayne, J. T., Worsnop, D. R., Ziemann, P. J., and Jimenez, J. L.:
1754 Chemically-resolved aerosol volatility measurements from two megacity field
1755 studies, Atmos. Chem. Phys., 9, 7161-7182, 10.5194/acp-9-7161-2009, 2009.
1756 Kalberer, M., Paulsen, D., Sax, M., Steinbacher, M., Dommen, J., Prevot, A. S. H.,
1757 Fisseha, R., Weingartner, E., Frankevich, V., Zenobi, R., and Baltensperger, U.:
1758 Science, 303, 1659, 2004.
1759 Lee, B. P., Li, Y. J., Yu, J. Z., Louie, P. K. K., and Chan, C. K.: Physical and chemical
1760 characterization of ambient aerosol by HR-ToF-AMS at a suburban site in Hong
1761 Kong during springtime 2011, Journal of Geophysical Research: Atmospheres,
1762 118, 8625-8639, 10.1002/jgrd.50658, 2013.
1763 Levy, M. E., Zhang, R., Zheng, J., Tan, H., Wang, Y., Molina, L. T., Takahama, S.,
1764 Russell, L. M., and Li, G.: Measurements of submicron aerosols at the
1765 California–Mexico border during the Cal–Mex 2010 field campaign, Atmos.
1766 Environ., 88, 308-319, http://dx.doi.org/10.1016/j.atmosenv.2013.08.062, 2014.
1767 Lo, J. C. F., Lau, A. K. H., Fung, J. C. H., and Chen, F.: Investigation of enhanced
1768 cross-city transport and trapping of air pollutants by coastal and urban land-sea
1769 breeze circulations, Journal of Geophysical Research: Atmospheres, 111, n/a-n/a,
1770 10.1029/2005JD006837, 2006.
1771 Murphy, B. N., Donahue, N. M., Robinson, A. L., and Pandis, S. N.: A naming
1772 convention for atmospheric organic aerosol, Atmos. Chem. Phys., 14, 5825-5839,
1773 10.5194/acp-14-5825-2014, 2014.
1774 O'Dowd, C. D., Jennings, S. G., Smith, M. H., and Cooke, W.: A high temperature
1775 volatility technique for determination of atmospheric aerosol composition,
1776 Journal of Aerosol Science, 23, Supplement 1, 905-908,
1777 http://dx.doi.org/10.1016/0021-8502(92)90558-D, 1992.
1778 Philippin, S., Wiedensohler, A., and Stratmann, F.: Measurements of non-volatile
1779 fractions of pollution aerosols with an eight-tube volatility tandem differential

mobility analyzer (VTDMA-8), Journal of Aerosol Science, 35, 185-203, http://dx.doi.org/10.1016/j.jaerosci.2003.07.004, 2004.

Pinnick, R., Jennings, S., and Fernandez, G.: Volatility of aerosols in the arid southwestern United States, Journal of the atmospheric sciences, 44, 562-576, 1987.

Rolph, G. D.: Real-time Environmental Applications and Display sYstem (READY) Website (http://www.ready.noaa.gov), 2016.

Rose, D., Wehner, B., Ketzel, M., Engler, C., Voigtländer, J., Tuch, T., and Wiedensohler, A.: Atmospheric number size distributions of soot particles and estimation of emission factors, Atmos. Chem. Phys., 6, 1021-1031, 10.5194/acp-6-1021-2006, 2006.

Rose, D., Gunthe, S. S., Su, H., Garland, R. M., Yang, H., Berghof, M., Cheng, Y. F., Wehner, B., Achtert, P., Nowak, A., Wiedensohler, A., Takegawa, N., Kondo, Y., Hu, M., Zhang, Y., Andreae, M. O., and Pöschl, U.: Cloud condensation nuclei in polluted air and biomass burning smoke near the mega-city Guangzhou, China – Part 2: Size-resolved aerosol chemical composition, diurnal cycles, and externally mixed weakly CCN-active soot particles, Atmos. Chem. Phys., 11, 2817-2836, 10.5194/acp-11-2817-2011, 2011.

Schauer, J. J., Mader, B. T., Deminter, J. T., Heidemann, G., Bae, M. S., Seinfeld, J. H., Flagan, R. C., Cary, R. A., Smith, D., Huebert, B. J., Bertram, T., Howell, S., Kline, J. T., Quinn, P., Bates, T., Turpin, B., Lim, H. J., Yu, J. Z., Yang, H., and Keywood, M. D.: ACE-Asia intercomparison of a thermal-optical method for the determination of particle-phase organic and elemental carbon, Environmental Science & Technology, 37, 993-1001, 10.1021/es020622f, 2003.

Stein, A. F., Draxler, R. R., Rolph, G. D., Stunder, B. J. B., Cohen, M. D., and Ngan, F.: NOAA's HYSPLIT Atmospheric Transport and Dispersion Modeling System, Bulletin of the American Meteorological Society, 96, 2059-2077, 10.1175/BAMS-D-14-00110.1, 2015.

Tan, H. B., Yin, Y., Gu, X. S., Li, F., Chan, P. W., Xu, H. B., Deng, X. J., and Wan, Q. L.: An observational study of the hygroscopic properties of aerosols over the Pearl River Delta region, Atmos. Environ., 77, 817-826, 10.1016/j.atmosenv.2013.05.049, 2013.

Tao, J., Zhang, L., Ho, K., Zhang, R., Lin, Z., Zhang, Z., Lin, M., Cao, J., Liu, S., and Wang, G.: Impact of PM2.5 chemical compositions on aerosol light scattering in Guangzhou — the largest megacity in South China, Atmospheric Research, 135–136, 48-58, http://dx.doi.org/10.1016/j.atmosres.2013.08.015, 2014.

Turpin, B. J., Cary, R. A., and Huntzicker, J. J.: An In Situ, Time-Resolved Analyzer for Aerosol Organic and Elemental Carbon, Aerosol Science and Technology, 12, 161-171, 10.1080/02786829008959336, 1990.

Twomey, S.: On the composition of cloud nuclei in the northeastern United States, J. Rech. Atmos, 3, 281-285, 1968.

Villani, P., Picard, D., Marchand*, N., and Laj, P.: Design and Validation of a 6-Volatility Tandem Differential Mobility Analyzer (VTDMA), Aerosol Science and Technology, 41, 898-906, 10.1080/02786820701534593, 2007.

Wehner, B., Philippin, S., Wiedensohler, A., Scheer, V., and Vogt, R.: Variability of non-volatile fractions of atmospheric aerosol particles with traffic influence, Atmos. Environ., 38, 6081-6090, http://dx.doi.org/10.1016/j.atmosenv.2004.08.015, 2004.

Wehner, B., Berghof, M., Cheng, Y. F., Achtert, P., Birmili, W., Nowak, A., Wiedensohler, A., Garland, R. M., Pöschl, U., Hu, M., and Zhu, T.: Mixing state of nonvolatile aerosol particle fractions and comparison with light absorption in the polluted Beijing region, Journal of Geophysical Research: Atmospheres, 114, D00G17, 10.1029/2008JD010923, 2009.

Wu, C., Ng, W. M., Huang, J. X., Wu, D., and Yu, J. Z.: Determination of Elemental and Organic Carbon in PM2.5 in the Pearl River Delta Region: Inter-Instrument (Sunset vs. DRI Model 2001 Thermal/Optical Carbon Analyzer) and Inter-Protocol Comparisons (IMPROVE vs. ACE-Asia Protocol), Aerosol Science and Technology, 46, 610-621, 10.1080/02786826.2011.649313, 2012.

Zhang, S. L., Ma, N., Kecorius, S., Wang, P. C., Hu, M., Wang, Z. B., Größ, J., Wu, Z. J., and Wiedensohler, A.: Mixing state of atmospheric particles over the North China Plain, Atmos. Environ., 125, Part A, 152-164, http://dx.doi.org/10.1016/j.atmosenv.2015.10.053, 2016.

Zhang, Y., Wang, X., Li, G., Yang, W., Huang, Z., Zhang, Z., Huang, X., Deng, W., Liu, T., Huang, Z., and Zhang, Z.: Emission factors of fine particles, carbonaceous aerosols and traces gases from road vehicles: Recent tests in an urban tunnel in the Pearl River Delta, China, Atmos. Environ., 122, 876-884, http://dx.doi.org/10.1016/j.atmosenv.2015.08.024, 2015.

Measurements of non-volatile aerosols with a VTDMA and their correlations with carbonaceous aerosols in Guangzhou, China

H. H. Y. Cheung[1], H. B. Tan[2], H. B. Xu[3], F. Li[2], C. Wu[1], J. Z. Yu[1,4] and C. K. Chan[1,5,6]

[1]{Division of Environment, Hong Kong University of Science and Technology, Hong Kong, China}

[2]{Institute of Tropical and Marine Meteorology, China Meteorological Administration, Guangzhou, China}

[3]{Sun Yat-sen University, Guangzhou, China}

[4]{Department of Chemistry, Hong Kong University of Science and Technology, Hong Kong, China}

[5]{Department of Chemical and Biomolecular Engineering, Hong Kong University of Science and Technology, Hong Kong, China}

[6]{School of Energy and Environment, City University of Hong Kong, Hong Kong, China}

Correspondence to: H. B. Tan (hbtan@grmc.gov.cn), C. K. Chan (chak.k.chan@cityu.edu.hk~~keckchan@ust.hk~~)

Abstract

Simultaneous measurements of aerosols of varying volatilities and carbonaceous matters were conducted at a~~n~~ suburban site ~~of~~in Guangzhou, China ~~were conducted~~ in February and March 2014 using a volatility tandem differential mobility analyzer (VTDMA) and an organic carbon/ elemental carbon (OC/EC) analyzer. Low-volatility (LV) particles, with a volatility shrinkage factor (*VSF*) at 300 ℃ exceeding 0.9, contributed to 5% of number concentrations of 40 nm particles and 11–15% of 80–300 nm particles. They were non-volatile materials externally mixed with the volatile ones and therefore did not evaporate significantly at 300 ℃. Non-volatile materials mixed internally with the volatile ones are referred to as the medium volatility (MV, $0.4 < VSF < 0.9$) and high volatility (HV, $VSF < 0.4$) particles. These MV and HV particles contributed to 57–71% of number concentrations for particles between 40 nm and 300 nm in size. The average EC and OC concentrations measured by the OC/EC analyzer were 3.4 ± 3.0 μg m^{-3} and 9.0 ± 6.0 μg m^{-3}, respectively. Non-volatile OC evaporating at 475 ℃ or above, together with EC, contributed to 67% of the total carbon mass. The diurnal variations in the volume fraction of the volatile materials, HV, MV and LV residuals were less than 15% for most of the particles except for the 40 nm ones, although a daily maximum and a daily minimum were still observed. Back trajectory analysis also suggests that over 90% of the air masses influencing the sampling site were well-aged as they were transported at low altitudes (below 1500 m) for over 40 h before arrival. Further comparison with the diurnal variations in the mass fractions of EC and non-volatile OC in $PM_{2.5}$ suggests that the non-volatile residuals may be related to both EC and non-volatile OC in the afternoon, during which the concentration of aged organics increased. The closure analysis of the total mass of LV and MV residuals and the mass of EC or the sum of EC and non-volatile OC also suggests that non-volatile OC, in addition to EC, was one of the components of the non-volatile residuals measured by the VTDMA in this study.~~In VTDMA, selected aerosols of 40 to 300 nm in mobility diameter were heated at elevated temperatures up to 300 ℃ and the size distributions of the residual particles were measured. Size dependent distributions were observed for both non-volatile and volatile materials (VM). The 40 nm particles were dominated by particles that completely vaporized (CV) at 300 ℃, with an average number fraction of about 0.4. Particles larger than 80 nm were dominated by the medium and low volatility (MV and LV, respectively) fractions, with average number fractions of 0.5 and 0.15 respectively. VM did not contribute separately to number fraction but contributed to over 50% of the total volume fraction for all sizes. In both number and volume fractions, diurnal variation was only observed for the high volatility (HV) group,~~

~~CV and VM in 40 nm particles, likely because these particles were related to fresh emissions. The little diurnal variation of larger particles could be attributed to non-locally aged aerosols. Closure analysis between the residual mass of LV+MV and mass of EC or EC+OC_{2-4} (sum of EC, OC_2, OC_3, and OC_4 of the OC/EC Analyzer) suggests that non-volatile materials measured by the VTDMA likely contain less volatile OC.~~

1 Introduction

Carbonaceous aerosols comprising organic carbon (OC) and elemental carbon (EC) or black carbon (BC) are one of the major light absorption constituents and are abundant in particulate matter (PM) (Rosen et al., 1978; Hansen et al., 1984; Japar et al., 1986; Chow et al., 1993; Horvath, 1993; Liousse et al., 1993; Fuller et al., 1999; Putaud et al., 2010; Tao et al., 2014; Zhang et al., 2015). In China, the worsening of visibility degradation associated with PM is of increasing concern in recent years. In particular, numerous studies on air pollution were carried out in different cities in China including the Pearl River Delta (PRD) region which is a fast-developing economic zone (Cheng et al., 2006; Wu et al., 2007; Andreae et al., 2008; Chan and Yao, 2008; Gnauk et al., 2008; Tan et al., 2013a). In 2007, the mass concentrations of EC and OC measured at an urban Guangzhou (GZ) site were reported to be from 6.8 to 9.4 μg m^{-3} and from ~~6.6~~13.4 to 22.5 μg m^{-3} respectively (Yu et al., 2010).

Soot particles are often characterized in terms of EC and BC, depending on whether they are measured thermally or optically (Penner and Novakov, 1996; Lavanchy et al., 1999; Cheng et al., 2011 and references therein). Their optical properties are distinct when they are freshly produced (Novakov et al., 2003). After aging processes such as cloud processing, reaction with other species and coagulation, their structure, shape, size, mixing state and thus optical properties change (Horvath, 1993; Liousse et al., 1993; Ghazi and Olfert, 2012). EC is typically measured by thermal method such as the OC/EC analyzer (Chow et al., 2007), BC are optically measured using instruments such as aethalometer (Hansen et al., 1984), multi-angle absorption photometer ~~(MAAP)~~ (Petzold and Schönlinner, 2004) and particle soot absorption photometer ~~(PSAP)~~ (Virkkula et al., 2005). However, it is not possible to retrieve the mixing state of soot particles from above techniques. To determine the mixing state of soot particles, single particle soot photometer ~~(SP2)~~ (Stephens et al., 2003), soot particle aerosol mass spectrometer ~~(SP-AMS)~~ (Onasch et al., 2012) and Volatility Tandem Differential Mobility Analyzer (VTDMA) (Philippin et al., 2004) have been used.

Ambient aerosols have varying volatility properties based on their chemical compositions. VTDMA was first introduced by Rader and McMurry (1986) to study the behavior of aerosols upon thermal treatment. Philippin et al. (2004) later developed a VTDMA which is capable of evaporating volatile materials in aerosols at temperatures up to 300 ℃. Non-volatile materials at 300 ℃, such as EC, non-volatile organics and sea salt, can internally mix with (or be coated with) volatile materials. ~~(VM) which evaporate during thermal treatment at elevated~~

~~temperatures. Based on the relative abundance of the non-volatile materials to VM, these internally mixed ambient aerosols can be categorized into three groups, namely the low volatility (LV), the medium volatility (MV) and the high volatility (HV) particles in VTDMA measurements (Wehner et al., 2004). When volatile materials exist as external mixtures with LV, MV and HV, they evaporate completely without leaving any residuals at elevated temperatures. They are referred as CV (completely vaporized) particles.~~ Note that the terms "volatile" and "non-volatile" are defined at the heating temperature of 300°C in the VTDMA. They are different from the volatilities defined under ambient conditions (Donahue et al., 2009; Murphy et al., 2014) or in other measurement techniques (Twomey, 1968; Pinnick et al., 1987; Huffman et al., 2009). The composition of these non-volatile residuals can vary spatially and temporally in VTDMA measurements. Previous studies have demonstrated good agreement between the mass of black carbon and the mass of particles with small volatile fractions, which experienced size reductions of 5 to 10% upon heating at 300 ℃ in the VTDMA. Various studies have also used an VTDMA to estimate the mixing states of soot particles. Particles with small volatile fractions are often assumed to be soot particles externally mixed with particles with volatile materials at 300 ℃. Particles with larger volatile fractions, which experienced size reductions of more than 10% upon heating at 300 ℃ in the VTDMA, were assumed to represent soot particles internally mixed (coated) with the volatile materials

~~An assumption often made in VTDMA measurements is that the majority of the non-volatile materials are EC. In some studies, the non-volatile materials measured in VTDMA poorly correlated with OC but gave better correlations with BC or light absorbing carbon (LAC)~~ (Philippin et al., 2004; Cheng et al., 2006; Frey et al., 2008; Wehner et al., 2009; Rose et al., 2011; Levy et al., 2014; Zhang et al., 2016). ~~On the other hand, Häkkinen et al. (2012) found that the mass fraction remaining (MFR) of non-BC residuals, which is the difference between the residual mass derived from a volatility differential mobility particle sizer (VDMPS) at 280 ℃ and black carbon mass derived from an aethalometer, is positively correlated with the mass fraction of organics measured by an AMS.~~

Organics ~~are also known as another contributor of~~also contribute to light absorption by atmospheric particles (Bond, 2001; Kirchstetter et al., 2004; Chen and Bond, 2010).~~However, because of its higher volatility compared to EC, they were often considered completely evaporated upon heating at temperatures above 300 ℃ in VTDMA studies. In recent years, it has been widely accepted organic aerosol exhibit a wide range of volatilities (Donahue et al.,~~

~~2011; Donahue et al., 2012). It is therefore possible, that a significant amount of non-volatile OC can exist together with EC in ambient aerosol, even after heating in a VTDMA.~~ Laboratory studies have shown that organic aerosols may form low volatility oligomers after aging for a long time (e.g. Kalberer et al., 2004). Huffman et al. (2009) showed that highly oxygenated, aged organic aerosols exhibited similar or lower volatility than the primary organic aerosols or the less oxygenated ones. Recently,~~On the other hand,~~ Häkkinen et al. (2012) found that the mass fraction remaining (MFR) of non-BC residuals, ~~which is~~i.e. the difference between the residual mass derived from a volatility differential mobility particle sizer ~~(VDMPS)~~ at 280 ℃ and black carbon mass derived from an aethalometer, is positively correlated with the mass fraction of organics measured by an AMS.

In this ~~paper~~study, ~~we report~~ simultaneous measurements of aerosols ~~of varying~~ volatility and carbonaceous matter were made at a~~n~~ suburban site ~~of~~ in Guangzhou, China during wintertime in February ~~to~~ and March 2014 using a VTDMA and a~~n~~ semi-continuous OC/EC analyzer, respectively. Volatility measurements were made for ambient aerosols ranging from 40 nm to 300 nm in diameter. Residuals remaining after heating at 300 ℃ in the VTDMA are referred to as non-volatile in this study. We report the average values, time series and diurnal variations in the number and volume fractions of the volatile and non-volatile materials, as well as the OC and EC concentrations. We examine the relationships of the non-volatile materials upon heating at 300 ℃ to EC and to the non-volatile OC, based on analyses of the diurnal patterns and mass closures of the OC/EC and VTDMA data. Finally, we discuss the influence of air mass origins on the volatility of the sampled aerosols and concentrations of OC and EC based on back trajectory analysis. ~~The term "volatile" components refer to those that evaporate at elevated temperatures and they may actually be semi-volatile under atmospheric conditions. We will first present the average, temporal and diurnal trends of the number and volume fractions of both non-volatile and volatile materials. We then conduct a closure analysis between the mass of non-volatile materials derived by the VTDMA and EC and OC measured by the OC/EC Analyzer to evaluate the significance of non-volatile OC in the VTDMA measurements.~~

2 Methodology

2.1 Experimental

2.1.1 Measurement details

The campaign was taken place at the China Meteorological Administration (CMA) Atmospheric Watch Network (CAWNET) Station in Panyu, Guangzhou, China in summer from July to September 2013 and winter from 6 February to 21 March 2014, which is operated by the Institute of Tropical and Marine Meteorology (ITMM) of the CMA. The Panyu station is located at the center of the PRD region and on the top of Dazhengang Mountain (23°00' N, 113°21' E) with an altitude of about 150 m (Figure S1 in Supplemental Information) (Tan et al., 2013a). It is about 120 m above the city average elevation and is surrounded by residential neighborhoods with no significant industrial pollution sources nearby. Measurements of particle number size distributions, volatility, mass concentrations of EC and OC were made in winter from 6 Feb to 21 Mar 2014. Some of the measurements were not made continuously due to maintenance work and hence only periods with both VTDMA and OC/EC measurements were analyzed.

2.1.2 VTDMA measurements

We used a custom-made VTDMA based on a Hygroscopic TDMA system developed in ITMM (Tan et al., 2013b), with the humidifier between the two DMAs replaced by a heated tube which effect evaporation of volatile materials. In our VTDMA system shown in Figure 1, ambient aerosols sampled by a $PM_{2.5}$ inlet first passed through a dryer at relative humidity below 20%. The dry aerosols then passed through a neutralizer and entered the first differential mobility analyzer (DMA_1) (Stream 1) to produce mono-disperse aerosols of diameter between 40 nm and 300 nm, D_0. The mono-disperse aerosols went either path (a) or (b) in ~~Figure~~ Fig. 1 after leaving DMA_1. In path (a), they (Stream 2) were directed to a condensation particle counter (CPC, TSI Model 3772) to obtain particle counts, N_{D0}. The particle number size distribution of the ambient aerosols, $dN/dlogD_p$, was also measured by varying the DMA_1 voltage (SMPS scan). Afterwards, the mono-disperse aerosols were directed via path (b) to a heated tube for volatility measurement (V-Mode) sequentially at 25 ℃, 100 ℃ and 300 ℃. The heating tube was a 1/2", 80 cm long stainless steel tube with an inner diameter of 8 mm. With a sample flow rate of 1 L min^{-1}, the resulting residence time in the heated section of the VTDMA was 2.4 s. The

estimated aerosol velocity on the center line was 0.33 m s^{-1}. Compared to the residence time of 0.3 s to 1 s in other VTDMA systems (e.g. Brooks et al., 2002; Philippin et al., 2004; Villani et al., 2007), the residence time in our VTDMA is assumed to be long enough for the volatile materials to be effectively vaporized. After leaving the heating tube, the flow entered a heat exchanger measuring 30 cm in length to ensure sufficient cooling before entering DMA_2.

Upon heating at 100 ℃ and ~~beyond~~above, volatile components of particles such as sulfate, nitrate and volatile organics would vaporize at different temperatures depending on their volatilities. A volatility shrinkage factor, *VSF*, is defined as the ratio of particle diameter after heating at temperature *T*, $D_{p,T}$, to that before heating, D_0, to indicate the size reduction of the ambient particles (Eq. (1)). The value of *VSF* is always smaller than or equal to one, depending on the amount of volatile materials vaporized at the heating temperature T.

$$VSF(T) = \frac{D_{p,T}}{D_0} \quad (1)$$

The *VSF* is also used to divide the particles into three groups, namely the low volatility (LV), medium volatility (MV) and high volatility (HV) particles. In this study, we focus on the measurements made at 300 ℃. The *VSF* ranges for LV, MV and HV particles upon heating at 300 ℃ are ~~larger than~~above 0.9, between 0.4 and 0.9 and ~~less than~~below 0.4, respectively (Fig~~ure 2b~~. 2) (Wehner et al., 2004; Wehner et al., 2009). The LV particles are assumed to represent EC particles externally mixed with the volatile materials, while MV and HV particles are assumed to represent EC particles internally mixed with volatile materials. While the volatile materials in the MV and HV particles are referred to as VM, those exist as external mixtures with the LV, MV and HV particles are referred to as completely vaporized (CV) particles. The CV particles evaporate completely without leaving behind any residuals at 300 ℃. Excluding particle diffusional and thermophoretic losses, the evaporation of VM and CV does not change the number concentrations of LV, MV and HV particles.

~~, resulting in the shrinking of particles and a~~The new size distribution, $dN'/d\log D_p$ of the remaining particles~~, i.e. the non-volatile materials in the LV/MV/HV aerosols~~ (hereafter ~~called~~ the residuals)~~. These size distributions of six selected diameters from DMA_1 (40 nm, 80 nm, 100 nm, 150 nm, 200 nm and 300 nm)~~ were measured by DMA_2 and CPC before they were heated at another temperature (Fig. 2b). Overall it took around one and a half to two hours to complete a cycle of measurements which consisted of SMPS scans and V-Mode measurements at 25 ℃, 100 ℃ and 300 ℃. At each temperature, the sampling time for six selected diameters

from DMA_1 (40 nm, 80 nm, 110 nm, 150 nm, 200 nm and 300 nm) took about half an hour and SMPS scans were made in-between. Hereafter, notations with the superscript prime refer to the LV~~/~~, MV or ~~/~~HV residuals measured by DMA_2 and CPC after heating, while the corresponding ones without the prime refer to the LV~~/~~, MV~~/~~ or HV residuals in ambient aerosols prior to heating.

~~Figure 2 illustrates how thermal treatment in the VTDMA affects the size distributions of the ambient aerosols. At each selected diameter D_0 (and at each temperature) in DMA_1 in the VTDMA, the particles include CV particles (purple) and LV, MV and HV particles that have VM (orange) internally mixed with the LV (blue), MV (green) and HV (red) residuals. After heating, the remaining particles form LV, MV and HV residuals without any CV or VM. Evaporation of VM and CV does not change the number concentrations of LV, MV and HV particles.~~

~~A volatility shrinkage factor, VSF, is defined as the ratio of particle diameter after heating, D_p, to that before heating, D_0, to indicate the size reduction of the ambient particles (Eq. (1)). The value of VSF is always smaller than or equal to one, depending on the amount of volatile materials vaporized,~~

~~$$VSF = \frac{D_p}{D_0} \quad (1)$$~~

~~The VSF range for LV, MV and HV are larger than 0.9, between 0.4 and 0.9 and less than 0.4, respectively (Figure 2b) (Wehner et al., 2004; Wehner et al., 2009).~~

~~Residual particles are either freshly emitted soot particles or other non-volatile material such as sea salt or crustal particles, which do not shrink significantly during heating (LV particles), or particles that exhibit a larger size change due to evaporation of volatile materials (MV and HV particles). Some volatile materials, such as sulfate and nitrate, are formed via chemical and/or photochemical reactions. They mix internally with the non-volatile materials during atmospheric aging process and evaporate at 300 ℃ in the VTDMA. Most of the organic species, including primary and secondary, also evaporated at this temperature. In urban areas, the majority of the non-volatile mass in submicron particles can be assumed to be soot (Kondo et al., 2006; Kuwata et al., 2007).~~

2.1.3 OC/EC measurements

A semi-continuous Sunset OC/EC Analyzer (Model 4) was used to measure $PM_{2.5}$ mass concentrations of organic carbon and elemental carbon, m_{OC} and m_{EC} respectively, on an hourly basis (Turpin et al., 1990; Birch and Cary, 1996; Wu et al., 2012). The OC/EC Analyzer adopts the ACE-Asia protocol (a NIOSH-derived protocol), where OC evaporates at four set temperatures of 310 ℃, 475 ℃, 615 ℃ and 870 ℃ with pure helium (He) as the carrier gas, and EC is combusted at temperatures between 550 ℃ and 870 ℃ under He and 2% oxygen (O_2)~~above 550 ℃~~ (Schauer et al., 2003; Wu et al., 2012). ~~Based on volatility and refractoriness,~~ ~~t~~The OC contents are named OC_1 to OC_4 based on the temperature protocol of the OC/EC analyzer (Table 1). The mass of EC determined at different temperatures will be grouped together for discussions~~ with OC_1 being most volatile~~. In the VTDMA measurements, there were volatile or semi-volatile OC which vaporize at 300 ℃ or below. These vaporized OC are assumed to be OC_1, which vaporizes at 310 ℃, although this OC/EC set temperature is slightly higher than the set temperature of 300 ℃ in the VTDMA. With this assumption, the residuals of the VTDMA at 300 ℃ (LV and MV residuals) are postulated to consist of (1) OC_2 to OC_4, which vaporize at 475 ℃ and above, and (2) EC and other refractory PM components. We have ignored the HV residuals as their contributions to the total volume of the particles are insignificant when compared to LV and MV residuals (~~see later~~Section 3.1). We will conduct a mass closure analysis based on the VTDMA and OC/EC measurements to examine this assumption.

2.2 Data analysis

2.2.1 Number fractions

The number fractions of LV, MV and HV residuals ($\Phi'_{N,LV}$, $\Phi'_{N,MV}$ and $\Phi'_{N,HV}$, with their sum being equal to unity) in Stream 2 on Fig. 1 were obtained from $dN'/d\log D_p$ measured by the CPC. However, these fractions ~~are not~~do not represent the actual number fractions of LV, MV and HV ~~residuals~~ particles ($\Phi_{N,LV}$, $\Phi_{N,MV}$ and $\Phi_{N,HV}$) ~~of the selected particles~~ before heating because they have not taken into account the CV particles and particle diffusional and thermophoretic losses. The number fraction of CV ($\Phi_{N,CV}$) is first obtained by considering the number fractions due to the residuals ($1-\Phi_{N,CV}$) and the number concentrations at a selected diameter D_0 before heating (N_{D0}) and after heating (N'):

$$N_{D_0} \times \eta_{D_0} \times \left(1 - \Phi_{N,CV}\right) = N' \quad (2)$$

where η_{D0} is the transport efficiency of particles.

Equation (2) assumes that η is the same for LV, MV and HV particles. η accounts for particle loss between DMA_1 and DMA_2 due to diffusion and thermophoretic forces (Philippin et al., 2004), and it varies with particle size and heating temperature. η at each particle diameter and VTDMA temperature was determined by laboratory calibrations with sodium chloride (NaCl) particles, which do not evaporate (i.e., $\Phi_{N,CV}$ = 0) at the ~~heating~~ temperatures used in our experiments. The transmission efficiency of NaCl of several selected diameters heated at temperatures between 50 ℃ and 300 ℃ is provided in the supplemental information (Fig. S2). From the known η and field measurements N_{D0} and N', $\Phi_{N,CV}$ was obtained from Eq. (2). Afterwards, $\Phi_{N,LV}$, $\Phi_{N,MV}$ and $\Phi_{N,HV}$ were obtained by renormalizing $\Phi'_{N,LV}$, $\Phi'_{N,MV}$ and $\Phi'_{N,HV}$ with (1-$\Phi_{N,CV}$) so that the sum of $\Phi_{N,LV}$, $\Phi_{N,MV}$, $\Phi_{N,HV}$ and $\Phi_{N,CV}$ equals to unity.

2.2.2 Volume fractions

The volume fractions of LV, MV, HV residuals and CV ($\Phi_{V,LV}$, $\Phi_{V,MV}$, $\Phi_{V,HV}$ and $\Phi_{V,CV}$) at each selected diameter D_0 are defined as the ratios of the volume of LV, MV, HV residuals and CV to the total volume of the mono-disperse particles before heating. By assuming that the residuals are in spherical shape, $\Phi_{V,LV}$, $\Phi_{V,MV}$ and $\Phi_{V,HV}$ can be calculated by:

$$\Phi_{V,i} = \frac{N_i \times \frac{\pi}{6} D_{p,i}^3}{N_{D_0} \times \frac{\pi}{6} D_0^3} = \Phi_{N,i} \times \frac{D_{p,i}^3}{D_0^3} \quad (3)$$

where N_i and $D_{p,i}$ are the number concentration and mean residual diameter of i = LV, MV or HV residuals.

For LV particles, it is assumed that D_0 and mean D_p are the same and hence $\Phi_{V,LV}$ is the same as $\Phi_{N,LV}$. For MV and HV particles, the mean D_p is smaller than D_0 due to the evaporation of volatile materials. The number weighted mean residual diameter (D_p) is calculated by:

$$D_{p,i} = \frac{\sum_j D_{p,i} \times N_{i,j}}{N_i} \quad (4)$$

where $D_{p,i}$ and $N_{i,j}$ are the residual diameter and number concentration of i = MV or HV at the 75 diameter bins (j) of *VSF*, respectively.

The volume fractions of the evaporated materials are calculated from the volume fractions of the residuals. The calculation for $\Phi_{V,CV}$ is similar to that for $\Phi_{V,LV}$. Since the particle has

completely vaporized, the vaporized volume is equivalent to the volume of the original particle. Hence, $\Phi_{V,CV}$ is the same as $\Phi_{N,CV}$:

$$\Phi_{V,CV} = \frac{N_{CV} \times \frac{\pi}{6} D_{p,CV}^3}{N_{Do} \times \frac{\pi}{6} D_o^3} = \Phi_{N,CV} \quad (5)$$

where $D_{p,CV} = D_0$. Since the sum of the total volume fraction of CV, VM and the residuals of LV, MV, HV equals to unity, $\Phi_{V,VM}$ was obtained after the above volume fractions were calculated. Furthermore, we also calculated the volume fraction remaining (*VFR*), defined as the volume ratio of the residuals to ~~their~~ its host particles, to aid ~~for MV and HV ($\Theta_{V,MV}$ and $\Theta_{V,HV}$) for~~ our discussions later:

$$\Theta VFR_{V,i} = \frac{N_i \times \frac{\pi}{6} D_{p,i}^3}{N_i \times \frac{\pi}{6} D_0^3} = \frac{D_{p,i}^3}{D_0^3} \quad (6)$$

where N_i and $D_{p,i}$ are the number concentration and mean residual diameter of i = MV or HV after heating, respectively.

2.2.3 Particle size distributions of number, volume and mass concentrations of LV, MV and HV residuals

Due to the differences in the size cuts of the VTDMA and the OC/EC Analyzer, log-normal fits extrapolated to 5 μm were applied to the particle number size distributions of the residuals of LV, MV and HV ($dN/dlogD_{p,i}$, where i = LV, MV or HV) to estimate the volume and then mass concentrations (calculated later) of the ambient aerosols for comparison with $PM_{2.5}$ OC/EC measurements. The volume size distributions ($dV/dlogD_{p,i}$) are calculated by:

$$\frac{dV}{dlogD_{p_i}} = \frac{dN}{dlogD_{p_i}} \times \frac{\pi}{6} D_{p,i}^3 \quad (7)$$

where $D_{p,i}$ is the mean residual diameter as defined in Section 2.2.2.

Volume (V) concentrations of LV, MV and HV residuals can then be calculated by integrating the area under the fitted curves. As we only focus on LV and MV, densities of 1.0 g cm^{-3} (Hitzenberger et al., 1999) and 1.5 g cm^{-3} are applied to V_{LV} and V_{MV} to obtain mass (m) concentrations of LV and MV residuals, respectively. The choice of the densities is based on the assumption that LV and MV residuals are dominated by soot and non-volatile OC, respectively.

3 Results and Discussions

3.1 Overview

The time series of meteorological conditions, particle number size distribution, $PM_{2.5}$, OC and EC concentrations during the campaign are presented in Fig. 3. Overall, the campaign came under the influence of the prevailing northerly wind with an average wind speed and temperature (± one standard deviation) of 1.73 ± 0.95 m s^{-1} and 14.8 ± 5.1 ℃, respectively. The average $PM_{2.5}$ concentration was 48 ± 26 μg m^{-3}. A few cold front periods were observed, during which the wind speed increased and the temperature decreased. In general, the low wind speed favored the accumulation of $PM_{2.5}$. OC concentrations ranged from 0.5 to 47.0 μg m^{-3} with an average of 9.0 ± 6.0 μg m^{-3}, while EC concentrations ranged from 0.2 to 23.0 μg m^{-3} with an average of 3.4 ± 3.0 μg m^{-3}. OC_1, the most volatile group among OC_1 to OC_4 in OC/EC analysis, accounted for one-third of the total carbon mass (Fig. 4).

On Feb 17, and Mar 12 and 17, the daily-averaged $PM_{2.5}$ concentrations exceeded 95 μg m^{-3}; they were nearly twice the daily-averaged values on other days (Fig. 3, shaded area in grey). Results of 72 h back trajectories (Stein et al., 2015; Rolph, 2016) showed that air masses arriving at the site on or before these three days mostly originated from the continental or oceanic area close to Eastern China (Fig. S3). The SMPS data also showed a mode near 100 nm with a high particle number concentration (Fig. 3).~~Figures 3 to 5 show the average values, time series and diurnal variation of $\Phi_{N,LV}$, $\Phi_{N,MV}$, $\Phi_{N,HV}$ and $\Phi_{N,CV}$ during the campaign, respectively. We will first discuss the trends of these number fractions and then the volume fractions. Finally, we attempt to conduct closure analysis for the non-volatile species (LV and MV residuals) with EC and OC_{2-4}. We focus only on the VTDMA data at 300 ℃ for comparison with the OC/EC data.~~

The temporal variation of the number concentration of MV particles having an initial diameter of 80 nm or above tracked reasonably well with the accumulation of $PM_{2.5}$ as particles aged and became more internally mixed (Fig. 3 and S4). Furthermore, a size dependence was observed for 80 nm to 300 nm MV particles. There were days, e.g., from Feb 24 to Mar 10, when the number concentration of 300 nm MV particles did not track well with $PM_{2.5}$. The mode of total particle number size distribution was below 100 nm and the number concentrations of 300 nm particles were low (Fig. 3). $PM_{2.5}$ tracked better with the number

concentrations of 80 nm to 150 nm MV particles (Fig. 4a to S4c) than those of 200 nm and 300 nm MV particles (Fig. S4d and S4e).

3.1.1 Number fractions

The average number fractions of CV and the residuals of LV, MV, and HV ($\Phi_{N,CV}$, $\Phi_{N,LV}$, $\Phi_{N,MV}$, and $\Phi_{N,HV}$) of 40 nm, 80 nm, 110 nm, 150 nm, 200 nm and 300 nm particles based on VTDMA measurements at 300 ℃ in Feb and Mar 2014 are shown in Figure 3. The average number and volume fractions of CV, HV, MV and LV in VTDMA measurements at 300 ℃ are summarized in Table 2. VM is internally mixed with (or coated on) MV and HV residuals, and hence it does not have a separate contribution to number concentrations. Overall, HV and MV particles, indicator for aged aerosols with internally mixed non-volatile and volatile materials, acounted for 57% to 71% of the total particle number concentration. Non-volatile materials (LV, MV and HV residuals) accounted for 15% to 26% of the total volume of selected particles before heating. While the CV and HV fractions were larger in the finest particles selected (D_0 = 40 nm), MV and LV were more abundant in larger particles (D_0 > 80 nm). As in Rose et al. (2006), fresh emissions like soot adsorbed or absorbed volatile materials during atmospheric processing. Smaller particles grew to a greater extent than the larger ones because of their higher ratios of surface area to volume. When they were heated in the VTDMA at 300 ℃, these smaller particles reduced more substantially in size, as reflected in the higher CV and HV fractions and lower MV and LV fractions. The higher abundance of MV and LV in larger size particles could also be explained by the non-volatile primary particles. Larger particles (D_0 > 80 nm) have more LV particles, while smaller particles have significantly more CV particles. At 40 nm, the mean ± standard deviation (SD) of $\Phi_{N,LV}$, $\Phi_{N,MV}$, $\Phi_{N,HV}$ and $\Phi_{N,CV}$ were 0.05 ± 0.026, 0.31 ± 0.097, 0.26 ± 0.097 and 0.38 ± 0.15 respectively. $\Phi_{N,CV}$ decreased while $\Phi_{N,HV}$, $\Phi_{N,MV}$ and $\Phi_{N,LV}$ increased as size increased from 40 nm to 80 nm and above. The lack of size dependence of number fractions for particles larger than 80 nm suggests that they may be the result of similar atmospheric processes. At 300 nm, the mean ± SD of $\Phi_{N,LV}$, $\Phi_{N,MV}$, $\Phi_{N,HV}$ and $\Phi_{N,CV}$ were 0.15 ± 0.047, 0.50 ± 0.125, 0.21 ± 0.097 and 0.14 ± 0.065 respectively. The large fraction of CV in 40 nm particles is likely due to nucleation of fresh emissions from more volatile primary sources or volatile secondary pollutants. Freshly emitted non-volatile primary sources such as EC and OC are in a larger size range. Larger particles also likely contain more internally mixed aged aerosols (secondary pollutants) than the smaller ones and these aged aerosols are likely more affected by meteorology. Yu et al. (2010) reported that the mass median aerodynamic

~~diameter~~condensation and droplet modes of ~~urban~~ EC and OC ~~in the condensation mode~~in urban sites of~~in~~ Guangzhou were approximately~~is about 380 nm~~ 400 nm and 900 nm, respectively. The mode of fresh EC emitted from vehicles is also approximately 400 nm (Huang et al., 2006). Larger particles also likely contain more internally mixed aged aerosols (secondary pollutants) than the smaller ones. Nevertheless, the detection limit of the downstream DMA and CPC in the VTDMA system is 10 nm. It was assumed that the residuals having a diameter below 10 nm were small enough to be considered as completely vaporized. However, such assumption would lead to an overestimation of CV and an underestimation of the non-volatile residuals for the finest particles selected (with an initial diameter of 40 nm). ~~Figure 4 shows the time series data of N_{LV}, N_{MV} and N_{HV}, $\Phi_{N,LV}$, $\Phi_{N,MV}$ and $\Phi_{N,HV}$, together with the mass concentration of $PM_{2.5}$. For 40 nm particles (Figure 4a and 4c), in both number concentrations and fractions, HV and MV were comparable and LV was very low. There was relatively little temporal variation of their concentrations and number fractions throughout the whole period. CV had a large fraction, varying between 0.2 and 0.6. For 300 nm particles (Figure 4b and 4d), CV, HV and LV fractions were small. N_{MV} tracks reasonably well with $PM_{2.5}$ mass because of its dominance in the number concentrations. Internally mixed soot particles, manifested as MV particles, play an important role in Guangzhou, especially during polluted days. CV had a rather stable fraction of about 0.15, much smaller than that for 40 nm particles.~~

3.2 Diurnal variations

Figure 5 shows the diurnal variation of the fraction of CV, HV residual, MV residual, LV residual and VM in the total volume of particles of dry initial diameters of 40, 150 and 300 nm. ~~number fractions. No obvious pattern of LV, MV, HV and CV was observed for particles larger than 80 nm.~~ For 40 nm particles, clear maximum and minimum of the fraction of CV ~~fraction~~, VM and HV residuals are observed at 08:00 ~~a.m.~~ and ~~01~~13:00 ~~p.m.~~, respectively. The diurnal variation of the HV and MV particles in 40 nm particles was clearer in terms of number fraction (Fig. S5). Furthermore, the trend of CV is opposite to those of VM, HV and MV. ~~For MV and HV, the average number concentrations increased since 08:00 a.m. and reached their maxima at 01:00 p.m.~~ The increase of CV in 40 nm particles and to a lesser extent of LV in 150 nm and 300 nm~~larger~~ particles in the morning ~~(Figure 5)~~ is consistent with traffic pattern, where freshly emitted volatile and non-volatile materials, likely OC and EC, are externally mixed and contributed to CV and LV, respectively. As time progresses in a day, the highly volatile species

(CV) which were freshly emitted in the morning, may evaporate and react to form less volatile particles and become VM instead of CV (Robinson et al., 2007). Alternatively, these CV particles could also coagulate with smaller particles to form VM containing particles. Less fresh emissions with more CV particles turning into VM on MV and HV particles can explain the trend that the number ~~concentration~~ and volume fractions of CV decreased while those of MV and HV increased (Fig. 5 and Fig. S5). ~~VM does not contribute to number fraction and its significance and diurnal variation will be discussed later in volume fraction. The lack of diurnal trends for particles larger than 80 nm suggests that they are dominated by aged particles accumulation likely due to low mixing height in the winter. Freshly emitted particles have little contributions to the number fractions.~~

~~3.2 Volume fractions~~

~~The average and diurnal variation of volume fractions of CV, the residuals of LV, MV, and HV, and VM are shown in Figure 6 and 7. Overall, the volume fractions of CV and VM are about 0.15 and 0.6, respectively (Figure 6), indicating that most of the original volume of the ambient particles has evaporated at 300 ℃. For 40 nm particles, CV and VM altogether contribute to almost 90% of the total volume. $\Phi_{V,LV}$, $\Phi_{V,MV}$ and $\Phi_{V,HV}$ are 0.15, 0.1 and less than 0.01, respectively. Size dependence of $\Phi_{V,CV}$, $\Phi_{V,LV}$, $\Phi_{V,MV}$ and $\Phi_{V,HV}$ are similar to number fractions: $\Phi_{V,CV}$ in 40 nm particles almost doubles and $\Phi_{V,LV}$ and $\Phi_{V,MV}$ are only half of those in 80 nm or larger particles, and is more dominant in larger size. CV are mostly found and hence contributed to $\Phi_{V,CV}$ in smaller particles while non-volatile materials contribute to $\Phi_{V,LV}$ in the larger particles.~~

~~The diurnal variation of $\Phi_{V,CV}$, $\Phi_{V,LV}$, $\Phi_{V,MV}$, $\Phi_{V,HV}$, $\Phi_{V,VM}$ and $\Theta_{V,MV}$ *and* $\Theta_{V,HV}$ (the volume ratio of the residuals to their host particles for MV and HV, respectively) are shown in Figure 7. Similar to the diurnal trends of the number fractions in Figure 5, there was no significant variation of $\Phi_{V,CV}$, $\Phi_{V,LV}$, $\Phi_{V,MV}$, and $\Phi_{V,HV}$ for all particle sizes except for 40 nm particles, where $\Phi_{V,VM}$ shows a trend opposite to $\Phi_{V,CV}$. The opposite trends of VM and CV can be explained by the trends of the number concentrations of MV+HV and CV. When there are more MV and HV particles, volume fraction of VM increases. Based on $\Theta_{V,MV}$ *and* $\Theta_{V,HV}$, about 70 to 80% of $\Phi_{V,VM}$ is from MV and there is no size dependence.~~

~~There was no obvious diurnal variation of $\Theta_{V,MV}$ and $\Theta_{V,HV}$ for all sizes (except for a minor peak at about 06:00 p.m. for $\Theta_{V,MV}$, which may be related to traffic), even for 40 nm particles where~~

~~there is an obvious diurnal trend of $\Phi_{V,VM}$, which is the volume ratio of volatile materials internally mixed with non-volatile components to total volume before heating.~~ We also used the diurnal variations in the volume fraction remaining (*VFR*), again defined as the volume ratio of the residual to its *host* particle (not to the total volume of all particles), to examine the size changes of the non-volatile residuals of HV and MV particles. The *VFR* of HV did not exhibit any obvious diurnal variations but the *VFR* of MV peaked near 18:00. The *VFR* of 40 nm MV particles increased after 14:00 while those of 150 nm and 300 nm MV particles increased after 15:00. Since the *VFR* of HV and MV were relatively constant during the day, t~~T~~he increase in VM fraction ~~$\Phi_{V,VM}$~~ after the morning rush hours is likely attributed to the increase in number concentrations of HV and MV particles ~~(N_{MV}) (Figure 5)~~ instead of changes in the amount of VM on the MV or HV residuals ~~since $\Theta_{V,MV}$ and $\Theta_{V,HV}$ are relatively constant~~.

~~Together with the lack of size dependence and diurnal variation on the different volatility components for particles of 80 nm or larger, the high volume contribution of VM and association with MV particles suggest that aerosols sampled at the Panyu station are moderately aged with a significant amount of volatile materials in this campaign.~~

The diurnal variations for particles larger than 80 nm were much less obvious than those for 40 nm particles in this study and in others (Rose et al., 2011; Cheng et al., 2012; Zhang et al., 2016). In winter, the atmosphere is more stable, resulting in a poorer dilution of aged particles with the less polluted aerosols from higher up (Rose et al., 2006). When the aged pollutants were trapped near the ground surface, the effect of aging of fresh emissions weakened. Therefore, although a daily maximum and a daily minimum were still observed for particles larger than 80 nm, the variation was mostly within 15%.

The diurnal variations in the mass fractions of OC and EC in $PM_{2.5}$ provided further insights to the observations above (Fig. 6). The OC and EC data on Mar 12 and 17 were excluded since they were more than two standard deviations higher than those on other days. Subtle morning peaks between 06:00 and 10:00 were observed for the volume fraction of LV residuals (Fig. 5). A similar peak was observed for the mass fraction of EC in $PM_{2.5}$ in the morning (Fig. 6). This suggests that LV particles may be related to the EC from vehicle emissions in the morning. This EC was relatively less aged and externally mixed with other volatile materials. In the late afternoon, LV residuals showed another peak between 17:00 and 19:00 whereas the mass fraction of EC in $PM_{2.5}$ exhibited a minimum at 15:00, after which it increased continuously.

The continuous increase in EC at night is likely related to the increase of heavy-duty diesel vehicles (Zhang et al., 2015), which was restricted during daytime (Bradsher, 2007).

Although OC_1 contributed to about half of the total OC mass, the diurnal variation in the mass fraction of OC in $PM_{2.5}$ was driven by the total mass of OC_2, OC_3 and OC_4 ($OC_{2\text{-}4}$), which reached a minimum between 05:00 and 09:00 and increased until 19:00. OC can be attributed to both primary and secondary sources. The increased mass fraction of OC in $PM_{2.5}$ and OC-to-EC ratio in the afternoon suggest that the sources of OC were less related to traffic but more to the aging and formation of secondary organic aerosols (Turpin et al., 1990; Chow et al., 1996). These OC_2, OC_3 and OC_4 may be highly oxygenated species or oligomers that are less volatile than primary or less oxygenated organics (Kalberer et al., 2004; Huffman et al., 2009).

It is interesting to note that the volume fraction of LV residuals and the *VFR* of MV particles at different sizes showed a dip in the afternoon (Fig. 5, third column from the left). The *VFR* of 40 nm MV particles showed a dip at 14:00 while those in 150 nm and 300 nm particles showed a dip at 15:00. The volume fraction of LV residuals in 150 nm and 300 nm particles reached a minimum at 13:00 and 15:00, respectively. Because EC decreased between 12:00 and 15:00, the increase in the volume fraction of LV residuals in 150 nm particles since 13:00 and the *VFR* of 40 nm MV particles since 14:00 may be related to the increased presence of aged organics as well as the EC particles which aged via coagulation and condensation.

3.3 Back trajectory analyses

We calculated the 72 h back trajectories of the air masses arriving at the sampling site (23°00′ N, 113°25′ E) at 4 h intervals (at 00:00, 04:00, 08:00, 12:00, 16:00 and 20:00 local time, UTC +8) using the PC version of the HYSPLIT4 (Hybrid Single Particle Lagrangian Integrated Trajectory, version 4) model (Stein et al., 2015; Rolph, 2016). Archived meteorological data from the Global Data Assimilation System (GDAS) 1-deg was employed and the receptor height was set at 500 m above ground level (a.g.l.). The 191 back trajectories calculated were grouped into six clusters based on their spatial distribution (Fig. 7).

Overall, the sampling site was mostly affected by northwesterly and northeasterly air masses. Cluster 1 and 3 are coastal and continental air masses, respectively, although both originated from the northeast. Clusters 4, 5 and 6 represent continental air masses originating from the northwest. Cluster 2 is a group of maritime air masses originating from the East China Sea northeast or east of Guangzhou. While air masses in cluster 6 were transported at relatively

high speeds and altitudes (over 3000 m a.g.l.), air masses in all the other clusters were transported at an altitude below 1500 m a.g.l. for over 40 h before arriving at the site. Nevertheless, air masses in cluster 6 only persisted for less than three days. Since the corresponding VTDMA and OC/EC data were sometimes unavailable, cluster 6 will be excluded from the following discussion.

The average $PM_{2.5}$, OC and EC concentrations associated with air masses from the northeast of Guangzhou (clusters 1, 2 and 3) were higher than those from the northwest (clusters 4 and 5, Table 3). Days associated with coastal and maritime air masses were more polluted than days associated with continental air masses for several reasons. First, south China as a region is often affected by the high pressure system moving eastward or southward from the continent out to sea in winter. When the maritime or coastal air streams entered from the southeast of the sampling site at Panyu, the atmosphere at the sampling site became more stable with low local wind speeds (e.g. the polluted days on Feb 17 and Mar 12, 16 and 17, Fig. 3 and S3). Local pollutants accumulated and the city was also affected by pollutants from the southeastern areas of the site (e.g. Shenzhen, Nansha and Dongguan). Second, land-sea breeze cycles were observed when the sampling site was under the influence of maritime air masses from Mar 18 to 20. During the day, southeasterly wind prevailed and the wind speed was higher. In the evening, the southeasterly wind was gradually replaced by a southwesterly or northwesterly wind and the wind speed decreased (Fig. 3). The cycle started again in the morning when the westerly wind was gradually replaced by southeasterly wind. Such land-sea breeze effects can result in an effective redistribution and accumulation of air pollutants within the PRD region (Lo et al., 2006).

Furthermore, $PM_{2.5}$ in the northeastern parts of China can exceed 200 μg m^{-3} due to both enhanced emissions from coal combustion for heating and poor dispersion during wintertime (Gu et al., 2014). Under the influence of the prevailing northerly or northeasterly wind in China, these pollutants were often transported to southern China and the East China Sea (Chen et al., 2012). Pollutants might also have accumulated when the maritime air masses spent about two days across Taiwan and the coast of south China. In contrast, continental air masses in cluster 5 moved slightly faster, and were often associated with the cold front period during which the local wind speed and pressure increased but the temperature decreased (Fig. 3). As the cold air masses passed through the city, dispersion and clearance of pollutants were promoted, resulting in lower $PM_{2.5}$ concentrations (Tan et al., 2013a). Therefore, unlike in other coastal cities like

Hong Kong (Lee et al., 2013), in Panyu maritime air masses could lead to more severe pollution than the continental ones in winter.

The five clusters were further analyzed to study the influence of air mass history on aerosol volatility. The number fractions of CV, HV, MV and LV of the six selected diameters in VTDMA measurements are regrouped based on the clusters as shown in Fig. 8. The total number fractions of the non-volatile residuals (sum of HV, MV and LV) were similar in all clusters. Maritime air masses (cluster 2) had a slightly higher fraction of LV particles while continental air masses originating from the northwest of the site (clusters 4 and 5) had a higher fraction of HV particles. Although the air masses in clusters 1 and 5 originated from farther away and traveled at relatively higher speeds than those in clusters 2, 3 and 4, all clusters involved transport at low altitudes (below 1500 m) for over 40 h, likely due to the generally lower mixing heights in winter. Therefore, aerosols in these air masses were all well-aged upon arrival (Wehner et al., 2009). This could be another reason for the lack of size dependence of the number, volume fractions and diurnal variation for particles larger than 80 nm. When the transported air masses mixed with local pollutants, the size dependence of the number fractions of different volatility groups as well as the aging of local emissions was further reduced.

We also examine at the volatility shrinkage factor (*VSF*) distributions of 40 nm, 110 nm and 300 nm particles upon heating at 300 ℃ (Fig. 9). Log-normal fittings with a three-peak solution were applied to the distributions. The average *VSF* modes of the peaks were located at 0.38 ± 0.021 (peak 1), 0.60 ± 0.066 (peak 2) and 0.95 ± 0.007 (peak 3), respectively. The standard deviation of the corresponding normal distribution (σ) of peak 3 was the smallest among the three peaks ($\sigma < 0.1$). For the same particle size, the *VSF* distributions in the *VSF* range between 0.3 and 0.8 in cluster 5 was relatively more uni-modal than those of other clusters (Fig. 9b and 9c). This suggests that the composition in cluster 5 was more homogeneous. Cluster 1 also consisted of long-range transported air masses but they likely passed through areas that are more polluted and mixed with different types of pollutants. Note that the fractions of HV, MV and LV have been traditionally defined based on the values of *VSF*, i.e. HV < 0.4; 0.4 < MV < 0.9; LV > 0.9 (Wehner et al., 2009). The *VSF* distributions above suggest that these definitions using *VSF* = 0.4 and 0.9 may need to be re-visited in the future.

3.4 New particle formation

Two new particle formation (NPF) events were observed in the campaign on Feb 20 and Mar 13 (Fig. 3). Since VTDMA data were not available during the NPF event on Mar 13, we only focus on the NPF event on Feb 20 which happened after a cold front under a low $PM_{2.5}$ concentration. On Feb 20, a sub-20 nm particle mode was first observed at 12:00. This particle mode grew continuously until it reached 120 nm at 02:00 on Feb 21. In VTDMA measurements, a sharp increase in the number concentration of HV particles having an initial diameter of 40 nm was observed at 17:00 on Feb 20 (Fig. 10). This event is likely related to the growth of the newly formed particles when they mixed with the volatile materials via condensation or adsorption. As these particles aged further, they grew larger as reflected in the increase in number concentrations of larger MV particles and the increase in $PM_{2.5}$ mass (Fig. 10). The growth of the newly formed particles can also be observed from the number size distributions of HV, MV and LV particles at different times on Feb 20 and 21 (Fig. 11). The mode of HV particles increased from 40 nm at 17:00 to 80 nm at 21:00 on Feb 20 Feb. The mode stayed at 80 nm while the corresponding number concentration decreased at 02:00 on Feb 21 Feb. In contrast, the number concentrations of MV particles grew continuously. The HV and MV particle concentrations and diameter modes underwent much smaller changes on the non-event day of Feb 28 (Fig. 11).

3.33.5 Closure analysis for LV, and MV residuals at 300°C, and OC/EC at 300°C and EC

Closure analysis of EC or EC+OC_{2-4} (the sum of EC, OC_2, OC_3, and OC_4) and the total mass of LV and MV residuals residuals of LV+MV is conducted (Figure 8. 12). Good correlations (R^2 > 0.9) for both EC and EC+OC_{2-4} the sum of EC, OC_2, OC_3, and OC_4 with the total mass of LV and MV residualsLV+MV were obtained. Nonetheless, the slope for the total mass of LV and MV residuals to the mass of EC m_{LV+MV} to m_{EC} (2.94) is more than two times of that for the total mass of LV and MV residuals to the sum of EC, OC_2, OC_3, and OC_4 m_{LV+MV} to $m_{EC+OC2-4}$ (1.22), indicating that EC alone cannot account for the total mass of LV and MV residualsmass of LV+MV. Including non-volatile OC (sum of OC_2 to OC_4) give better mass closure for with the total of LV and MV residuals. LV+MV and tThis observation further supports our initial postulation that LV and MVthe non-volatile residuals which remained intact upon heating at 300 ℃ in the VTDMA may contain a significant amount of non-volatile OC. However, mass of EC+OC_{2-4} the total mass of EC, OC_2, OC_3, and OC_4 do not explain all the mass of LV+MVLV

and MV residuals. A possible explanation could be that the vaporizing temperatures of some OC_1 are close to the upper limit (310 ℃), hence they were not completely vaporized in the heated tube and remained in non-volatile residuals~~LV+MV~~. The presence of other refractory materials and the assumption made about the density of LV and MV are two other possible explanations.~~, as well as errors during the measurements, could also be a reason for the difference. The extrapolated lognormal fitting of the size distribution of nonvolatile particles can cause errors if the mode diameter of the fitting is beyond the range of measurements of the VTDMA.~~

Other possible errors for the closure could be related to the different heating environments in the VTDMA and the OC/EC analyzer. In the OC/EC analyzer, OC was measured when the samples were heated in the presence of a non-oxidative carrier gas (He). ~~It should be noted that the heating environment in a VTDMA is different from that of an OC/EC Analyzer. In the VTDMA, aerosols were heated in the presence of oxygen, while in the OC/EC Analyzer, samples were heated in the presence of helium for OC. In the presence of oxygen, it is possible that OC_{2-4} in the aerosols may have evaporated in the VTDMA even at 300 ℃.~~ In the VTDMA, aerosols were heated in air which contained O_2. Therefore, some "OC_{2-4}" that evaporated at 475 ℃ or above in the OC/EC analyzer may have been oxidized at 300 ℃ in the VTDMA. Charring of organic matter could also occur (Philippin et al., 2004). Further study is needed to quantify the effect of oxygen on the oxidation of OC in the VTDMA. The extrapolated lognormal fitting of the size distribution of non-volatile particles can also cause errors if the mode diameter of the fitting is beyond the VTDMA's range of measurements~~ of the VTDMA~~. While the VTDMA measured the size distribution of particles between 10 nm and 400 nm in diameter, the OC/EC analyzer took into account particles up to 2.5 μm in diameter. Yu et al. (2010) reported three EC and OC modes between 0.4 μm and 10 μm in ambient aerosols in Guangzhou: 0.4, 0.9 and 5 μm. The 0.4 μm mode accounted for 44% to 49% of the measured EC but only 17% to 20% of the measured OC.

4 Conclusions

This study presents the first VTDMA measurements in a suburban area of Guangzhou in the Pearl River Delta, China during wintertime. The LV fraction was assumed to be EC particles. These particles were externally mixed with volatile materials at 300 ℃ and contributed to less than 20% of the total particle number concentration at the sampling site. The diurnal variations

in the number and volume fractions of LV, MV and HV were much less obvious in this study than in other studies likely because of the more stable atmosphere and poorer dilution of aged aerosols in winter. Back trajectory analysis showed that the measured $PM_{2.5}$, EC and OC concentrations were higher when the sampling site came under the influence of maritime and coastal air masses originating from the east or northeast of the site. These observations are attributed to the high pressure system on the continent, the prevailing northerly wind and the enhanced pollution from north China in winter. Long-range transport continental trajectories were often associated with the cold front periods during which the dispersion of pollutants was promoted. The number fractions of LV, MV and HV particles did not show much variations among the clusters, likely because the air masses in all clusters were transported at low altitudes (below 1500 m) for over 40 h. They were therefore well-aged upon arrival at the site.

While previous studies have demonstrated soot as a major component of the non-volatile residuals at 300 ℃ measured by the VTDMA, this work identified non-volatile organics as another possible component. The diurnal variations in the LV fractions and the size of the MV residuals may be related to the variation in the abundance of both EC and non-volatile OC, which evaporated at 475 ℃ and above in the OC/EC analyzer. Analyses of the diurnal variations in the LV fractions and the *VFR* of MV particles, the latter of which reflects the change in size of the non-volatile materials in the MV particles, suggest that the increase in non-volatile fractions and size in the early afternoon may be related to the increase in non-volatile OC in addition to the effects of EC coagulation and condensation. The mass closure analysis of EC and non-volatile OC and the total mass of LV and MV residuals also suggest that non-volatile OC may have contributed to non-volatile residuals in our VTDMA measurements.

~~This study presents the first VTDMA measurements in the PRD, China. The measured volatility characteristics of ambient aerosols reflect the difference of the freshly emitted 40 nm particles and the aged bigger ones (80 nm to 300 nm). The 40 nm particles had 50% of particles that completely evaporated at 300 ℃. Particles larger than 80 nm were more aged and contained volatile components (VM) internally mixed with non-volatile residuals (MV) and VM contributed to over 50% of the total volume fraction for all particles. From the mass closure analysis of the VTDMA data and OC/EC data, it is likely that the non-volatile residuals at 300 ℃ observed in VTDMA also contained some less volatile OC (OC_{2-4}).~~

~~Cheng et al. (2009) performed an aerosol optical closure to investigate the aerosol light absorption coefficient and single scattering albedo using the soot mixing states determined by a VTDMA in Yufa, Beijing. It is possible that some less volatile OCs (OC_{2-4}) also absorb light.~~

~~The mixing state is a key parameter for accurately assessing the climatic impacts of soot particles (Jacobson, 2001). In this study, we found that externally mixed soot particles contribute to about 10% for 40 nm particles and about 15% for 80 nm and larger particles in number concentration. Such external mixing needs to be accounted for in assessing climatic impacts of soot particles in the region.~~

Supplemental Information~~: Location of the measurement site~~

Fig. S1. Location of the measurement site.

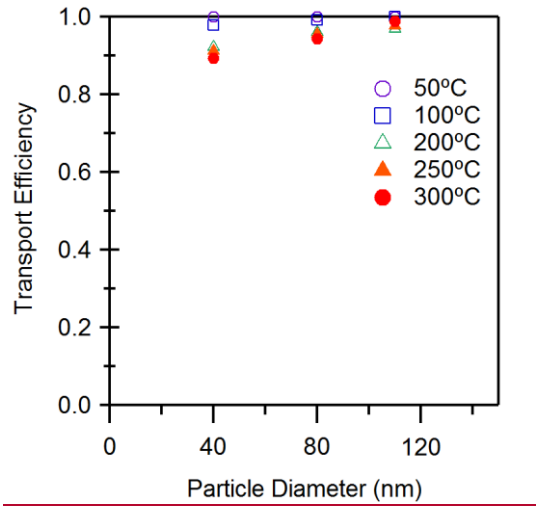

Fig. S2. Transport efficiency of NaCl in the VTDMA as a function of particle diameter and heating temperature.

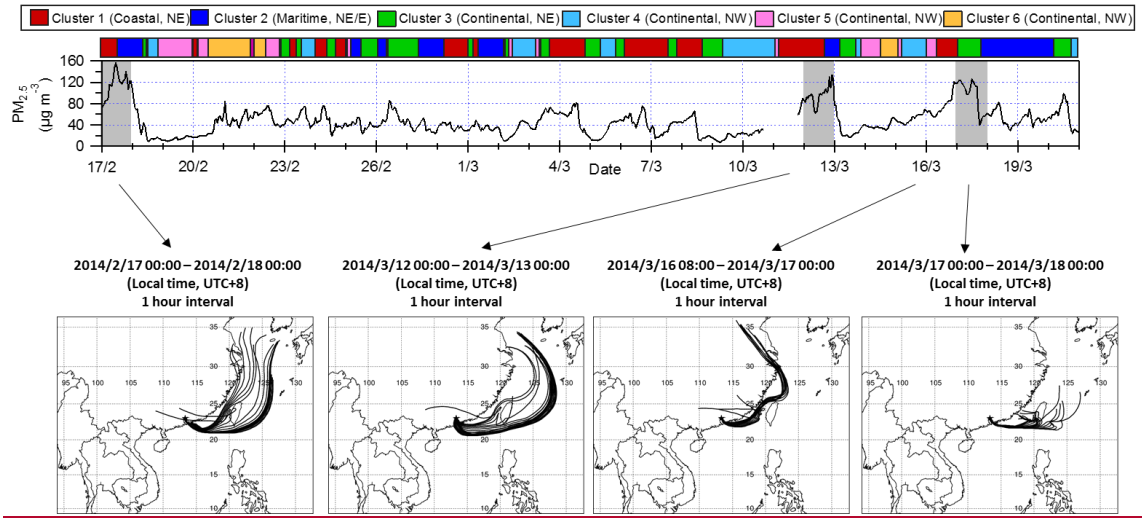

Fig. S3. Time series of $PM_{2.5}$ concentrations and 72 h back trajectories at hourly intervals on Feb 17, and Mar 12, 16 and 17.

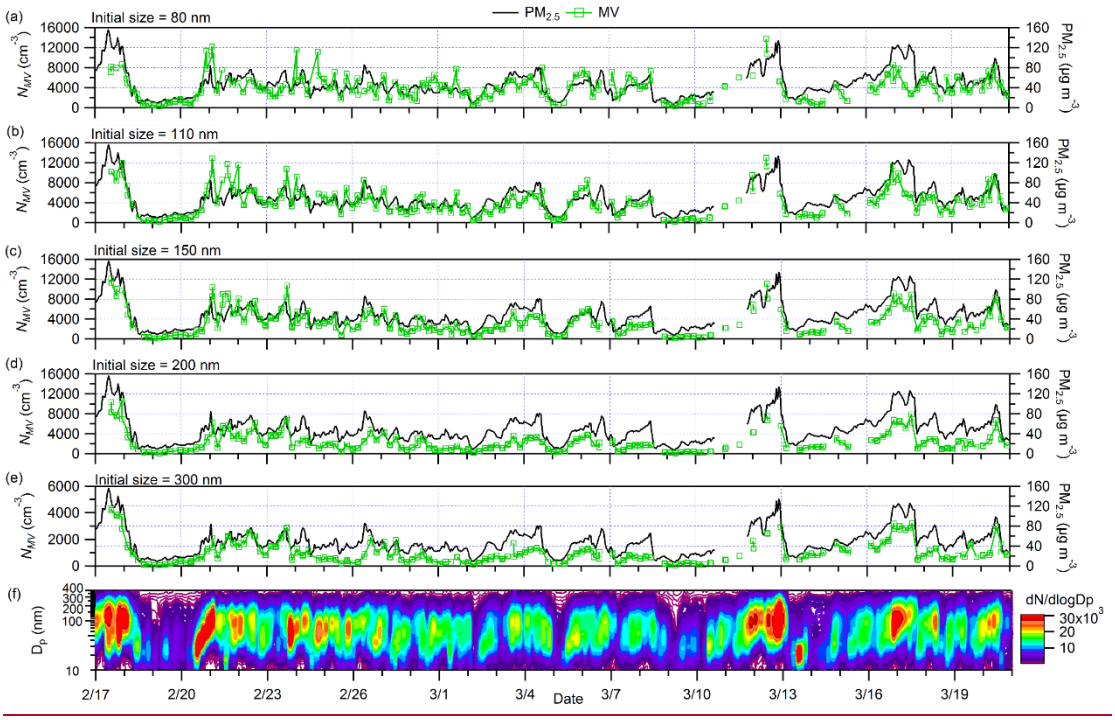

Fig. S4. (a–e) Time series of number concentrations of MV particles having initial diameters of 80 nm to 300 nm and (f) particle number size distributions during the campaign. Time series of $PM_{2.5}$ concentrations are plotted on the right axis in (a) to (e).

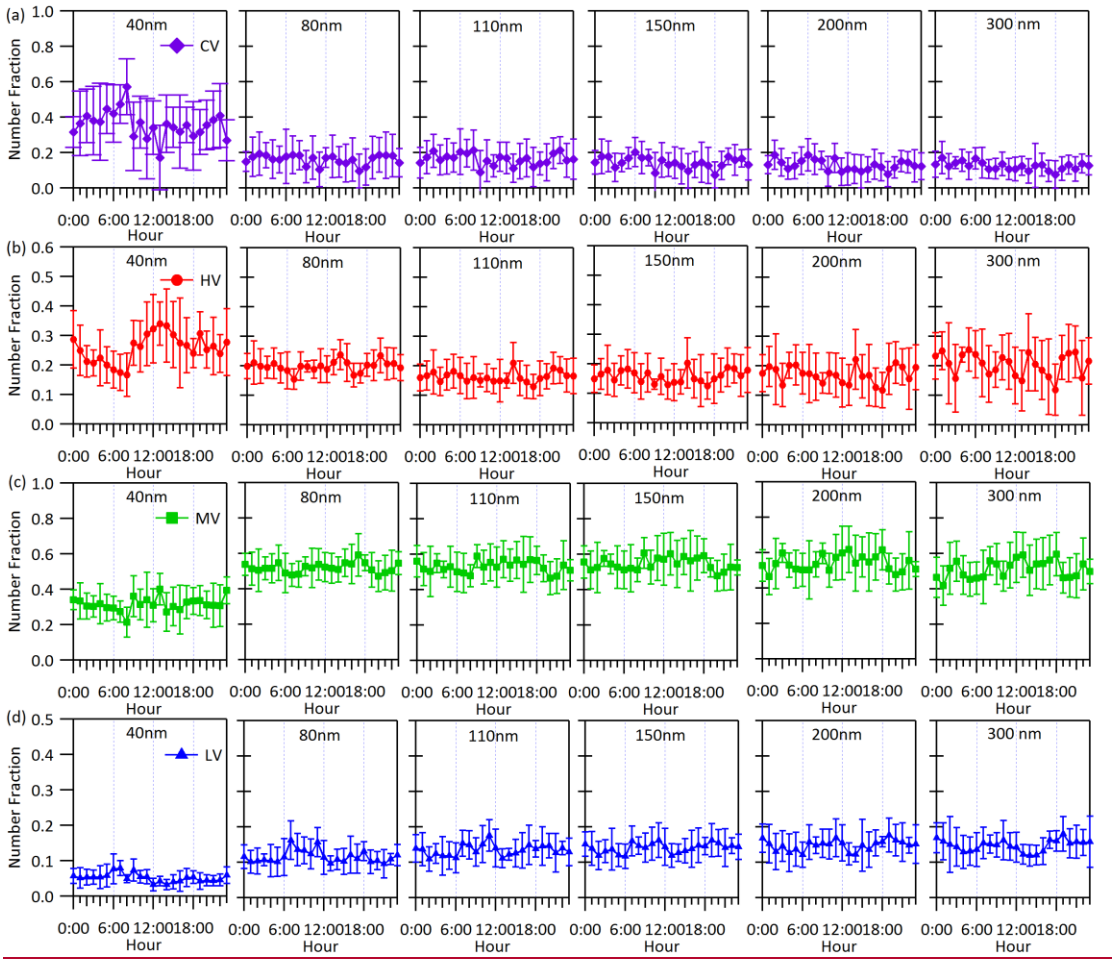

Fig. S5. (a–d) Diurnal variations in the number fractions of CV, HV, MV and LV particles having (from left to right) the six selected diameters ranging from 40 nm to 300 nm. Error bars represent one standard deviation.

Acknowledgements

This work is supported by the Research Grants Council of the Hong Kong Special Administrative Region, China (Project No. 600413), the Natural Science Foundation of China (Grant 41375156), Special Research and Development Fund for Research Institutes (2014EG137243) and the National Key Project of Basic Research (2011CB403403).

References

Andreae, M. O., Schmid, O., Yang, H., Chand, D., Zhen Yu, J., Zeng, L.-M., and Zhang, Y.-H.: Optical properties and chemical composition of the atmospheric aerosol in urban Guangzhou, China, Atmos. Environ., 42, 6335-6350, http://dx.doi.org/10.1016/j.atmosenv.2008.01.030, 2008.

Birch, M. E., and Cary, R. A.: Elemental carbon-based method for monitoring occupational exposures to particulate diesel exhaust, Aerosol Science and Technology, 25, 221-241, 10.1080/02786829608965393, 1996.

Bond, T. C.: Spectral dependence of visible light absorption by carbonaceous particles emitted from coal combustion, Geophysical Research Letters, 28, 4075-4078, 10.1029/2001GL013652, 2001.

Bradsher, K.: Trucks power China's economy, at a suffocating cost., The New York Times, NY, USA, http://www.nytimes.com/2007/12/08/world/asia/08trucks.html, 2007.

Brooks, B. J., Smith, M. H., Hill, M. K., and O'Dowd, C. D.: Size-differentiated volatility analysis of internally mixed laboratory-generated aerosol, Journal of Aerosol Science, 33, 555-579, http://dx.doi.org/10.1016/S0021-8502(01)00192-6, 2002.

Burtscher, H., Baltensperger, U., Bukowiecki, N., Cohn, P., Hüglin, C., Mohr, M., Matter, U., Nyeki, S., Schmatloch, V., Streit, N., and Weingartner, E.: Separation of volatile and non-volatile aerosol fractions by thermodesorption: instrumental development and applications, Journal of Aerosol Science, 32, 427-442, http://dx.doi.org/10.1016/S0021-8502(00)00089-6, 2001.

Chan, C. K., and Yao, X.: Air pollution in mega cities in China, Atmos. Environ., 42, 1-42, 10.1016/j.atmosenv.2007.09.003, 2008.

Chen, B., Du, K., Wang, Y., Chen, J., Zhao, J., Wang, K., Zhang, F., and Xu, L.: Emission and transport of carbonaceous aerosols in urbanized coastal areas in China, 2012.

Chen, Y., and Bond, T. C.: Light absorption by organic carbon from wood combustion, Atmos. Chem. Phys., 10, 1773-1787, 10.5194/acp-10-1773-2010, 2010.

Cheng, Y., He, K.-b., Duan, F.-k., Zheng, M., Du, Z.-y., Ma, Y.-l., and Tan, J.-h.: Ambient organic carbon to elemental carbon ratios: Influences of the measurement methods and implications, Atmos. Environ., 45, 2060-2066, http://dx.doi.org/10.1016/j.atmosenv.2011.01.064, 2011.

Cheng, Y. F., Eichler, H., Wiedensohler, A., Heintzenberg, J., Zhang, Y. H., Hu, M., Herrmann, H., Zeng, L. M., Liu, S., Gnauk, T., Brüggemann, E., and He, L. Y.: Mixing state of elemental carbon and non-light-absorbing aerosol components derived from in situ particle optical properties at Xinken in Pearl River Delta of China, Journal of Geophysical Research: Atmospheres, 111, D20204, 10.1029/2005JD006929, 2006.

Cheng, Y. F., Berghof, M., Garland, R. M., Wiedensohler, A., Wehner, B., Müller, T., Su, H., Zhang, Y. H., Achtert, P., Nowak, A., Pöschl, U., Zhu, T., Hu, M., and Zeng, L. M.:

Influence of soot mixing state on aerosol light absorption and single scattering albedo during air mass aging at a polluted regional site in northeastern China, Journal of Geophysical Research: Atmospheres, 114, D00G10, 10.1029/2008JD010883, 2009.

Cheng, Y. F., Su, H., Rose, D., Gunthe, S. S., Berghof, M., Wehner, B., Achtert, P., Nowak, A., Takegawa, N., Kondo, Y., Shiraiwa, M., Gong, Y. G., Shao, M., Hu, M., Zhu, T., Zhang, Y. H., Carmichael, G. R., Wiedensohler, A., Andreae, M. O., and Pöschl, U.: Size-resolved measurement of the mixing state of soot in the megacity Beijing, China: diurnal cycle, aging and parameterization, Atmos. Chem. Phys., 12, 4477-4491, 10.5194/acp-12-4477-2012, 2012.

Chow, J. C., Watson, J. G., Lowenthal, D. H., Solomon, P. A., Magliano, K. L., Ziman, S. D., and Richards, L. W.: PM10 and PM2.5 compositions in California's San Joaquin Valley, Aerosol Science and Technology, 18, 105-128, 1993.

Chow, J. C., Watson, J. G., Lu, Z., Lowenthal, D. H., Frazier, C. A., Solomon, P. A., Thuillier, R. H., and Magliano, K.: Descriptive analysis of PM2.5 and PM10 at regionally representative locations during SJVAQS/AUSPEX, Atmos. Environ., 30, 2079-2112, http://dx.doi.org/10.1016/1352-2310(95)00402-5, 1996.

Chow, J. C., Yu, J. Z., Watson, J. G., Hang Ho, S. S., Bohannan, T. L., Hays, M. D., and Fung, K. K.: The application of thermal methods for determining chemical composition of carbonaceous aerosols: A review, Journal of Environmental Science and Health Part A, 42, 1521-1541, 2007.

Donahue, N. M., Robinson, A. L., and Pandis, S. N.: Atmospheric organic particulate matter: From smoke to secondary organic aerosol, Atmospheric Environment, 43, 94-106, http://dx.doi.org/10.1016/j.atmosenv.2008.09.055, 2009.

Donahue, N. M., Epstein, S. A., Pandis, S. N., and Robinson, A. L.: A two-dimensional volatility basis set: 1. organic-aerosol mixing thermodynamics, Atmos. Chem. Phys., 11, 3303-3318, 10.5194/acp-11-3303-2011, 2011.

Donahue, N. M., Kroll, J. H., Pandis, S. N., and Robinson, A. L.: A two-dimensional volatility basis set – Part 2: Diagnostics of organic-aerosol evolution, Atmos. Chem. Phys., 12, 615-634, 10.5194/acp-12-615-2012, 2012.

Frey, A., Rose, D., Wehner, B., Müller, T., Cheng, Y., Wiedensohler, A., and Virkkula, A.: Application of the Volatility-TDMA Technique to Determine the Number Size Distribution and Mass Concentration of Less Volatile Particles, Aerosol Science and Technology, 42, 817-828, 10.1080/02786820802339595, 2008.

Fuller, K. A., Malm, W. C., and Kreidenweis, S. M.: Effects of mixing on extinction by carbonaceous particles, Journal of Geophysical Research: Atmospheres, 104, 15941-15954, 10.1029/1998JD100069, 1999.

Ghazi, R., and Olfert, J. S.: Coating Mass Dependence of Soot Aggregate Restructuring due to Coatings of Oleic Acid and Dioctyl Sebacate, Aerosol Science and Technology, 47, 192-200, 10.1080/02786826.2012.741273, 2012.

Gnauk, T., Müller, K., van Pinxteren, D., He, L.-Y., Niu, Y., Hu, M., and Herrmann, H.: Size-segregated particulate chemical composition in Xinken, Pearl River Delta, China: OC/EC and organic compounds, Atmos. Environ., 42, 6296-6309, http://dx.doi.org/10.1016/j.atmosenv.2008.05.001, 2008.

Gu, J., Du, S., Han, D., Hou, L., Yi, J., Xu, J., Liu, G., Han, B., Yang, G., and Bai, Z.-P.: Major chemical compositions, possible sources, and mass closure analysis of PM2.5 in Jinan, China, Air Quality, Atmosphere & Health, 7, 251-262, 10.1007/s11869-013-0232-9, 2014.

Häkkinen, S. A. K., Äijälä, M., Lehtipalo, K., Junninen, H., Backman, J., Virkkula, A., Nieminen, T., Vestenius, M., Hakola, H., Ehn, M., Worsnop, D. R., Kulmala, M., Petäjä, T., and Riipinen, I.: Long-term volatility measurements of submicron atmospheric aerosol in Hyytiälä, Finland, Atmos. Chem. Phys., 12, 10771-10786, 10.5194/acp-12-10771-2012, 2012.

Hansen, A. D. A., Rosen, H., and Novakov, T.: The Aethalometer - An Instrument for the Real-Time Measurement of Optical-Absorption by Aerosol-Particles Sci. Total Environ., 36, 191-196, 10.1016/0048-9697(84)90265-1, 1984.

Hitzenberger, R., Jennings, S. G., Larson, S. M., Dillner, A., Cachier, H., Galambos, Z., Rouc, A., and Spain, T. G.: Intercomparison of measurement methods for black carbon aerosols, Atmos. Environ., 33, 2823-2833, http://dx.doi.org/10.1016/S1352-2310(98)00360-4, 1999.

Horvath, H.: Atmospheric light absorption—A review, Atmospheric Environment. Part A. General Topics, 27, 293-317, http://dx.doi.org/10.1016/0960-1686(93)90104-7, 1993.

Huang, X.-F., Yu, J. Z., He, L.-Y., and Hu, M.: Size Distribution Characteristics of Elemental Carbon Emitted from Chinese Vehicles: Results of a Tunnel Study and Atmospheric Implications, Environmental Science & Technology, 40, 5355-5360, 10.1021/es0607281, 2006.

Huffman, J. A., Docherty, K. S., Aiken, A. C., Cubison, M. J., Ulbrich, I. M., DeCarlo, P. F., Sueper, D., Jayne, J. T., Worsnop, D. R., Ziemann, P. J., and Jimenez, J. L.: Chemically-resolved aerosol volatility measurements from two megacity field studies, Atmos. Chem. Phys., 9, 7161-7182, 10.5194/acp-9-7161-2009, 2009.

Japar, S. M., Brachaczek, W. W., Gorse Jr, R. A., Norbeck, J. M., and Pierson, W. R.: The contribution of elemental carbon to the optical properties of rural atmospheric aerosols, Atmospheric Environment (1967), 20, 1281-1289, http://dx.doi.org/10.1016/0004-6981(86)90163-0, 1986.

Kalberer, M., Paulsen, D., Sax, M., Steinbacher, M., Dommen, J., Prevot, A. S. H., Fisseha, R., Weingartner, E., Frankevich, V., Zenobi, R., and Baltensperger, U.: Science, 303, 1659, 2004.

Kirchstetter, T. W., Novakov, T., and Hobbs, P. V.: Evidence that the spectral dependence of light absorption by aerosols is affected by organic carbon, Journal of Geophysical Research: Atmospheres, 109, D21208, 10.1029/2004JD004999, 2004.

Kondo, Y., Komazaki, Y., Miyazaki, Y., Moteki, N., Takegawa, N., Kodama, D., Deguchi, S., Nogami, M., Fukuda, M., Miyakawa, T., Morino, Y., Koike, M., Sakurai, H., and Ehara, K.: Temporal variations of elemental carbon in Tokyo, Journal of Geophysical Research: Atmospheres, 111, D12205, 10.1029/2005JD006257, 2006.

Kuwata, M., Kondo, Y., Mochida, M., Takegawa, N., and Kawamura, K.: Dependence of CCN activity of less volatile particles on the amount of coating observed in Tokyo, Journal of Geophysical Research: Atmospheres, 112, D11207, 10.1029/2006JD007758, 2007.

Lavanchy, V. M. H., Gäggeler, H. W., Nyeki, S., and Baltensperger, U.: Elemental carbon (EC) and black carbon (BC) measurements with a thermal method and an aethalometer at the high-alpine research station Jungfraujoch, Atmos. Environ., 33, 2759-2769, http://dx.doi.org/10.1016/S1352-2310(98)00328-8, 1999.

Lee, B. P., Li, Y. J., Yu, J. Z., Louie, P. K. K., and Chan, C. K.: Physical and chemical characterization of ambient aerosol by HR-ToF-AMS at a suburban site in Hong Kong during springtime 2011, Journal of Geophysical Research: Atmospheres, 118, 8625-8639, 10.1002/jgrd.50658, 2013.

Levy, M. E., Zhang, R., Zheng, J., Tan, H., Wang, Y., Molina, L. T., Takahama, S., Russell, L. M., and Li, G.: Measurements of submicron aerosols at the California–Mexico border during the Cal–Mex 2010 field campaign, Atmos. Environ., 88, 308-319, http://dx.doi.org/10.1016/j.atmosenv.2013.08.062, 2014.

Liousse, C., Cachier, H., and Jennings, S. G.: Optical and thermal measurements of black carbon aerosol content in different environments: Variation of the specific attenuation cross-section, sigma (σ), Atmospheric Environment. Part A. General Topics, 27, 1203-1211, http://dx.doi.org/10.1016/0960-1686(93)90246-U, 1993.

Lo, J. C. F., Lau, A. K. H., Fung, J. C. H., and Chen, F.: Investigation of enhanced cross-city transport and trapping of air pollutants by coastal and urban land-sea breeze circulations, Journal of Geophysical Research: Atmospheres, 111, n/a-n/a, 10.1029/2005JD006837, 2006.

Murphy, B. N., Donahue, N. M., Robinson, A. L., and Pandis, S. N.: A naming convention for atmospheric organic aerosol, Atmos. Chem. Phys., 14, 5825-5839, 10.5194/acp-14-5825-2014, 2014.

Novakov, T., Ramanathan, V., Hansen, J. E., Kirchstetter, T. W., Sato, M., Sinton, J. E., and Sathaye, J. A.: Large historical changes of fossil-fuel black carbon aerosols, Geophysical Research Letters, 30, 4, 10.1029/2002gl016345, 2003.

O'Dowd, C. D., Jennings, S. G., Smith, M. H., and Cooke, W.: A high temperature volatility technique for determination of atmospheric aerosol composition, Journal of Aerosol Science, 23, Supplement 1, 905-908, http://dx.doi.org/10.1016/0021-8502(92)90558-D, 1992.

Onasch, T. B., Trimborn, A., Fortner, E. C., Jayne, J. T., Kok, G. L., Williams, L. R., Davidovits, P., and Worsnop, D. R.: Soot Particle Aerosol Mass Spectrometer: Development, Validation,

and Initial Application, Aerosol Science and Technology, 46, 804-817, 10.1080/02786826.2012.663948, 2012.

Penner, J. E., and Novakov, T.: Carbonaceous particles in the atmosphere: A historical perspective to the Fifth International Conference on Carbonaceous Particles in the Atmosphere, Journal of Geophysical Research: Atmospheres, 101, 19373-19378, 10.1029/96JD01175, 1996.

Petzold, A., and Schönlinner, M.: Multi-angle absorption photometry—a new method for the measurement of aerosol light absorption and atmospheric black carbon, Journal of Aerosol Science, 35, 421-441, http://dx.doi.org/10.1016/j.jaerosci.2003.09.005, 2004.

Philippin, S., Wiedensohler, A., and Stratmann, F.: Measurements of non-volatile fractions of pollution aerosols with an eight-tube volatility tandem differential mobility analyzer (VTDMA-8), Journal of Aerosol Science, 35, 185-203, http://dx.doi.org/10.1016/j.jaerosci.2003.07.004, 2004.

Pinnick, R., Jennings, S., and Fernandez, G.: Volatility of aerosols in the arid southwestern United States, Journal of the atmospheric sciences, 44, 562-576, 1987.

Putaud, J. P., Van Dingenen, R., Alastuey, A., Bauer, H., Birmili, W., Cyrys, J., Flentje, H., Fuzzi, S., Gehrig, R., Hansson, H. C., Harrison, R. M., Herrmann, H., Hitzenberger, R., Hüglin, C., Jones, A. M., Kasper-Giebl, A., Kiss, G., Kousa, A., Kuhlbusch, T. A. J., Löschau, G., Maenhaut, W., Molnar, A., Moreno, T., Pekkanen, J., Perrino, C., Pitz, M., Puxbaum, H., Querol, X., Rodriguez, S., Salma, I., Schwarz, J., Smolik, J., Schneider, J., Spindler, G., ten Brink, H., Tursic, J., Viana, M., Wiedensohler, A., and Raes, F.: A European aerosol phenomenology – 3: Physical and chemical characteristics of particulate matter from 60 rural, urban, and kerbside sites across Europe, Atmos. Environ., 44, 1308-1320, http://dx.doi.org/10.1016/j.atmosenv.2009.12.011, 2010.

Rader, D. J., and McMurry, P. H.: Application of the tandem differential mobility analyzer to studies of droplet growth or evaporation, Journal of Aerosol Science, 17, 771-787, 1986.

Robinson, A. L., Donahue, N. M., Shrivastava, M. K., Weitkamp, E. A., Sage, A. M., Grieshop, A. P., Lane, T. E., Pierce, J. R., and Pandis, S. N.: Rethinking organic aerosols: Semivolatile emissions and photochemical aging, Science, 315, 1259-1262, 10.1126/science.1133061, 2007.

Rolph, G. D.: Real-time Environmental Applications and Display sYstem (READY) Website (http://www.ready.noaa.gov), 2016.

Rose, D., Wehner, B., Ketzel, M., Engler, C., Voigtländer, J., Tuch, T., and Wiedensohler, A.: Atmospheric number size distributions of soot particles and estimation of emission factors, Atmos. Chem. Phys., 6, 1021-1031, 10.5194/acp-6-1021-2006, 2006.

Rose, D., Gunthe, S. S., Su, H., Garland, R. M., Yang, H., Berghof, M., Cheng, Y. F., Wehner, B., Achtert, P., Nowak, A., Wiedensohler, A., Takegawa, N., Kondo, Y., Hu, M., Zhang, Y., Andreae, M. O., and Pöschl, U.: Cloud condensation nuclei in polluted air and biomass burning smoke near the mega-city Guangzhou, China – Part 2: Size-resolved aerosol

chemical composition, diurnal cycles, and externally mixed weakly CCN-active soot particles, Atmos. Chem. Phys., 11, 2817-2836, 10.5194/acp-11-2817-2011, 2011.

Rosen, H., Hansen, A. D. A., Gundel, L., and Novakov, T.: Identification of the optically absorbing component in urban aerosols, Applied Optics, 17, 3859-3861, 10.1364/AO.17.003859, 1978.

Schauer, J. J., Mader, B. T., Deminter, J. T., Heidemann, G., Bae, M. S., Seinfeld, J. H., Flagan, R. C., Cary, R. A., Smith, D., Huebert, B. J., Bertram, T., Howell, S., Kline, J. T., Quinn, P., Bates, T., Turpin, B., Lim, H. J., Yu, J. Z., Yang, H., and Keywood, M. D.: ACE-Asia intercomparison of a thermal-optical method for the determination of particle-phase organic and elemental carbon, Environmental Science & Technology, 37, 993-1001, 10.1021/es020622f, 2003.

Stein, A. F., Draxler, R. R., Rolph, G. D., Stunder, B. J. B., Cohen, M. D., and Ngan, F.: NOAA's HYSPLIT Atmospheric Transport and Dispersion Modeling System, Bulletin of the American Meteorological Society, 96, 2059-2077, 10.1175/BAMS-D-14-00110.1, 2015.

Stephens, M., Turner, N., and Sandberg, J.: Particle identification by laser-induced incandescence in a solid-state laser cavity, Applied Optics, 42, 3726-3736, 10.1364/AO.42.003726, 2003.

Tan, H. B., Yin, Y., Gu, X. S., Li, F., Chan, P. W., Xu, H. B., Deng, X. J., and Wan, Q. L.: An observational study of the hygroscopic properties of aerosols over the Pearl River Delta region, Atmos. Environ., 77, 817-826, 10.1016/j.atmosenv.2013.05.049, 2013a.

Tan, H. B., Xu, H. B., Wan, Q. L., Li, F., Deng, X. J., Chan, P. W., Xia, D., and Yin, Y.: Design and Application of an Unattended Multifunctional H-TDMA System, Journal of Atmospheric and Oceanic Technology, 30, 1136-1148, 10.1175/JTECH-D-12-00129.1, 2013b.

Tao, J., Zhang, L., Ho, K., Zhang, R., Lin, Z., Zhang, Z., Lin, M., Cao, J., Liu, S., and Wang, G.: Impact of PM2.5 chemical compositions on aerosol light scattering in Guangzhou — the largest megacity in South China, Atmospheric Research, 135–136, 48-58, http://dx.doi.org/10.1016/j.atmosres.2013.08.015, 2014.

Turpin, B. J., Cary, R. A., and Huntzicker, J. J.: An In Situ, Time-Resolved Analyzer for Aerosol Organic and Elemental Carbon, Aerosol Science and Technology, 12, 161-171, 10.1080/02786829008959336, 1990.

Twomey, S.: On the composition of cloud nuclei in the northeastern United States, J. Rech. Atmos, 3, 281-285, 1968.

Villani, P., Picard, D., Marchand*, N., and Laj, P.: Design and Validation of a 6-Volatility Tandem Differential Mobility Analyzer (VTDMA), Aerosol Science and Technology, 41, 898-906, 10.1080/02786820701534593, 2007.

Virkkula, A., Ahlquist, N. C., Covert, D. S., Arnott, W. P., Sheridan, P. J., Quinn, P. K., and Coffman, D. J.: Modification, Calibration and a Field Test of an Instrument for Measuring

Light Absorption by Particles, Aerosol Science and Technology, 39, 68-83, 10.1080/027868290901963, 2005.

Wehner, B., Philippin, S., Wiedensohler, A., Scheer, V., and Vogt, R.: Variability of non-volatile fractions of atmospheric aerosol particles with traffic influence, Atmos. Environ., 38, 6081-6090, http://dx.doi.org/10.1016/j.atmosenv.2004.08.015, 2004.

Wehner, B., Berghof, M., Cheng, Y. F., Achtert, P., Birmili, W., Nowak, A., Wiedensohler, A., Garland, R. M., Pöschl, U., Hu, M., and Zhu, T.: Mixing state of nonvolatile aerosol particle fractions and comparison with light absorption in the polluted Beijing region, Journal of Geophysical Research: Atmospheres, 114, D00G17, 10.1029/2008JD010923, 2009.

Wu, C., Ng, W. M., Huang, J. X., Wu, D., and Yu, J. Z.: Determination of Elemental and Organic Carbon in PM2.5 in the Pearl River Delta Region: Inter-Instrument (Sunset vs. DRI Model 2001 Thermal/Optical Carbon Analyzer) and Inter-Protocol Comparisons (IMPROVE vs. ACE-Asia Protocol), Aerosol Science and Technology, 46, 610-621, 10.1080/02786826.2011.649313, 2012.

Wu, D., Bi, X. Y., Deng, X. J., Li, F., Tan, H. B., Liao, G. L., and Huang, J.: Effect of atmospheric haze on the deterioration of visibility over the Pearl River Delta, Acta Meteorol. Sin., 21, 215-223, 2007.

Yu, H., Wu, C., Wu, D., and Yu, J. Z.: Size distributions of elemental carbon and its contribution to light extinction in urban and rural locations in the pearl river delta region, China, Atmos. Chem. Phys., 10, 5107-5119, 10.5194/acp-10-5107-2010, 2010.

Zhang, S. L., Ma, N., Kecorius, S., Wang, P. C., Hu, M., Wang, Z. B., Größ, J., Wu, Z. J., and Wiedensohler, A.: Mixing state of atmospheric particles over the North China Plain, Atmos. Environ., 125, Part A, 152-164, http://dx.doi.org/10.1016/j.atmosenv.2015.10.053, 2016.

Zhang, Y., Wang, X., Li, G., Yang, W., Huang, Z., Zhang, Z., Huang, X., Deng, W., Liu, T., Huang, Z., and Zhang, Z.: Emission factors of fine particles, carbonaceous aerosols and traces gases from road vehicles: Recent tests in an urban tunnel in the Pearl River Delta, China, Atmos. Environ., 122, 876-884, http://dx.doi.org/10.1016/j.atmosenv.2015.08.024, 2015.

Table 1. Temperature (T) and residence time (RT) protocol of the semi-continuous Sunset OC/EC analyzer (Wu et al., 2012)

Carbon Fraction	Carrier Gas	T (℃)	RT (s)
OC_1	He	310	80
OC_2		475	60
OC_3		615	60
OC_4		870	90
EC_1	He and 2% O_2	550	45
EC_2		625	45
EC_3		700	45
EC_4		775	45
EC_5		850	45
EC_6		870	45

Table 2. Summary of average number and volume fractions in VTDMA measurements at 300 ℃.

Diameter (nm)	40	80	110	150	200	300
Number fraction						
CV	0.380 ± 0.153	0.174 ± 0.097	0.188 ± 0.081	0.167 ± 0.074	0.153 ± 0.070	0.141 ± 0.065
HV	0.255 ± 0.097	0.198 ± 0.052	0.165 ± 0.055	0.163 ± 0.064	0.178 ± 0.081	0.214 ± 0.097
MV	0.314 ± 0.097	0.513 ± 0.089	0.515 ± 0.098	0.530 ± 0.105	0.523 ± 0.116	0.497 ± 0.125
LV	0.051 ± 0.026	0.113 ± 0.040	0.132 ± 0.041	0.140 ± 0.041	0.146 ± 0.044	0.148 ± 0.047
Volume fraction						
VM	0.503 ± 0.131	0.600 ± 0.082	0.580 ± 0.073	0.590 ± 0.066	0.602 ± 0.064	0.627 ± 0.064
CV	0.361 ± 0.168	0.163 ± 0.105	0.166 ± 0.098	0.148 ± 0.086	0.134 ± 0.080	0.127 ± 0.073
HV	0.014 ± 0.005	0.011 ± 0.003	0.008 ± 0.002	0.007 ± 0.003	0.007 ± 0.003	0.007 ± 0.003
MV	0.070 ± 0.025	0.112 ± 0.024	0.112 ± 0.025	0.115 ± 0.026	0.109 ± 0.027	0.091 ± 0.025
LV	0.052 ± 0.026	0.114 ± 0.040	0.134 ± 0.044	0.140 ± 0.042	0.148 ± 0.048	0.148 ± 0.047

Table 3. Summary of concentrations of $PM_{2.5}$, OC, EC and the ratio of OC to EC (OC/EC) in the five clusters.

	Cluster				
	Coastal	Maritime	Continental		
	1	2	3	4	5
Origin (to the site)	NE	NE/E	NE	NW	NW
$PM_{2.5}$ (μg m^{-3})	58.5 ±24.4	58.9 ±30.9	47.5 ±28.4	33.9 ±15.9	33.8 ±19.3
OC (μg m^{-3})	10.8 ±6.01	10.84 ±7.22	10.13 ±6.89	5.51 ±3.3	7.32 ±2.75
EC (μg m^{-3})	4.38 ±2.97	4.98 ±4.21	3.43 ±3.12	1.8 ±0.98	2.46 ±0.59
OC/EC	2.83 ±1.05	2.62 ±1.03	3.65 ±1.6	3.18 ±1.26	2.94 ±0.73

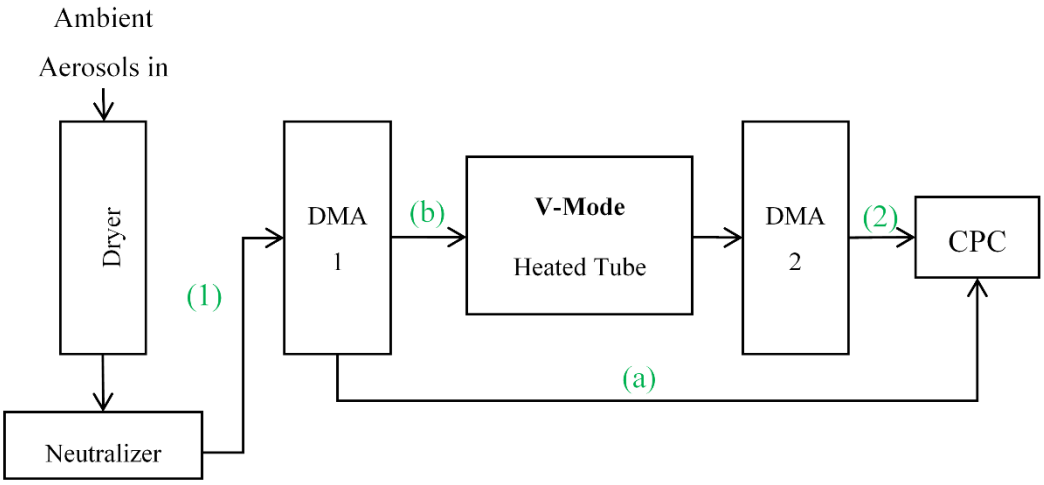

Fig. 1. Schematic diagram of the volatility tandem differential mobility analyzer (VTDMA).

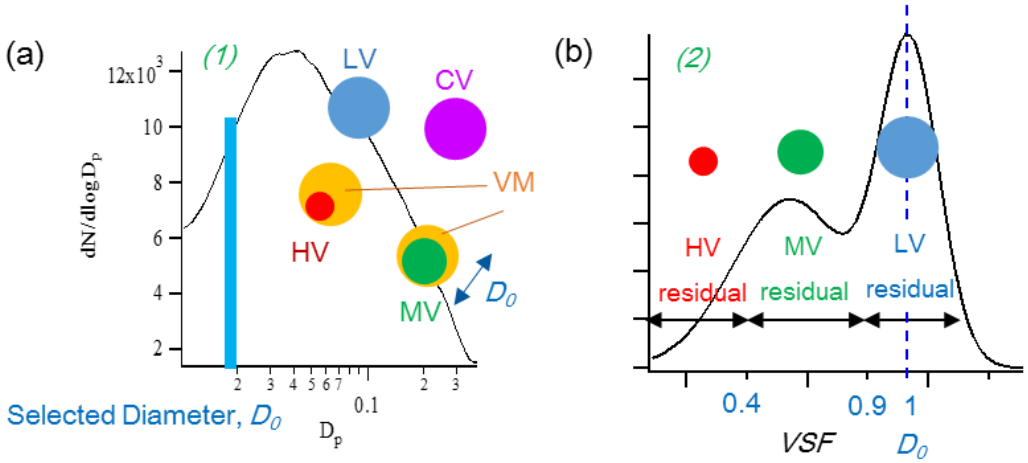

Fig. 2. Examples of particle size distributions of ~~(left)~~ (a) ambient aerosols before entering DMA_1 and ~~(right)~~(b) residuals of the size-selected particles (D_0) after heating. at 300 ℃. The distributions in Fig. 2a and 2b~~The left and right distributions~~ correspond to (1) and (2) in Figure 1 respectively. Residuals are divided into three groups—LV (blue), MV (green) and HV (red)—based on their *VSF*~~volatilities~~. CV (purple) and VM (orange) are vaporized and hence not measured as residuals. VM appears as coating for illustration purposes only. It does not necessarily reflect the morphology of the particles.

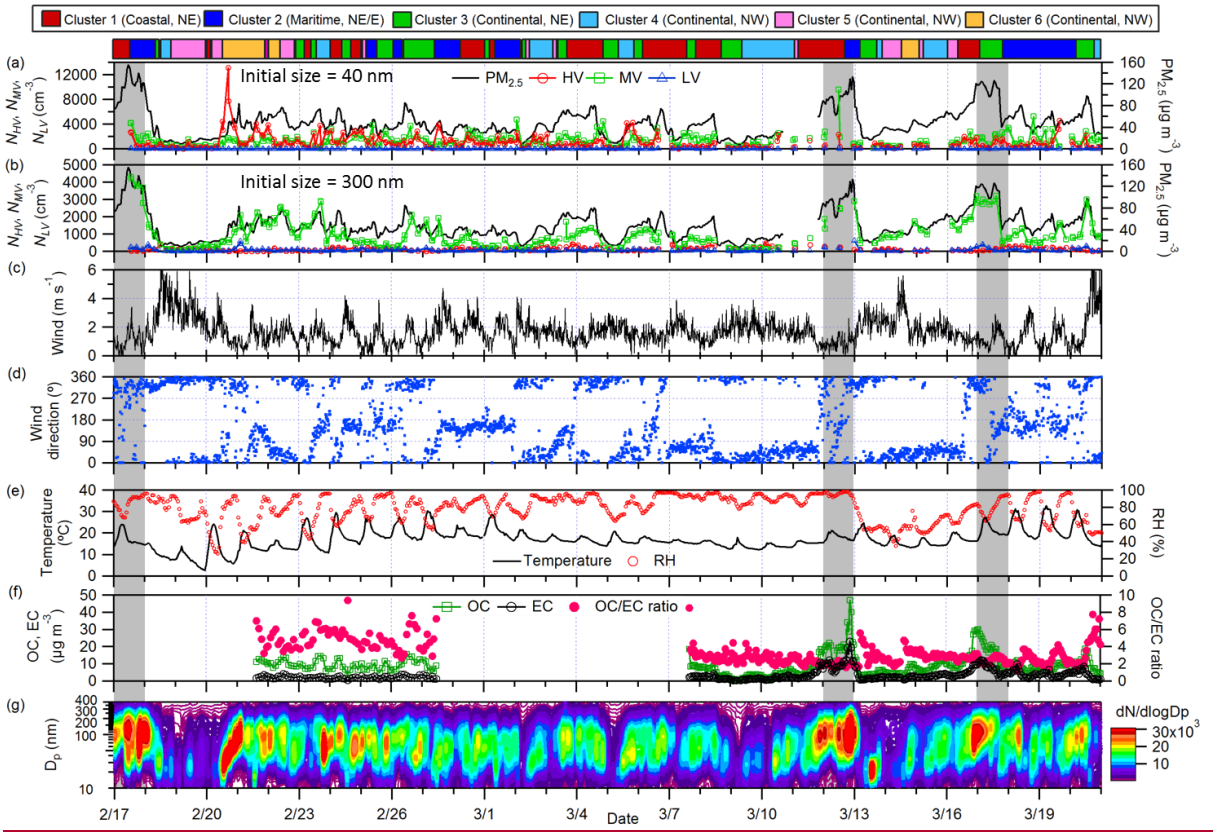

Fig. 3. Temporal variation of number concentrations of HV, MV and LV in 40 nm and 300 nm particles, $PM_{2.5}$, major meteorological parameters, OC and EC concentrations, OC-to-EC ratio and particle number size distributions in the campaign. Air mass clusters are depicted at the top and the shaded areas indicate days with daily-averaged $PM_{2.5}$ concentrations exceeding 95 μg m^{-3}.

~~Figure 3. Average number fractions of CV (purple), HV (red), MV (green) and LV (blue) particles of six selected particle dry diameters (40 nm, 80 nm, 110 nm, 150 nm, 200 nm and 300 nm) in Feb and Mar 2014.~~

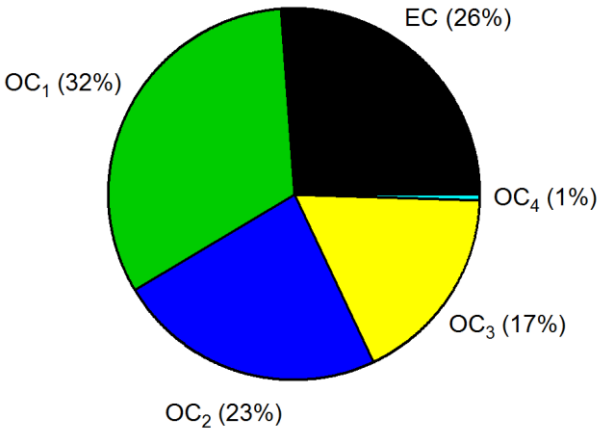

Fig. 4. Average mass fractions of EC, OC_1, OC_2, OC_3 and OC_4 in $PM_{2.5}$.

~~Figure 4. Time series of number concentrations of (a) 40 nm and (b) 300 nm HV (circle (red)), MV (square (green)), and LV (triangle (blue)) particles; number fractions of (c) 40 nm and (d) 300 nm CV (purple), HV (red), MV (green) and LV (blue) particles during the measurement period from 17 Feb to 20 Mar 2014. Time series of mass concentrations of $PM_{2.5}$ (solid line (black)) are plotted on the right axis of each plot.~~

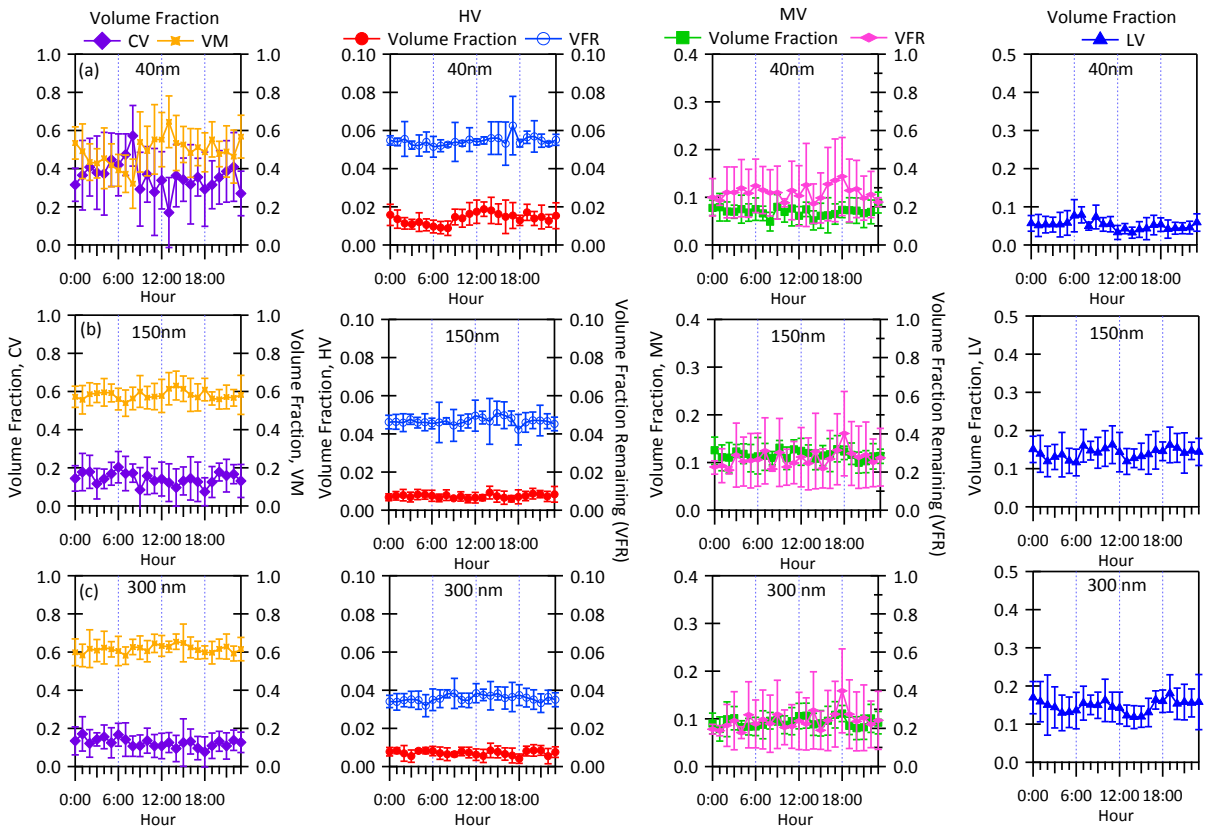

Fig. 5. Diurnal variations in volume fractions of (columns from left to right) CV, VM, HV residuals, MV residuals and LV residuals in (a) 40 nm, (b) 150 nm and (c) 300 nm particles. Diurnal variations in the volume fraction remaining (*VFR*) of HV and MV particles are plotted on the right axis. Error bars represent one standard deviation.

~~Figure 5. Diurnal variation in number fractions of CV (diamond (purple)), HV (circle (red)), MV (square (green)) and LV (triangle (blue)) particles that are 40 nm, 80 nm, 110 nm, 150 nm, 200 nm and 300 nm in dry size.~~

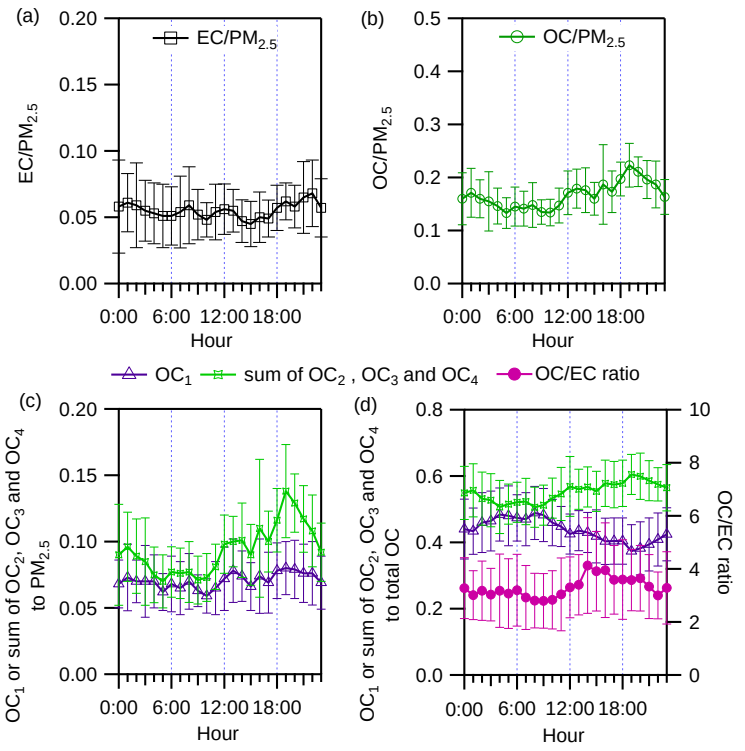

Fig. 6. Diurnal variations in the mass fractions of EC, OC, OC_1 and the sum of OC_2, OC_3 and OC_4 in $PM_{2.5}$, the ratio of OC to EC, mass fractions of OC_1 and the sum of OC_2, OC_3 and OC_4 to total OC in February and March. Error bars represent one standard deviation.

~~Figure 6. Overall average volume fractions of VM (orange), CV (purple), HV (red), MV (green), and LV (blue) particles as a function of particle diameter.~~

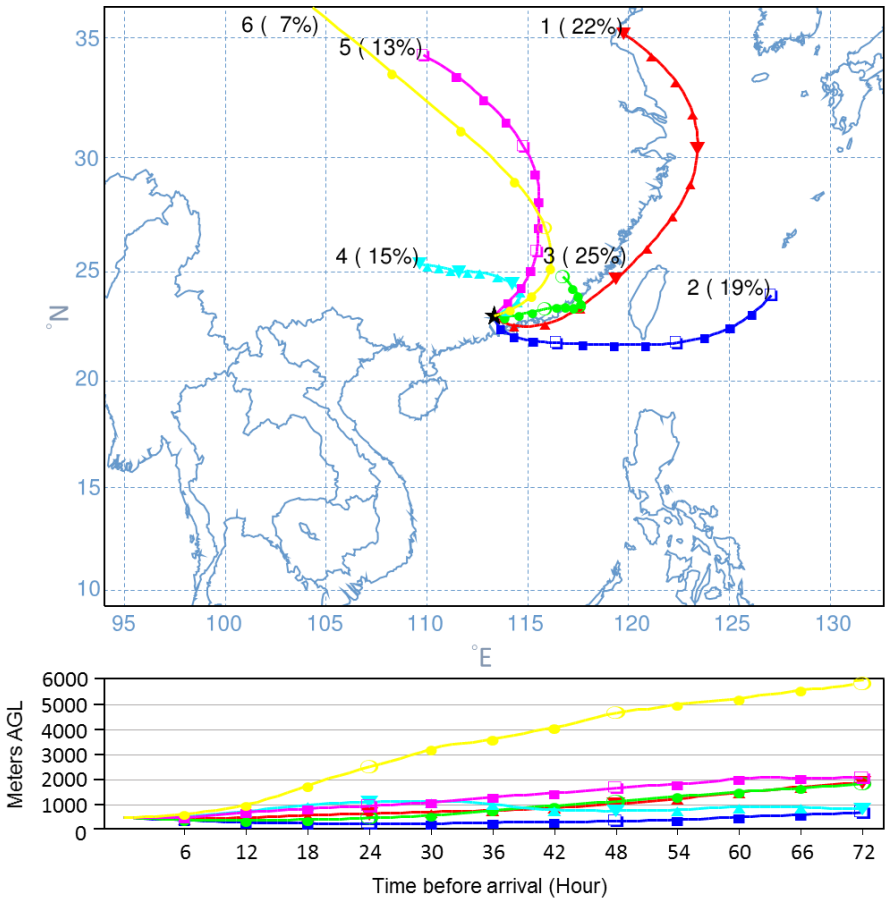

Fig. 7. Mean back trajectories of the six types of air masses arriving at the sampling site.

~~Figure 7. Diurnal variation in (left axis) $\Phi_{V,VM}$ (cross (orange)), $\Phi_{V,CV}$ (diamond (purple)), $\Phi_{V,HV}$ (circle (red)), $\Phi_{V,MV}$ (square (green)), $\Phi_{V,LV}$ (triangle (blue)), (right axis) $\Theta_{V,HV}$ (solid line (red)) and $\Theta_{V,MV}$ (dashed line (green)) particles that are 40 nm, 80 nm, 110 nm, 150 nm, 200 nm and 300 nm in dry size.~~

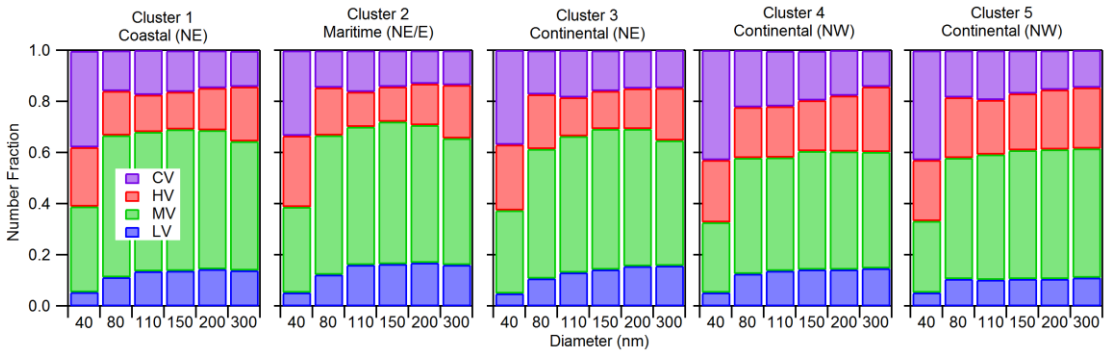

Fig. 8. Average number fractions of CV, HV, MV and LV in clusters 1 to 5 at different selected diameters.

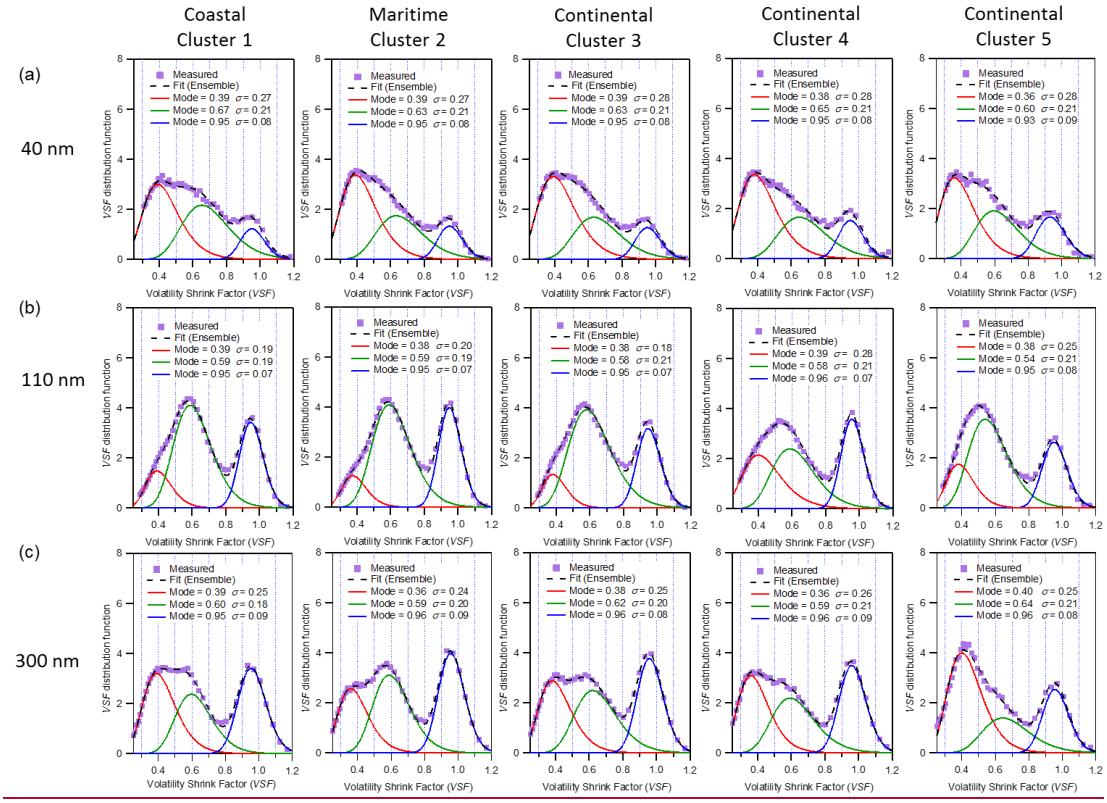

Fig. 9. Volatility shrinkage factor (*VSF*) distribution function in different clusters. Solid and dotted lines are the peaks fitted with log-normal function and the ensemble distributions, respectively.

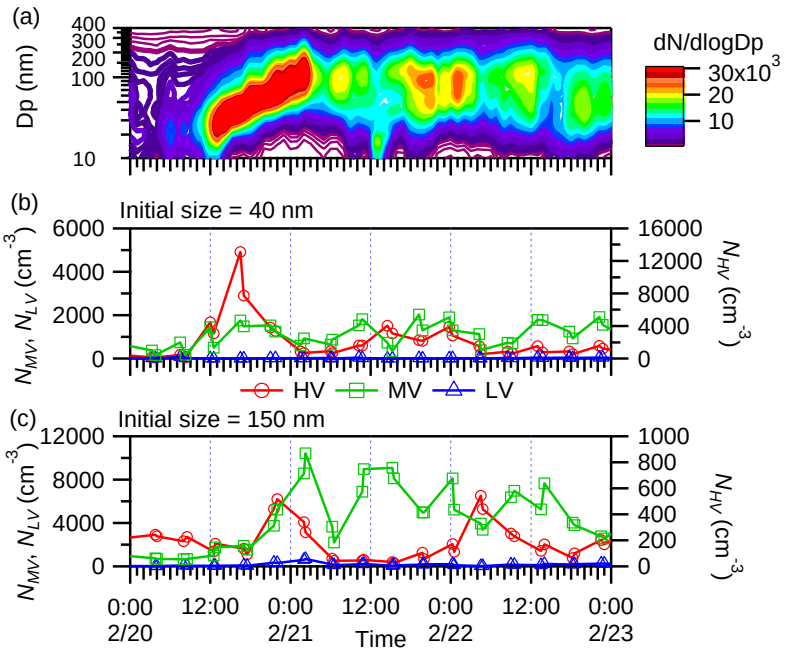

Fig. 10. Time series of (a) particle number size distribution, (b) number concentrations of HV, MV and LV in 40 nm particles and (c) number concentrations of HV, MV and LV in 150 nm particles.

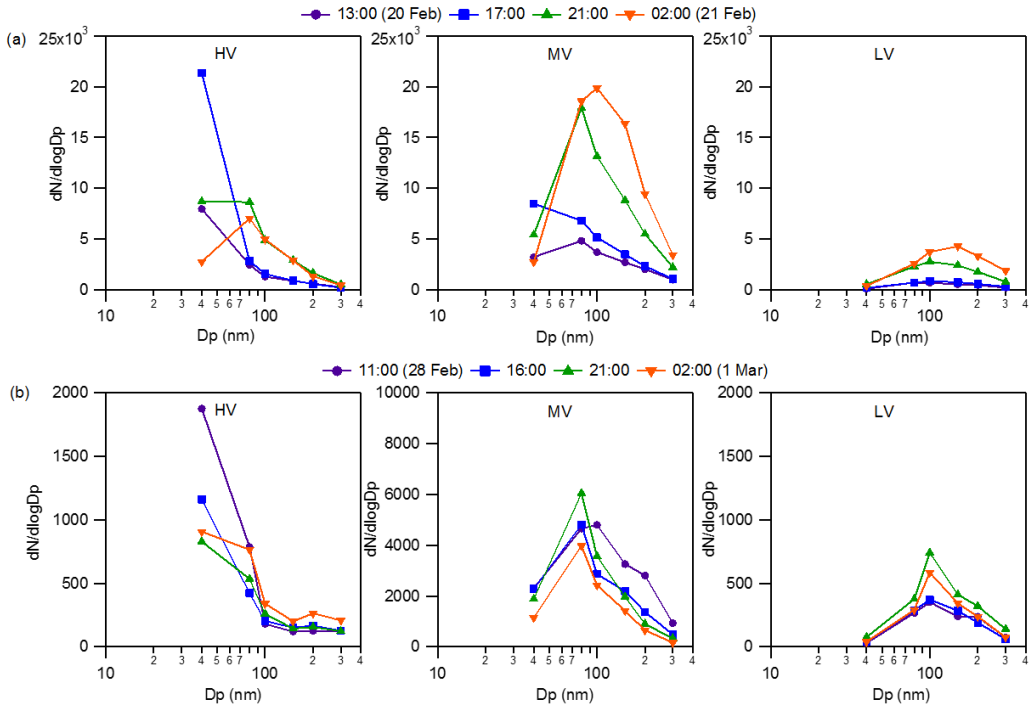

Fig. 11. Particle number size distribution of (columns from left to right) HV, MV and LV particles (a) at 13:00, 17:00, 21:00 on 20 Feb and 02:00 on 21 Feb and (b) at 11:00, 16:00, 21:00 on 28 Feb and 02:00 on 1 Mar.

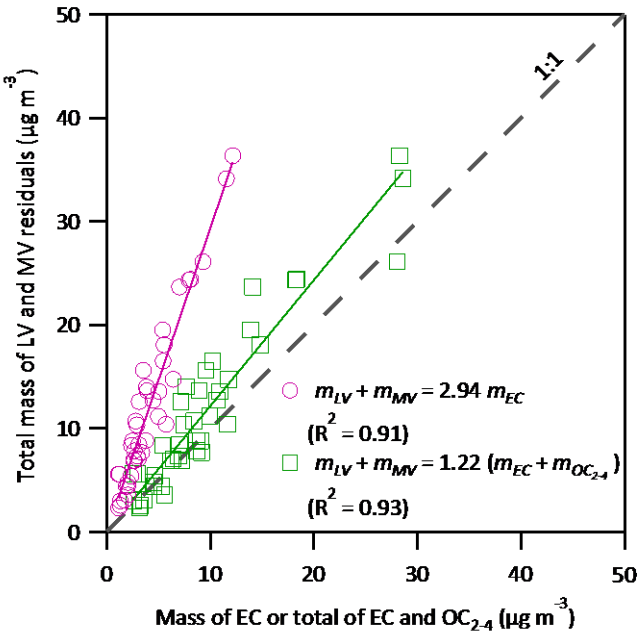

Fig. ~~8~~12. Closure analysis of the total mass of LV and MV residuals ~~(LV+MV)~~ from VTDMA at 300 ℃ and measured mass of EC or total of EC and $OC_{2\text{-}4}$ from the OC/EC analyzer.